

POLITECNICO DI TORINO

DIMEAS – Dipartimento di Ingegneria Meccanica e Aerospaziale

Corso di Laurea Magistrale in Ingegneria Meccanica



Tesi di Laurea Magistrale

DESIGN OF THE BODY OF AN ELECTRIC SUPERCAR

Academic supervisor:

Prof. Giancarlo Genta

Company supervisor:

Ing. Alessandro Genta

Candidate:

Óscar Lorenzo Rodríguez

Academic year 2017/2018

DESIGN OF THE MODEL OF AN ELECTRIC SUPERCAR
ÓSCAR LORENZO RODRÍGUEZ

To my family, your support
and encouragement was worth more
than I can express on paper.

My thanks and appreciations also
to my colleagues, who have willingly helped
me out sharing with me their knowledge.

Abstract

In the last decades, the automotive sector has experienced great progress in reached velocity, comfort or security. These new conditions, together with a stricter legislation, lead to new requirements that the fabricants have to face in the market. One of the fields where the companies are spending their effort and time is the aerodynamics. New technologies that help to understand how the exterior of the car and the air interact have been developed and improved, being CFD (Computer Fluid Dynamics) simulations one of the most used tools.

In this project, an aerodynamic study was performed using as an object the LVCHI 'La Venere' supercar model, presented in the Geneva Car Show 2018. The work in the company ANKERS and the direct contact with the client constructor of the vehicle allowed to perform this study with good accuracy. The external design in this type of sportive cars is very important due to the high velocities that can be reached. In addition, as this is an electric model, the reduction of the drag force can contribute to increase autonomy, key factor in the competence of this type of cars.

To perform this CFD study, different programs have been used. First, the initial geometry of the car, in form of surfaces, has been cleaned, prepared and meshed with the software Hypermesh of Altair. The simulations were performed with two different solvers, AcuSolve and OpenFOAM, to validate the method and be sure that the obtained output represented the reality. Finally, the different results were analysed with several post-processing software.

To have a bigger accuracy in the conclusions, two velocities, 160 km/h and 275 km/h, have been simulated, speeds that the car studied in this project can reach. With the analysis of the results, the components of the car with the greatest contribution can be identified, and some modifications were being proposed and discussed to improve the aerodynamic efficiency of the model.

The studied geometry includes a good number of details, to simulate accurately the flux around the car and be near to the reality conditions. The part of the suspensions and brakes that are in direct contact with the air are included, to take into account their influence on the flux of the wheelhouses. Another important feature that are included is the internal flow through the heat exchanger of the car. The air ducts, entering on the front spoiler and exiting to the wheelhouses, hood and bottom of the car were modelled. On the other hand, the behaviour of the radiator is included with a local porous zone, configured on the two used solvers.

Key words: CFD, Drag and lift coefficients, Downforce, Electric supercar

Table of contents

I. INTRODUCTION	1
1. General introduction	1
2. State of art.....	2
2.1. Evolution of aerodynamics	2
2.2. Evolution of car aerodynamics	5
2.3. Previous studies	8
3. Objectives	10
4. Structure of the document.....	11
5. Basic definitions	14
II. MODELS	16
6. Physical model.....	16
6.1. Properties of the fluid.....	16
6.2. Bernouilli's principle	20
6.3. Venturi effect.....	21
6.4. Reynolds number	22
6.5. Aerodynamic forces	23
6.6. Aerodynamic coefficients	26
6.7. Boundary layer.....	27
6.8. Parameter y -plus	28
6.9. Wake and flow separation.....	29
6.10. Darcy and Forchheimer law	30
7. CFD model	32
7.1. Fluid governing equations	33
7.2. Spatial discretization.....	35
7.3. Turbulent models	37
7.4. Spalart Allmaras turbulent model	38
III. NUMERICAL METHODOLOGY.....	40
8. Geometry.....	40
9. Spatial discretization	47

9.1. Bi-dimensional discretization	48
9.2. Three-dimensional discretization.....	51
9.3. Discretization quality and component organization.....	54
10. Solver configuration.....	57
10.1. AcuSolve solver	57
10.2. Heat exchanger configuration.....	61
10.3. Simulation launch.....	64
10.4. OpenFOAM solver	65
11. Post-Processing.....	68
11.1. AcuSolve results	68
11.2. OpenFOAM results	69
IV. MESH CONVERGENCE	70
V. VALIDATION OF THE METHOD	75
VI. SIMULATED CASES	78
12. Base case.....	78
13. Proposed modifications	79
13.1. Added rear spoiler.....	79
13.2. Different car inclination	80
13.3. Optimized air ducts	81
13.4. Other possible modifications	83
VII. RESULTS	85
14. Results of the base case.....	85
14.1. Numerical output	85
14.2. Contour results.....	88
14.3. Streamlines of the air flux	92
14.4. Pressure profiles.....	96
14.5. Study of the lateral flux.....	97
15. Results of the proposed modifications.....	101
15.1. Results with the added rear spoiler	101
15.2. Results with the different car inclination.....	110
15.3. Results with optimized air ducts	114
VIII. CONCLUSIONS	123
IX. BIBLIOGRAPHY	130

List of figures

Figure 2.1 : Wright brothers on their first manned flight [2].....	5
Figure 2.3 : 1921 Alfa Romeo G1 [4]	6
Figure 2.2 : 2016 Alfa Romeo Giulietta [5]	6
Figure 2.4 : Volkswagen XL1 [7]	7
Figure 6.1 : Pressure coefficient contour example	20
Figure 6.2 : Venturi effect basic scheme [16]	21
Figure 6.3 : Principal aerodynamic forces acting on a car	25
Figure 6.4 : Boundary layer in a horizontal surface	27
Figure 6.5 : Y-plus contour result	29
Figure 6.6 : Example of the wake zone in a car.....	30
Figure 6.7 : Experimental curve of the heat exchanger	32
Figure 7.1 : Element quality examples [18].....	37
Figure 7.2 : Principal turbulent models scheme	37
Figure 8.1 : General view of the received geometry.....	41
Figure 8.2 : Geometry of the interior ducts and heat exchanger	42
Figure 8.3 : Geometry of the added rear spoiler	42
Figure 8.4 : Detail of the simulated wheels	42
Figure 8.5 : Cleaning process, first step	43
Figure 8.6 : Cleaning process, second step	44
Figure 8.7 : Cleaning process, third step	44
Figure 8.8 : General measures of the domain.....	45
Figure 9.1 : Front view of the mesh	49
Figure 9.2 : Back view of the mesh	49
Figure 9.3 : Discretization of the interior ducts	50
Figure 9.4 : Wheel view of the mesh	50
Figure 9.6 : Discretization of the suspension component	51

Figure 9.5 : Mesh of the wheel and brake disk	51
Figure 9.7 : General view of the mesh	51
Figure 9.8 : Boundary selection panel	52
Figure 9.9 : Tetramesh parameters panel	53
Figure 9.10 : Refinement boxes in the model.....	53
Figure 9.11 . Division of the surfaces in the model	55
Figure 9.12 : Principal components of the model	56
Figure 9.13 : Ground division in the wheels	56
Figure 10.1 : Residual evolution during simulation	59
Figure 10.2 : Experimental curve of the heat exchanger	62
Figure 10.3 : Streamlines on the heat exchanger	63
Figure 10.4 : Launch panel of AcuSolve	64
Figure 10.5 : General case structure of OpenFOAM	65
Figure 10.6 . Velocity file in OpenFOAM.....	66
Figure 11.1 : Discretization with 9 mm of minimum element size.....	72
Figure 11.2 : Discretization with 1 mm of minimum element size.....	72
Figure 11.1 : Pressure contour in OpenFOAM.....	76
Figure 11.2 : Pressure contour in AcuSolve	76
Figure 11.3 : Velocity contour in OpenFOAM.....	77
Figure 11.4 : Velocity contour in AcuSolve	77
Figure 12.1 : Base geometry	78
Figure 13.1 : Geometry of the added rear spoiler	79
Figure 13.2 : Geometry before the inclination	80
Figure 13.3 : Geometry after the inclination	81
Figure 13.4 : Comparation of the interior redesign, symmetry plane.....	82
Figure 13.5 : Comparation of the interior redesign, interior ducts	82
Figure 13.6 : Comparation of the interior redesign, lateral view	82
Figure 14.1 : Pressure contour.....	89
Figure 14.2 : Velocity contour.....	89
Figure 14.3 : Wall shear stress contour	90

Figure 14.4 : Y-plus contours.....	91
Figure 14.5 : Eddy viscosity contour	91
Figure 14.6 : Streamlines of the exterior air flux	94
Figure 14.7 : Streamlines through the interior ducts of the car	95
Figure 14.8 : Pressure profile of the standard geometry.....	96
Figure 14.9 : Pressure value at 1 cm from the window corner.....	97
Figure 14.10 : Lateral pressure at $z = 0.35$ m	98
Figure 14.11 : Lateral pressure at $z = 0.45$ m	98
Figure 14.12 : Lateral pressure at $z = 0.55$ m	99
Figure 14.13 : Lateral pressure at $z = 0.254$ m	99
Figure 14.14 : Exterior streamlines of the lateral flux	100
Figure 15.1 : Pressure comparison with the rear spoiler.....	103
Figure 15.2 . Velocity comparison with the rear spoiler	104
Figure 15.3 : Wake zone comparison with the rear spoiler	104
Figure 15.4 . Pressure values comparison.....	105
Figure 15.5 : Pressure contour comparison	106
Figure 15.6 : Eddy viscosity contour without the rear spoiler	107
Figure 15.7 : Eddy viscosity contour with the rear spoiler.....	107
Figure 15.8 : Streamline comparison with the rear spoiler	108
Figure 15.9 : Pressure profile comparison	109
Figure 15.10 : Numerical results with the modified inclination	110
Figure 15.11 : Velocity contour in the base case	112
Figure 15.12 : Velocity contour after the inclination	112
Figure 15.13 : Velocity values in the base case.....	112
Figure 15.14 : Velocity values after the inclination.....	113
Figure 15.15 : Pressure values in the base case.....	114
Figure 15.16 : Pressure values after the inclination	114
Figure 15.17 : Pressure at symmetry plane in standard air ducts	115
Figure 15.18 : Pressure at symmetry plane in modified air ducts	116
Figure 15.19 : Pressure at interior standard air ducts	116

Figure 15.20 : Pressure at interior modified air ducts.....	117
Figure 15.21 : Eddy viscosity contour at standard air ducts.....	118
Figure 15.22 : Eddy viscosity contour at modified air ducts.....	118
Figure 15.23 : Streamlines of interior flux in the standard case	119
Figure 15.24 : Streamlines of interior flux in the modified case	120
Figure 15.25 : Interior standard streamlines with a different seed	121
Figure 15.26 : Interior modified streamlines with a different seed	121

List of tables

Table 8.1 : Measures of the wind tunnel	45
Table 8.2 : measures of the car model.....	46
Table 8.3 : Computation of the rotation of the wheels	47
Table 9.1 : Parameters used for the 2D mesh.....	48
Table 9.2 : Boundary layer parameters.....	52
Table 9.3 : Maximum element sizes in the refinement boxes.....	54
Table 9.4 : Components defined in HyperMesh	55
Table 10.1 : General parameters of the simulation	58
Table 10.2 : Summary of the boundary conditions.....	59
Table 10.3 : Wheels and ground configuration in the 160 km/h case.....	60
Table 10.4 : Wheels and ground configuration in the 270 km/h case.....	61
Table 10.5 : Heat exchanger fluid configuration.....	62
Table 10.6 : General configuration of the constant folder in OpenFOAM	67
Table 10.7 : General simulation parameters in OpenFOAM.....	67
Table 11.1 : Cases of the convergence process	71
Table 11.1 : Validation result	75
Table 14.1 : Aerodynamic coefficient of the base case	86
Table 14.2: Numerical results of the base case	86
Table 14.3 : Aerodynamic contributions in the base case	87
Table 15.1 : Numerical comparison with the added rear spoiler	101
Table 15.2 : Aerodynamic contributions with the rear spoiler	102
Table 15.3 : Aerodynamic contributions with the changed inclination.....	111

List of formulas

(2-1) Newton drag force law	3
(6-1) Definition of the density	16
(6-2) Law of ideal gases	17
(6-3) Definition of kinematic viscosity	17
(6-4) Sutherland law	17
(6-5) Total pressure components	18
(6-6) Expression of the dynamic pressure	18
(6-7) Pressure coefficient definition	19
(6-8) Pressure coefficient alternative expression	19
(6-9) Bernouilli principle	20
(6-10) Simplified Bernouilli principle	20
(6-11) Reynolds number	22
(6-12) Expression of the drag force	24
(6-13) Expression of the lift force	25
(6-14) Y+ parameter expression	28
(6-15) Momemtum equation with porous contribution	31
(7-1) Transport Reynolds Theorem	33
(7-2) Continuity equation	34
(7-3) Momemtum equation	34
(7-4) Momemtum definition	34
(7-5) Momemtum equation applied to a fluid volume.....	34
(7-6) First law of thermodynamics	35
(7-7) Energy equation	35

List of symbols

Fundamental magnitudes

M	Mass
L	Length
T	Time
\emptyset	Temperature

Constants

g	Gravity [LT^{-2}]
R_{air}	Ideal gases constant [$L^2T^{-2}\emptyset$]
C_S	Sutherland constant [\emptyset]

Fluid properties

ρ	Density [ML^{-3}]
μ	Viscosity [$ML^{-1}T^{-1}$]
ν	Kinematic viscosity [L^2T^{-1}]

Field properties

T	Temperature [\emptyset]
V	Volume [L^3]
p	Pressure [$ML^{-1}T^{-2}$]
q	Dynamics pressure [$ML^{-1}T^{-2}$]
m	Mass [M]
v	Velocity [LT^{-1}]
Re	Reynolds number [-]
τ	Shear stress [$ML^{-1}T^{-2}$]
C_p	Pressure coefficient [-]

Aerodynamic properties

C_D	Drag coefficient [-]
C_L	Lift coefficient [-]

Others

z	Reference height [L]
A	Frontal area [L^2]
\vec{n}	Normal vector [-]

I. INTRODUCTION

1. General introduction

The automotive industry is in continuous growth. New advances and stricter norms that affect the sector force the companies to develop and improve new technologies and studies to be competitive.

As the car, without any doubt, is the most popular land transport system, used widely all over the world, regulations focus in this sector to reduce the contamination, and to improve the passenger safety and comfort.

The European Union imposes new norms in the field of emissions that are more restrict, and this makes the fabricants of the automotive sector to adapt to the new rules. With the objective of reducing the harmful substances emitted to the atmosphere, the companies focus in designing new and more efficient propulsive systems, advanced components to save energy and the design of the external shape of the car, to reduce the aerodynamic resistance induced by the contact with the air.

In the recent decades, the focus in the aerodynamic studies has grown due to the importance of reducing the consumption of the vehicle with the reduction of the drag force. Additionally, forces induced by the air in the car have great influence in the security because of the possibility of increasing the downforce that contributes to have a better grip between the tyres and the road. Comfort is another field that is affected, because of the possibility of reducing vibrations and noise with an appropriate exterior design. [1]

Electric cars, raising in the past decades especially due to the increase of the traditional fuel prices, have the challenge of improving their autonomy in order to be more competitive and attractive in the market. Efficient external designs can help widely in this task, as the reduction of the drag force affect positively to save the energy used by the vehicle.

This kind of studies only have a good reason to be applied when the speed is at least 100 km/h, otherwise the effects of aerodynamic forces are almost negligible. The new velocities that can be reached with the modern model cars give to these studies

even more value as the aerodynamic forces increase with the velocity to the power of two. This explains why the studies are applied especially on the type of cars that are more sportive, as it is the case of the electric model studied in this project.

Aerodynamic studies are performed in different ways, as real scale experiments or in wind tunnels, but a type of analysis that is more and more used is the CFD (Computer Fluid Dynamics) simulations. This method allows studying many different conditions with a software that solves the equations of the fluid and therefore predict how the model behaves with those conditions in the real world. This kind of studies, nowadays widely used in many different sectors, has experiment a great progress due to the increasing performance of new computers, making them more accessible.

Aerodynamic simulations are nowadays more complex in comparison with the past, therefore the number of details and components that can be added to the studied model are greater. In addition to the external shapes of the car, the internal flux of the air that refrigerates the engine and other parts as suspensions and brakes are usually included in the CFD studies. In the present document, it is explained the process of simulations of an electric sportive car, with a high level of detail that make the model very similar to the reality.

After this type of CFD studies, the next step that follows usually in the market is to perform experimental test in a real wind tunnel, to prove the results obtained in a computer. Obviously, the final part of the process is to jump to a real road and drive the car, testing its behaviour in a circuit.

2. State of art

2.1. Evolution of aerodynamics

Aerodynamics is a part of the fluid dynamics concerning with the study of the principles of the flow of gases and the generated forces on a solid body within the flow. Various properties of the fluid have to be taken into account in order to solve a problem in this field, as the velocity, pressure or density, as functions of space and

time. After understanding the flow pattern, the next step is to compute or estimate the forces and moments that act on the solids within the flow. [2]

Aerodynamics is well known for affecting the design of aircrafts or other vehicles, but its influence is greater. In addition, it plays an important role in the design of bridges, buildings or ventilation passages. Town planners need to consider the air behaviour in their designs in order to reduce pollution and increase the comfort in outer spaces.

During the history, many images and studies were carried out related with aerodynamics and flights. Aristotle or Galileo Galilei recorded some observations about aerodynamic effects, but the first governing laws were not developed until the seventeenth century.

The first person to develop a theory related with the air resistance, making him the world's first aerodynamicist. During his work Newton thought that the drag was produced due to the dimensions of the body, the fluid density and the velocity raised to the second power. Although his ideas were not entirely correct, it turned out that his conclusions were valid for low-flow speeds. Newton developed also a law for the drag force on an inclined flat plate, the expression is:

$$F = \rho \cdot S \cdot V^2 \cdot \sin^2(\theta) \quad (2-1)$$

Where F is the drag force, ρ the fluid density, S the area of the plate, V the velocity of the flow and θ the inclination angle. Nowadays we know this equation is not correct unless the flow is hypersonic but the contribution of Newton to the aerodynamic field is beyond doubt. This formula could make people thought that flight was more difficult than actually is, as the drag is closer to being linear with the inclination angle. The lack of knowledge at this point in the history explain the delay on the arrival of the manned flight.

George Cayley was the first to separate the drag and lift contributions of the force, which are present on any vehicle. Cayley believed that the propulsion in a flying machine was necessary to counteract the drag force in order to achieve the flight. During his studies, he looked to nature searching for aerodynamic shapes with low drag, as some aquatic animals as the trout. Fish bodies are shaped in order to have a

very low resistance with the water, their cross-sections are very close to the modern low-drag air foils designed nowadays.

All these empirical findings caused some resistance experiments to be carried out during the eighteenth and nineteenth centuries. During this period Jean Rond d'Alembert, Gustav Kirchhoff and Lord Rayleigh developed drag theories from the experiments. Claude-Louis Navier and George Gabriel Stokes wrote the equations of the fluid behaviour with friction. At this time, the experiments may consist on immersing objects in water or simply drop them from a high altitude, like flat plates from the Eiffel Tower.

Francis Herbert Wenham constructed the first wind tunnel in 1871, a much more precise way to measure the air resistance on an object. The studied body is placed within an artificial, uniform stream of air, where the velocity is known. The object used in these experiments are generally smaller than in practice, this makes necessary the invention of a method to relate small scale models to their real-life counterpart. Osbourne Reynolds, who invented the dimensionless Reynolds number, and experiment with laminar to turbulent flow transition, did this. At the end of the nineteenth century the first professional organization dedicated to aeronautics was born, the Royal Aeronautical Society of Great Britain.

At this period, two problems were still to be solved in order to achieve the manned flight. One was the creation of low-drag high-lift aerodynamic wings. The second one was the determination of the power needed in the flight process. Some non-scientifically enthusiasts tested various flying machines but with little success.

In 1889, Charles Renard became the first person to estimate in the power needed for sustainable flight. The study of the bird wings by this French aeronautical engineer and other German colleagues help them to conclude that a human could not fly with its own power with wings attached to their arms. The design of thin and curved airfoils was starting to be highly tested due to its high lift and low drag.

In 1893 all the scientific work around the world was summarised in a book by Octave Chanute, helping to those interested in this field. The information of this publication and the personal assistance of Chanute helped the Wright brothers to reach the necessary knowledge to fly the first manned aircraft on December the 17th, 1903; an image of this successful moment is shown in the figure 2.1. This achievement

arrived after a long race with another scientist around the world. This first flight confirmed and discarded a great number of aerodynamics theories, as the above-mentioned Newton drag force. After this moment, the efforts were more organised between scientist and aviators, leading to the modern aerodynamics.

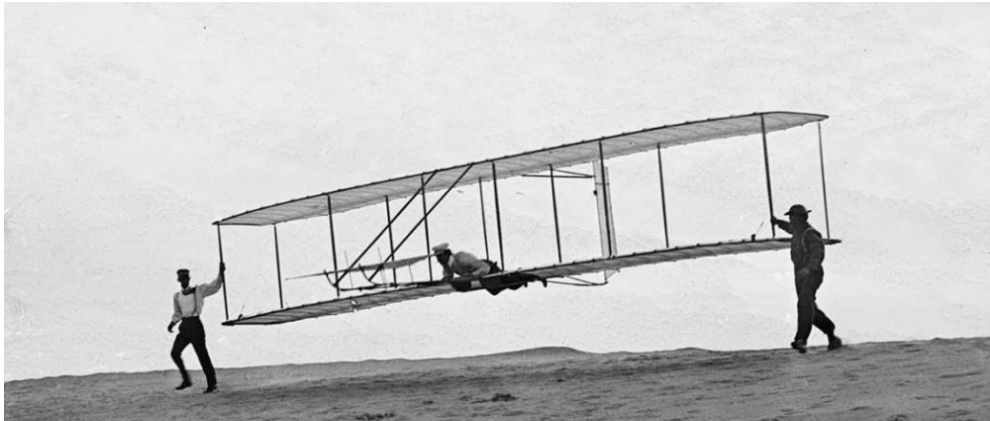


Figure 2.1 : Wright brothers on their first manned flight (2)

In the evolution of this field, the aeronautic sector has a very important role, due to the very high velocities reached and the vital interaction between plane and air. Much progress was applied first in this sector and then they influenced to other fields, like the automotive one, which is treated in this project and explained in the next part of the document. [3]

2.2. Evolution of car aerodynamics

The early history of automobile is characterised by the arrival of many different technologies that tried to find the most efficient propulsion system. However, as the knowledge in fluid dynamics grew and new fabrication systems were possible, the later periods were defined by trends in exterior styling, size and other utilities.

When the first car models appeared, in the late XIX century, the design and the technical efforts were focused on the engine and the entire propulsion system in order

to reach higher velocities. The external shape was not taken into account nor the effects of the air in the car movement.

In the early XX century, cars started to be produced in series, but the effort of the fabricants were still focused principally in the improvement of mechanic components, like transmission or engine. External design was influenced by esthetical criteria and not by engineering aims.

In the middle XX century, the aerodynamic studies showed that the shapes of the cars in that time were not efficient, and from that moment, the design changed drastically, with shorter front parts, lower heights and generally more rounded shapes.

In the figure 2.3 and 2.4, we can distinguish clearly some of the differences in the external design of the current model cars with respect to the old ones. In this case, we have a comparison with two Alfa Romeo models. On the left, the first model made by the company, the Alfa Romeo G1 of 1921 [4], a car with six cylinders, 6.3 litres and able to have 70 CV. This model had great mechanic characteristics if we compare it with other cars of the same time as the Fort T, more popular and with a power of 20 CV. On the right, the modern Alfa Romeo Giulietta 2016 [5], as an example of a car made with the nowadays knowledge and criteria.



Figure 2.3 : 1921 Alfa Romeo G1 [4]



Figure 2.2 : 2016 Alfa Romeo Giulietta [5]

The new designs aim to reduce the so-called drag force, which represent the resistance the air generates to the object within it. The lower this value is, the higher the velocities the car can reach and the lower the fuel consumption will be a very important parameter due to the increasing prices of fossil fuels. Therefore, a good

understanding of this phenomenon is necessary in order to focus the effort in a good direction. Generally, the drag in vehicle aerodynamics is comprised of three forces: The frontal pressure, the rear vacuum and the effect of the friction on the surface of the vehicle. [6]

Considering this, together with computer and wind tunnel experiments, automotive engineers have the tools and are able to produce much more efficient cars. However, it is debated whether these models would be sold or not, due to its increasing price and the nowadays aesthetic criterion. The most aerodynamic car in the world is the Volkswagen XL1, which can be seen in the figure 2.4, with a drag coefficient of 0.19. This car gets up to 300 miles per gallon and offers a very low resistance to the airflow due to its general shape that adapts to the streamlines and the covered wheels together with other details.



Figure 2.4 : Volkswagen XL1 [7]

Sportive cars nowadays have higher drag coefficients, that can be around 0.3 as the case of the model of this project, because they are designed looking to optimise other aspects, as the lift coefficient. These aerodynamic concepts are defined in the theory part of this document. [8]

Other transport systems, like the mentioned planes, but also motorbikes, trains and even ships had a similar evolution from the growing fluid knowledge and the new

tools that showed up and gave the possibility of doing more accurate experiments, like wind tunnels and the CFD software simulations.

2.3. Previous studies

Many different studies have been carried out about this topic. Every model that is in the market was first analysed in its design phase. Many projects can be found and in order to have a good reference some of them are listed in this part. The used software, the studied parameters, the proposed modifications and the type of presented results of these studies have been taken into account in order to write and structure this project.

W. Kieffer, S. Moujaes and N. Armbya [9] wrote in 2006 their study of the aerodynamic characteristics in a Formula Mazda race car, focusing on the rear and front wings. Due to the very competitive environment of the racing sector, generally this kind of studies are not published, or they do but only when they are already obsolete. For this reason, Kieffer and his colleagues wanted to perform this analysis to share their knowledge and help teams that compete in minor leagues. In their study, they simulate with a k-e turbulent model the flow in the wings of the car, and they focus on the ground effect on the bottom part of the Formula Mazda. They presented graphically the results, as the pressure and velocity distributions, and lift and drag coefficients for the different angles of attack of the front wing. It was concluded that the ground effect has a big impact on the lift force acting on the car and that the angle of attack affects directly the lift and drag coefficients.

Satyan Chandra et al [10] performed in 2011 their study about the airflow effects and dynamics of a PACE Formula 1 race car. The goal of the analysis was to maximize the down force and minimize the drag during high-speed situations. Their simulations included efficient meshing techniques and realistic loading conditions to understand the behaviour of the car. Optimizations of the wing orientations and improvement of some outer surfaces of the model were carried out. The CFD simulations pointed out that the current front and rear wings did not generate the desired down force, therefore these parts needed a redesign.

Mohd Aliff Bin Mohd Nor and Aswatha Narayana [11] studied the effect of two different rear spoilers varying the angles of attack on a sedan concept model car. The aim of the study was to understand the contributions of these components to the lift and drag coefficients, and to compare the results of the different cases graphically. After the simulations, it could be concluded that the behaviour of the car with a rear wing is improved compared with the model without it. Besides, the NACA 0012 wing give better results than the plate spoiler. Negative angles of attack are not positive as they contribute to lifting the car. This thesis also included an extensive discussion of numerical solution and the output obtained with the simulations.

Sneh Hetawal et al [12] wrote in 2014 their paper about the aerodynamic study of a Formula rear-engine SAE car. The goal of the analysis was to compare the aerodynamic behaviour of this model with and without front spoiler. Formula SAE is a design competition, at college level, where students of universities all over the world compete with open-wheel formula cars. The CFD analysis of these lightweight cars is done to reduce the drag force, enhancing the stability. For this study, the ANSYS Fluent software was used, performing a turbulent simulation with the k-epsilon model. The results were shown in the form of velocity contours and drag force comparison. Three models were tested, a standard one, without front wing and with a cut section at the firewall. It is concluded that the third model shows better aerodynamic characteristics than the other two.

S.M. Rakibul Hassan et al [13] studied in 2014 different aspects that affect the car competition sector, as drag reduction techniques such as rear underbody modifications and exhaust gas redirection towards separation zones in the rear part. About 50 to 60% of total energy fuel is lost to overcome the drag force that affects the car during a race. For this reason, optimising the exterior shapes of these models to reduce the drag is one of the main concerns in race vehicle aerodynamics. Performing a CFD simulation using a k-epsilon turbulent model, the drag coefficient of the car was found to be 0.32, and the different proposed modifications can reduce it up to 22% with rear bottom redesign and 9.5% with exhaust gas redirection. They also concluded that the negative pressure in the rear part, together with the separation zone, could be reduced and therefore the drag coefficient improved.

3. Objectives

This document was written to explain the aerodynamic analysis of an electric supercar, throughout several CFD simulations. The standard geometry was used to find out possible aspects where a redesign could be applied, after that, some modifications were proposed and tested in order to improve the car's behaviour.

Besides, another objective of this project was to compare the result of two different CFD solvers. The geometry of the model was discretized with the same pre-processing program. After that, the standard car was simulated with AcuSolve and OpenFOAM, which will be explained later in this document, in order to validate the used method and the obtained results.

Finally, the output of the simulations was analysed, focusing principally in the following parameters and visual results:

- Drag coefficient
- Lift coefficient
- Car balance (moment coefficient)
- Maximum and minimum pressure on the car's surfaces
- Maximum and minimum velocities on the domain
- Pressure contours
- Velocity contours
- Eddy coefficient contours
- Wall shear stress contours
- Surface's y -plus contours

In addition to these results, it was also interesting to extract some animations of the streamlines of the air flux. Due to the paper format of the document it is not possible to show them here, but some static images were included on the project.

After the analysis of this first simulation, corresponding with the standard geometry, some modifications were proposed and computed as well, showing the change that was reached through a direct comparison. These changes were the

addition of a little rear spoiler, the modifications of the inclinations of the car and finally a redesign of the internal air ducts of the vehicle.

The motivation behind this work is to conclude which is the aerodynamic behaviour of this specific electric model car. A deep study of all the possible variables that affect is necessary in order to find a good optimization, very important in the electric sector to be able to compete with fossil fuel models.

Besides, in these studies the simulation of the air flux throughout the radiator of the car was included. Generally, this aspect is not included in this type of CFD studied due to the needed details and the high computational power that comes with it. In order to be as close as possible to real conditions, the simulation of the air entering by the front spoiler, passing through the heat exchanger and going out to the suspensions, bottom of the vehicle and the hood is taken into account.

All these details, included in the final simulations of the project, allow us to think that the obtained results represent accurately the behaviour and characteristics of the real car.

4. Structure of the document

This document is divided into nine different parts, in order to explain clearly all the information related with the study and to have all content well organised. In the following points each of these parts are described:

- The first part represents a general **introduction** to the topic of the project. It has four divisions; in the first one, the document is introduced, explaining the basic ideas of the study, together with the motivation and strategies followed. The second one represents the state of art, where the previous work in the field of automotive aerodynamics is explained, as the evolution of the CFD studies, the changes of the car industry and previous studies that were useful in order to write the present paper. The third one is used to list the main and secondary goals of the project, together with the motivation of the study. The structure of the document is the fourth part, where the reader is at this moment, and finally the last has definitions of some basic concepts used in the document, to make the reading more understandable.

- The second part, based mainly on **theory**, is divided into two chapters. In the first one some general parameters, definitions about fluid dynamics and other concepts that were used during the study process are explained. The goal of this part is to cover the main theory, and throughout the document, some references calling to this chapter can be found. On the other hand, the second one represents a more specific theory related with the CFD simulations, as the equations solved by the software, the process of discretization of the studied domain or the turbulent model used to compute the solution.
- Third part contains the **methodology** followed during all the study process. Starting from the received geometry, that has to be cleaned and prepared for the simulations, the discretization of the domain, called mesh generation, and the configuration of the solvers, used to compute the simulated cases. The main steps followed during the process are described, presenting all the introduced parameters and problems that can be encountered, with the objective to facilitate all the needed information to repeat what it has been done. Finally, the post-processing programs used to analyse all the obtained output are listed, with the type of results opened with each of them.
- The fourth one represents the **mesh convergence** performed in this project. This kind of studies are necessary to know the optimal size of the elements in which we discretise out domain. This knowledge allows us to simulate efficiently the different cases, not losing unnecessary time with a too refined mesh that gives the same output or not being able to get a stable result with a too big mesh size. To perform this study several simulations were carried out with the solver OpenFOAM, due to its higher computational velocity, varying the general size of the mesh, refinement boxes and boundary layers. After the analysis of some results as the drag and lift coefficient, maximum pressure and velocity or the oscillations of the numerical output, the optimal mesh were obtained. Once this conclusion was reached, the rest of the cases were performed with this strategy of discretization, taking into account the details that were added for the definitive simulations.

- Fifth part of the document contains the **validation** of the used method. This is an essential component of a numerical study, useful to know if the followed procedure is correct and the obtained results valid. For the validation, two solvers were used: AcuSolve and OpenFOAM. The comparison between these two CFD-specialised programs let us know the correctness of the method. The control variable in this case was the drag coefficient of the model car and also some visual results obtained with both software as pressure and velocity contours. The evaluation of these parameters allowed concluding that the used method is valid.
- Part six shows what are the **simulated cases** during the study. A general explanation and objective of each simulation can be found, this includes the standard geometry and two possible modifications. Besides, proposed future work that can be done to complete the study is also written.
- The seventh part contains all the obtained **results** of the simulated cases. In order to make the content more understandable, an explanation of each figure and table is included, as well as the conclusion that can be directly extracted from them. This is the most visual and important part of the document, as it has all the output from the studies.
- The **conclusions** that can be extracted from the whole study are contained on the part eight. Here the final comments are written, the most important data summarised, as well as an evaluation about the aerodynamic behaviour of this electric supercar. In addition, a final comment about the possibility of additional modifications that can be applied to the car model is included.
- The final and ninth part of the document contains the **bibliography**. The most important references, as books, articles or web pages that were used to write and be able to simulate correctly the model are included. This could allow the readers to perform, if they want, a deeper research about the project topic.

5. Basic definitions

- **CAD:** Computer Aided Design, it is the informatics sector where software technologies are used to aid in the creation, modification, analysis or optimization of a design. The goal of these technologies is to improve the productivity and quality of the designer and improve the communication through the generated documents.
- **FEM:** Finite Element Method, numeric technique that is used to solve through approximations a problem described by differential equations with partial derivatives. The computations are reduced to a system of algebraic equations.
- **CFD:** Computational Fluid Dynamics, method that uses numerical analysis to solve and analyse fluid flow problems using computational resources. Workstations are used to perform the calculations required to simulate interactions between fluids and solids, defined by boundary conditions.
- **Mesh:** The Finite Element Method discretise the domain with the creation of the so-called mesh, made by finite elements that can be triangles or squares for a 2D domain, and tetrahedral and hexahedral elements for the 3D one, principally.
- **Air ducts:** Conduits or passages used on different applications as heating or ventilation. The fluid flow passes through its interior and arrives to the desired destiny. Possible pressure losses can create recirculation that must be eliminated to improve the flow efficiency.
- **Heat exchanger:** Also called radiator, it is used to transfer heat between two fields, which can be a solid and a fluid or two fluids. In the case of two fluids, a solid wall to prevent a mixing process may separate them, or they can be on direct contact. These components are used on space heating, air conditioning, refrigeration and other applications.

- **Tire:** Ring-shaped component that is surrounding the wheel's rim. It transfers the load of the car from the axle, through the wheel to the ground, providing traction on its contact with the road. Generally, the tyres are pneumatically inflated.
- **Hood:** Component of a car that covers the engine and allow access to its compartment for maintenance or repair scope. It may present air vents through which the flow from the heat exchanger exits to the exterior.
- **Bumper:** Part of the bodywork of a vehicle that has the function of prevent, limit or decrease the damage due to a collision at low velocity. Generally, this element has not the capacity to reduce the damage caused by high-velocity crashes.
- **Windshield:** Also called windscreen, it is the front window of a vehicle as a car, aircraft, bus, motorbike or tram. Two sheets of glass make the modern versions of this component with a plastic layer laminated between them.
- **Spoiler:** Also called wing, an aerodynamic element can be fixed or variable, used to obtain a high-pressure zone on a specific space. Generally, on a land vehicle, these elements help to increase the downforce. However, on an aircraft its function is the opposite. Car with a sportive design present this kind of component on different parts, named as side skirts, rear skirts, etc.
- **Turbulence:** On fluid dynamics, a turbulent flow is characterised by a high value of inertial forces, which cannot be dumped with viscous forces. The movement of its particles is then chaotic, following path that are not ordinated as in the laminar case.
- **Vortex:** In fluid dynamics, a vortex is a phenomenon that takes place on turbulent regime. The path of the particle revolves around an axis line, straight or curved. Vortices are created generally on low-pressure zones and may be eliminated or reduced in order to have an efficient flow on car aerodynamics.

II. MODELS

In order to do this project, it was necessary the knowledge of some general aspects related with the fluid mechanics and more precisely with the external aerodynamic of a vehicle. For this reason, in this part some concepts are defined, using for this the bibliography [14].

6. Physical model

In this part of the document, different concepts related with the theory of fluid mechanics are explained. More precisely the ones related with aerodynamics used in this project.

6.1. Properties of the fluid

The analysis of the behaviour of the air when it is in contact with an object requires the knowledge of some general properties of the fluid that are explained below.

6.1.1. Density

Density is a property defined as the amount of mass that is in a determined volume. In fluids, density can be different from one point to another. If we consider little sphere of volume ∂V centred in a specific point with a mass ∂m , the density of this point would be then:

$$\rho = \lim_{\partial V \rightarrow 0} \frac{\partial V}{\partial m} [kg/m^3] \quad (6-1)$$

In this project, external airflow of a car, the ideal gas formula has been used to know which density value to introduce in the simulations, the expression is:

Law of ideal gases:

$$p \cdot V = m \cdot R \cdot T \rightarrow \frac{m}{V} = \rho = \frac{p}{R \cdot T} \quad (6-2)$$

Where p is the pressure in Pascal, V is the volume in m^3 , m is the mass in kg, R is the constant of air with a value of $286.7 \text{ J}/(\text{kg} \cdot \text{K})$, T is the temperature in K and ρ is the density in kg/m^3 .

With standard conditions in pressure of 1 atmosphere (101325 Pa) and a temperature of $15 \text{ }^\circ\text{C}$ (288 K), the density of air is $1.225 \text{ kg}/m^3$, introduced value in all simulated computations.

6.1.2. Viscosity

Viscosity (μ) is the property of a fluid of resistance of tangential deformations and it influence in a direct way in the forces that it induces in an object in its interior. When a fluid has a very high viscosity, higher shear forces will affect the solid in comparison with a less viscous fluid.

Another parameter, called kinematic viscosity, is represented with the symbol ν . To compute it, the following expression is used:

$$\nu = \frac{\mu}{\rho} [m^2/s] \quad (6-3)$$

Where ν is the kinematic viscosity in m^2/s , μ is the viscosity or absolute viscosity in $\text{kg}/(\text{m} \cdot \text{s})$ and ρ is the density in kg/m^3 .

To compute the air viscosity in this case, the relation between this property and the temperature has been used through the Sutherland law:

Sutherland law:

$$\mu = \mu_0 \cdot \frac{T_0 + C_s}{T + C_s} \cdot \left(\frac{T}{T_0}\right)^{3/2} [kg/m \cdot s] \quad (6-4)$$

Where μ is the viscosity in $\text{kg}/(\text{m}\cdot\text{s})$, T is the temperature in K, μ_0 is the reference viscosity ($1.71\cdot 10^{-5} \text{ kg}/\text{m}\cdot\text{s}$) in the reference temperature T_0 (273 K) and C_s is the Sutherland constant in Kelvin, that is 120 K in the air case.

In the simulations of this project, with a supposed temperature of 15 °C, the viscosity value is $1.79\cdot 10^{-5} \text{ kg}/\text{m}\cdot\text{s}$.

6.1.3. Pressure

Pressure is a physical magnitude that related the force and the surface where it is applied. When a solid is in the interior of a fluid, several forces are applied perpendicularly to its faces due to the molecular movement of the particles of, for example, the air.

In the applied pressure, we can distinguish two different terms that together make the total value:

$$pressure_{TOTAL} = pressure_{STATIC} + pressure_{DYNAMIC} \quad (6-5)$$

Static pressure is the one generated with independence of its velocity or movement. This pressure acts homogeneously in all directions and perpendicularly. When a fluid is in repose the static pressure would be the same as the total one.

On the other hand, **dynamic pressure** depends on the velocity and fluid density and it is applied in the movement direction. Its expression is:

$$q = \frac{1}{2} \cdot \rho \cdot v^2 [Pa] \quad (6-6)$$

Being q the dynamic pressure in Pascal, ρ the density in kg/m^3 and v the fluid velocity in m/s .

6.1.4. Pressure coefficient

To create the different pressure contours of the obtained results the pressure coefficient (C_p) has been used. The reason behind this is the fact that this is a non-dimensional quantity, so it allows performing easy comparisons between different

conditions simulated or even between the results of this document and the ones of other projects.

This parameter permits to determine easily the deviation of the static pressure in an evaluated point with respect to the pressure of the free flux, far from the perturbations the solid is generating in the fluid. It is expressed in the following way:

$$c_p = \frac{p - p_\infty}{\frac{1}{2} \cdot \rho_\infty \cdot V_\infty^2} \quad (6-7)$$

Where C_p is the pressure coefficient, dimensionless quantity, p is the static pressure in the studied point, p_∞ the pressure of the free flux, ρ_∞ is the density of the fluid and V_∞ the velocity of the free flux, the same magnitude as the solid in the interior of the fluid, as we have a fixed car in the simulations.

If we apply the expression using the Bernoulli equation, considering incompressible fluid and no losses, we obtain:

$$c_p = 1 - \left(\frac{V}{V_\infty}\right)^2 \quad (6-8)$$

Where V is the velocity of the fluid in the evaluated point and V_∞ the free flux velocity.

Considering this, when we see a pressure contour like in figure 6.1, a negative C_p means that the fluid velocity in that point is higher than in the free flux, something that may be caused by the shape of the solid. A C_p value equal to zero means that both velocities are the same and a C_p value equal to 1 indicates zero velocity and maximum pressure, situations that occurs in the front part of the car.

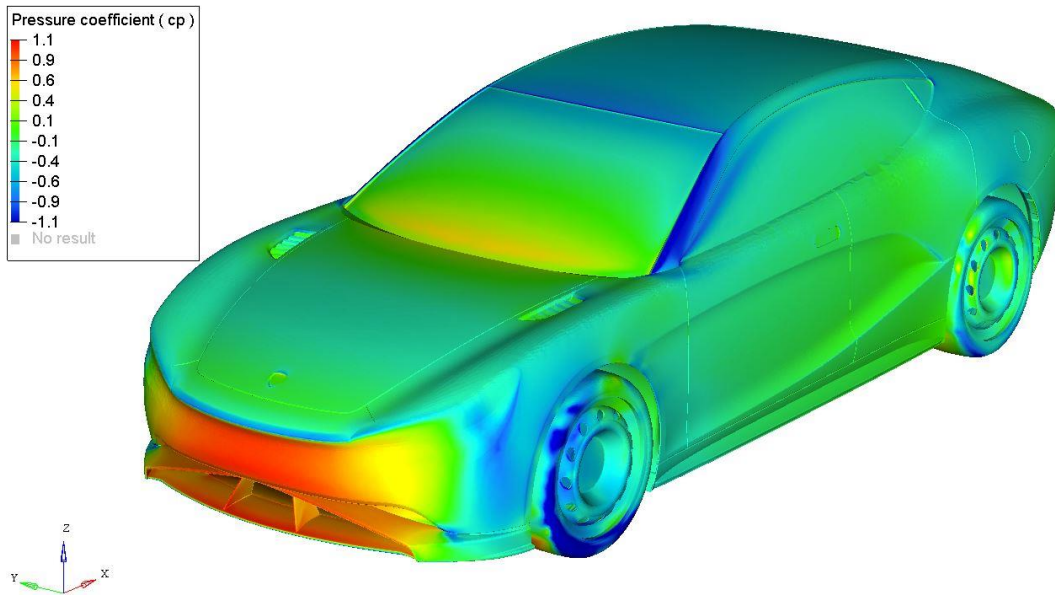


Figure 6.1 : Pressure coefficient contour example

6.2. Bernoulli's principle

Bernoulli principle is used to explain how the behaviour of the fluid with an energy balance is. The equation is applied an incompressible and no viscous fluids and the main conclusion that is extracted from it is that the total energy is always constant throughout the evaluated flow line.

$$p + \frac{1}{2} \cdot \rho \cdot v^2 + \rho \cdot g \cdot z = cte \quad (6-9)$$

Where p is the static pressure of the fluid, ρ is the density, V is the velocity magnitude, g is the value of the acceleration of gravity (9.81 m/s^2) and z is the height with respect to a reference.

If we consider a constant height through all the flow line, the third component, potential energy, can be simplified, and the expression is then:

$$p + \frac{1}{2} \cdot \rho \cdot v^2 = cte \quad (6-10)$$

First term corresponds with the static pressure and the second with the dynamic one, the sum of both is the total pressure, that remains constant. This expression

allows to correlate two important variables of the flux, pressure and velocity. If one of them increases, the other decreases to maintain the energy balance.

Since this expression is applied to non-viscous fluids, it is used to study the flux in the exterior of the boundary layer of the solid, where viscosity can be considered zero. This principle is important to understand how the forces are generated in a solid in contact with a fluid.

One possible example is the vertical force that a car experiments when it's moving. Due to the different velocities of the air in the upper and lower sides, different pressures take place as well, resulting in a force, that in the best case will be pointing to the ground.

6.3. Venturi effect

The so-called Venturi effect is the phenomenon in which a fluid that fluxes on a conduct decreases its pressure and increases its velocity when it passes through a smaller section on the duct. This is the general explanation, with a closed duct as it can be seen on the figure 6.2. If the increase of velocity is sufficiently high, the pressure might arrive to negative values, causing in the fluid of the second tube an aspiration phenomenon. This principle can be applied to a great variety of other applications, as in the wings of an aircraft or in the vehicle aerodynamic field, with the so-called ground effect. [15]

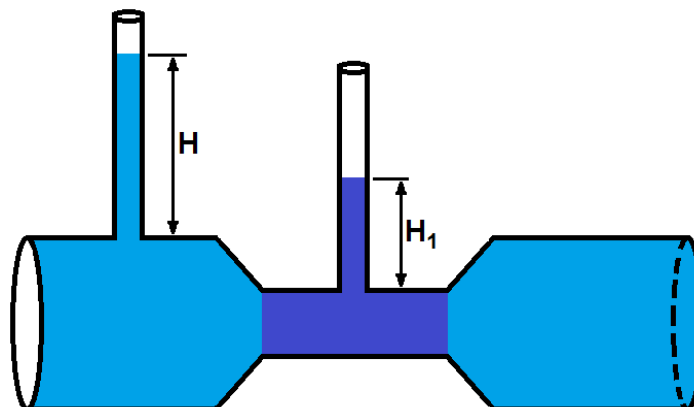


Figure 6.2 : Venturi effect basic scheme (16)

The ground effect takes place on the lower part of the cars because the air that flows between the bottom of the vehicle and the ground increases its velocity when this gap decreases. This generates a low-pressure zone on the lower surfaces of the car, that contributes to have a good grip of the car with the road, generally a positive phenomenon on vehicle dynamics. The advantage of this characteristic is the possibility of increase the downforce of the model without the inclusion of additional elements as wings, components that increase the drag force. This phenomenon has been widely analysed in the results of the project, simulating its change with two different ground inclinations of the car.

6.4. Reynolds number

Reynolds number is a useful parameter to determine the kind of fluid we have, it can be seen as the relation between inertial and viscous stresses, its expression is:

$$Re = \frac{\rho \cdot v \cdot L}{\mu} = \frac{\textit{inertial stresses}}{\textit{viscous stresses}} \quad (6-11)$$

Where Re is the Reynolds number (dimensionless), ρ and μ are the density and viscosity of the studied fluid, v is the flux velocity and L is the characteristic length of the object.

When Re has a low value, all perturbations are dumped but when it is increased inertial forces have greater importance and a turbulent flow is reached. This type of fluids, with random movements, are more difficult to describe with models.

In this project, the studied case can be considered mainly laminar, but there's always a wake zone with turbulence caused by the flow separation in the rear part of the car. This affects negatively the drag coefficient importantly so new designs always try to reduce this zone.

6.5. Aerodynamic forces

In this part, the principal aerodynamic forces that affect a solid in contact with a fluid are described.

6.5.1. Drag force

A body in contact with a fluid experiment a force in a direction parallel to the flux and opposite to the body movement. This force is the same with independence of which the fluid or the solid is moving. To study this force is of great importance in the transport industry, where the fluid is generally air, since it affects directly in the fuel consumption or in the maximum velocities the vehicle can reach.

The drag force can be divided in two components: drag due to pressure, that depends directly on the shape of the object in contact with the fluid, and the drag due to friction, generated by shear stresses, highly connected with the viscosity of the fluid.

In order to understand the pressure component, it is necessary to study the disturbance the object cause on the fluid because of its shape, generating a wake zone. The flux tries to follow the shape of the solid but at a certain point a separation occurs, and a turbulent wake zone is created. The pressure in the rear part is then lower in comparison with the front part, this creates a force that is in the opposite direction with respect to the movement.

The goal of the design is to delay as much as possible the separation phenomena, using aerodynamic shapes, achieving to lower the drag force.

On the other hand, the friction component is created by the shear stresses acting in the object projected to the movement direction. In the boundary layer in contact with the solid, an energy dissipation that make the fluid slower is produced, this helps the separation of the flow and the consequent wake zone.

Generally, the pressure component in a car is the most important due to the typical shapes that these vehicles have. The friction component is usually neglected, but the higher is the length of the vehicle, the more important the friction will be. In all cases, the pressure component is always the one that contributes the most.

The expression of the drag force is the following:

$$F_D = \frac{1}{2} \cdot \rho \cdot V^2 \cdot C_D \cdot A \text{ [N]} \quad (6-12)$$

Being F_D the drag force, ρ the fluid density, v the velocity, C_D the drag coefficient and A the frontal area of the studied object. As it was explained before, it's important to consider the drag when the vehicle is designed, nowadays multiple experiments and improvements try to find the most efficient shapes and components in order to reduce the power required to move the vehicle.

6.5.2. Lift force

The lift force affects a body inside a fluid in perpendicular direction to the movement. This component is very important in the study of aeronautic transport, as it is the force opposite to the weight and responsible of allowing the flight.

In land transport, its study is related with the grip the vehicle has with the road, being directly connected with security.

In a real case, this force depends almost exclusively on the distribution of pressure around the vehicle, therefore, its shape will have great influence. As we saw in the Bernoulli principle, the pressure decreases with the velocity to the power of two, this means that the parts where the flux is faster will have lower pressure and vice versa.

Due to the shape of vehicles, generally the flux must do more distance in the upper part in comparison with the lower one, this creates lower pressure in this part and a positive lift force in the car that tries to lift it. Sportive cars are designed in order to have this force in direction to the ground, improving the grip with the road. This so-called downforce increases the curve behaviour of the vehicle.

The expression the lift force is the following:

$$F_L = \frac{1}{2} \cdot \rho \cdot V^2 \cdot C_L \cdot A \text{ [N]} \quad (6-13)$$

Where F_L is the lift force, ρ is the fluid density, v is the velocity, C_L is the lift coefficient and A is the reference area of the body. As it happens with the drag, it exists a clear dependence with the object size and its orientation with respect to the flux direction.

6.5.3. Lateral force

Together with the drag and lift, a lateral force can affect a body in the interior of a fluid. This is not usually studied because the vehicle is symmetric with respect to the middle plane and due to this the magnitude of the lateral force is in theory zero.

In some cases, as when more than one car is simulated, a curve situation is studied, or a wind force is introduced in the experiment, this component of the aerodynamic forces can be considered.

In the figure 6.3, the principal aerodynamic forces are represented, acting in the car model studied in this project. The point where they are applied is the centre of pressure.

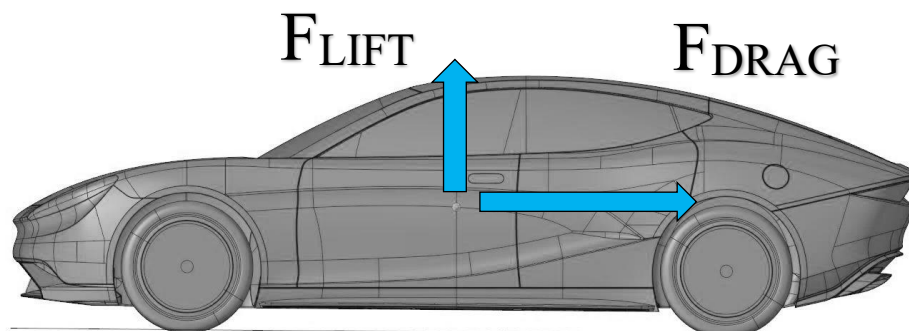


Figure 6.3 : Principal aerodynamic forces acting on a car

6.6. Aerodynamic coefficients

6.6.1. Drag coefficient

Drag coefficient is a dimensionless parameter used to quantify what is the resistance acting in a moving object in the interior of a fluid. As it has no units, is a useful magnitude to compare various cases and extract easier conclusions.

This coefficient is not constant with a certain geometry, as is directly dependent on the Reynolds number. The type of fluid, laminar or turbulent, influence in the separation point of the boundary layer.

Generally, due to the high difficulty of calculating the frontal area of a car, the so-called Resistance Factor (RF) is used, defined as the product of the drag coefficient and the frontal area ($C_D \cdot A$). This is the obtained value in the experiments and where the design affects directly.

6.6.2. Lift coefficient

This dimensionless number, analogous to the drag coefficient, quantify the lift that a body feels in a fluid, that can be positive or negative depending on the direction of the force perpendicular to the flux.

This parameter is relevant when plane wings are studied, where its variation with the angle of attack of the flux is determined.

6.6.3. Moment coefficient

As in the case of C_D and C_L , the moment coefficient (C_M) can be useful to understand how the forces can affect the equilibrium of the vehicle. Its value depends on the axis used for the computation and its position with respect to the body. In this project is especially interesting to determine the moment around the y axis (horizontal and perpendicular to the car movement), as it gives information on how the rear part of the car is lifting at high velocities, something that is negative for the safety and good performance of the car.

6.6.4. Aerodynamic efficiency

To compute the aerodynamic efficiency of a certain geometry, the relation C_L/C_D is generally used. As this value grows it means that the downforce (positive) is increasing and the drag decreasing, which is clearly an improvement in the performance of the studied model.

6.7. Boundary layer

The boundary layer is the part of the fluid affected by the presence of an object on its interior. This zone exists due to the viscosity of the fluid and it will be higher if this fluid is more viscous. In the points in contact with the solid walls the velocity of the fluid is considered zero and at a certain distance, equal to the thickness of the boundary layer, its magnitude is equal to $0.99U$, being U the velocity of the free flux, at a point situated far from the object and not affected by it.

In the figure 6.4 is shown the shape of the boundary layer in a horizontal surface.

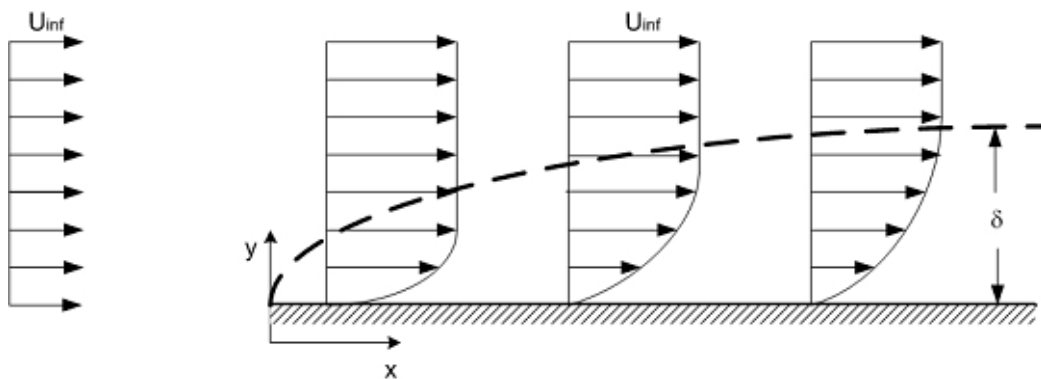


Figure 6.4 : Boundary layer in a horizontal surface

The study of the boundary layer is important to understand the aerodynamic forces in an object in the interior of a fluid. As we saw in the Bernoulli principle, the velocity variation in the fluid create pressure differences that are the responsible of the forces like drag and lift.

In general, it does not have a big numerical effect in land transport as the air viscosity is very low, but its introduction is needed in order to simulate in a correct way the flux near the walls.

When the vehicle is very long in the movement direction, as in the case of a train, the effect of the boundary layer increase as the region affected by the solid is more important.

6.8. Parameter y-plus

In order to study accurately the viscous effects near the walls of the object the spatial discretization in these zones must be specially designed. The y plus parameter is used to see if the cells near the walls are correctly sized, its expression is the following:

$$y^+ = \frac{y \cdot u_T}{\nu} ; \quad u_T = \sqrt{\frac{\tau_w}{\rho}} \quad (6-14)$$

Where y is the distance to the wall, u_t the friction velocity, ν the kinematic viscosity, ρ the density and τ_w the wall shear stress.

The important thing is to have the centroid of the nearest cell to the wall at a certain distance in order to take into account the viscous effects of the fluid. As we see, this distance depends on various factors as the type of fluid and its velocity.

When the studied case increases the velocity of the free stream, the distance to the wall of the first element have to decrease in order to maintain a certain y-plus parameter. Curve shapes, that produce an acceleration on the flow, also have to be taken into account during this computation, as in these zones the distance of the first centroid should be lower to maintain the same y-plus.

In the results part of this document, some contours of the y-plus parameter on the surfaces of the car and ground are shown, to be sure we are under admissible limits. Next figure 6.5 show one of these contours, as we see, the parameter doesn't exceed the value of 100 on the car's surfaces and on the close ground. This is achieved

with the creation of a controlled boundary layer on these parts, as it will be explained later on the document.

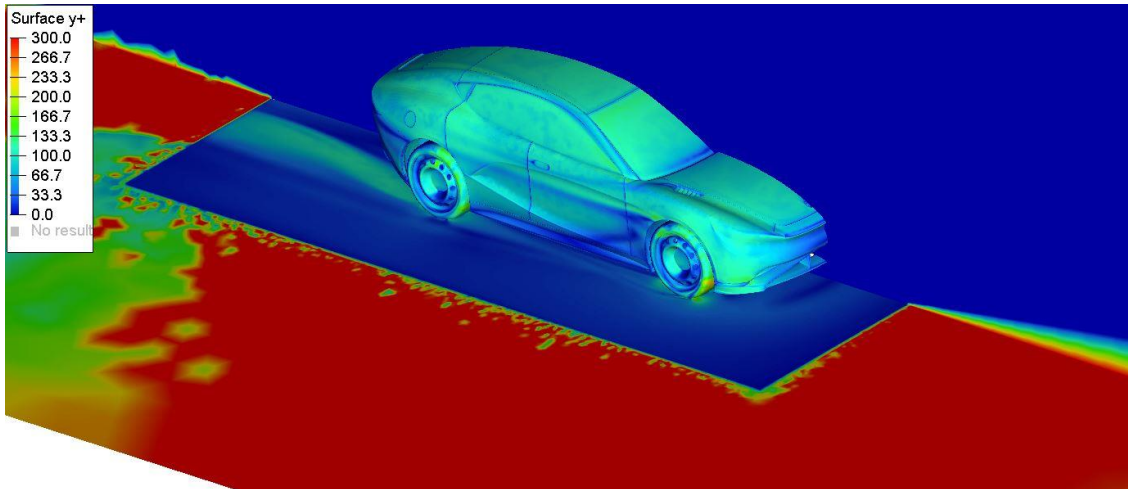


Figure 6.5 : Y-plus contour result

6.9. Wake and flow separation

Due to energy dissipation, the fluid decelerates when it's moving near the object's surface. This causes a separation point after a certain distance between the solid and the fluid.

The generated zone, the so-called wake, has low pressure due to the recirculating flux. The size of this region depends highly on the shape of the solid, aerodynamic designs help the fluid to follow the object's surfaces easier, delaying the separation point and reducing the wake zone size.

The next image in the figure 6.6 is an example of this effect, in the car studied in this project. The contour represents the velocity of the flux, which decelerates in the rear part of the vehicle and even recirculates. The separation is easily viewed in this image with the blue colour.

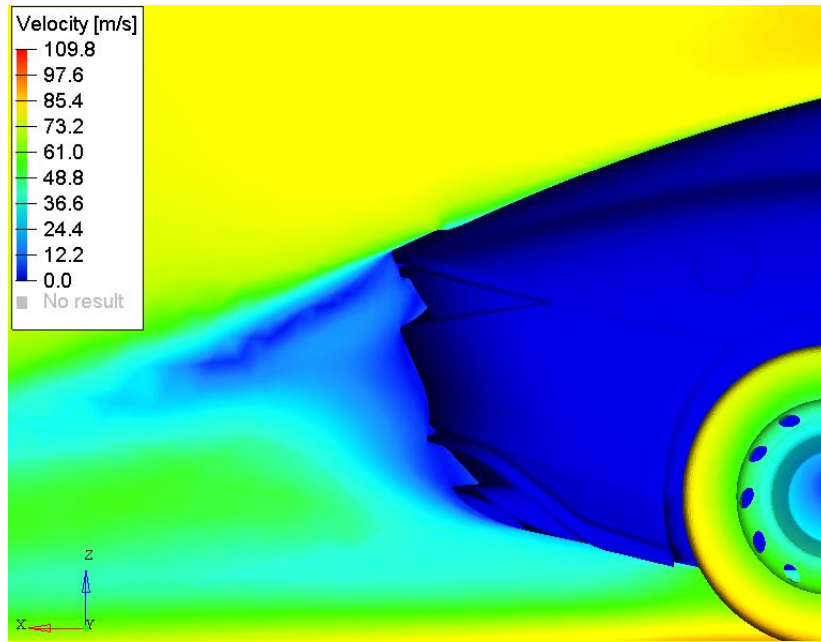


Figure 6.6 : Example of the wake zone in a car

6.10. Darcy and Forchheimer law

In order to simulate the interior flux through the radiator of the vehicle, a specific strategy have to be followed to be able to model the same effects that this component has in the air. A real heat exchanger of a car forces the fluid to flow on a certain direction, being very difficult for the particles to move on the other two. In addition, the pressure of the fluid decreases while it is on the interior, due to the physical barrier it finds on its movement. All this is modelled as a region on the domain with a defined permeability, coincident with the volume the real heat exchanger occupies on the vehicle.

The configuration of the solvers, AcuSolve and OpenFOAM, is similar and it is based on the same law, introducing two parameters: Darcy and Forchheimer coefficients. On the methodology part of this document the procedure is explained but on this chapter the definition of this coefficients, its influence on the solvers and the expressions and curve used to compute them are shown. [17]

The addition of a porous media on the domain modify the momentum equation on that volume as follows:

$$\frac{\rho}{\phi} \frac{\partial u}{\partial t} + \rho u \cdot \nabla u + \nabla p + Rf = \nabla \cdot \tau + \rho b \quad (6-15)$$

Where ρ is the density of the fluid, ϕ the porosity, u the velocity vector and f the porous media contribution.

This additional term can be expressed as follows:

$$f_i = \left(\frac{C_{DARCY} u}{k_i} + \frac{C_{FORCH} \rho}{\sqrt{k_i}} |u| \right) u_i$$

Where the term can be divided on its three component in space f_x , f_y and f_z . In general, the fluid is going to flow on the x-direction (we substitute the index i by x). As it was explained before, the air loses pressure while it's on the radiator's interior and this phenomenon can be expressed with the two coefficients as:

$$\frac{\nabla P}{L} = \left(\frac{C_{DARCY} u}{k_x} + \frac{C_{FORCH} \rho}{\sqrt{k_x}} |u| \right) u_x$$

The expression can be simplified and written as a curve formula, with the two usual terms A and B depending on the wanted coefficients.

$$\nabla P = A u + B u^2$$

$$A = \frac{C_{DARCY} u L}{k_x} \quad B = \frac{C_{FORCH} \rho L}{\sqrt{k_x}}$$

Finally, this expression is compared with an experimental curve of the real heat exchanger we want to model in our study, obtaining the terms A and B of the previous formula and computing the two coefficients. To do this we have to know that L is the length on the current direction (x), μ the dynamic viscosity of the fluid and k_x the permeability on the x -direction, which is equal to 1. On the other two directions in space its value is equal to 0.001, to model the resistance the radiator imposes.

The following figure 6.7 shows the experimental curve used on this project. The final expressions of the Darcy and Forchheimer coefficients are also written. The numerical values are shown on the numerical methodology part, as well as the procedure to introduce the parameters in order to configurate the porous zone on both solvers.

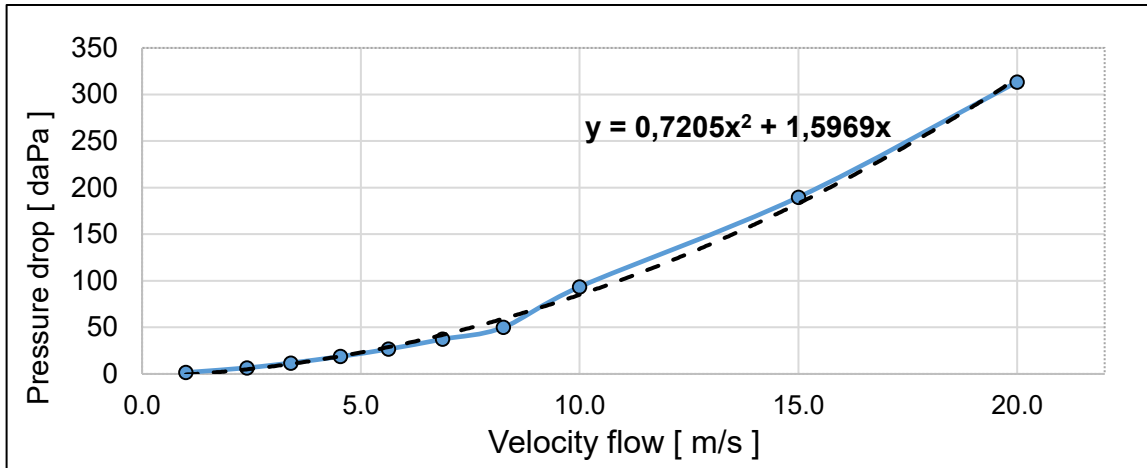


Figure 6.7 : Experimental curve of the heat exchanger

$$C_{DARCY} = \frac{A k_x}{\mu L} \quad C_{FORCH} = \frac{B \sqrt{k_x}}{\rho L}$$

7. CFD model

In this part of the document, the general concepts that affect the CFD simulations are explained, and specifically the ones related with the software used in this project, described in the following chapters.

After a first review of the general theory related with the fluid dynamics, other concepts, more specific of this project were explained, like the turbulent model used for the simulations. To write this part of the memory, some bibliography was looked for the fluid theory [14].

The CFD, Computer Fluid Dynamics, is a part of fluid dynamics related and dedicated to the study and analysis of the fluxes and their interaction with solid objects. To know how will be the behaviour of the fluid in a specific situation some

dedicated programs can be used. This software, using a model, solve the equations that govern the flux movement and properties.

CFD studies are relatively young because the first practical applications were carried out around the middle 20th century. In the last decades, with the great technology advances and the improvement of the computer performance, the CFD simulations have had a great impulse and nowadays they are accessible to a great number of users, much more than in the past.

In the actual market this type of studies are highly used by firm from many different sectors, like for fabrication technologies. In the transport industry they allow to know how the air-vehicle interaction is and permit to optimize the design in order to achieve specifications of fuel consumption or security before to reach more advanced steps of the construction process.

7.1. Fluid governing equations

The basic equations that model the fluid behaviour and that have to be solved when its behaviour is simulated are the continuity equation, the moment or Navier-Stokes equation and the energy equation. Generally, to name them all, the term Navier-Stokes equations is used.

Although the complete process is not described here, in order to obtain these expressions, the Transport Reynolds Theorem was used, useful to know the property variations of the fluid in the studied control volume.

This theorem has the following expression:

$$\frac{d}{dt} \int_{FV} \varphi \cdot dV = \frac{d}{dt} \int_{CV} \varphi \cdot dV + \oint_{CS} \varphi \cdot (\vec{V} \cdot \vec{n}) \cdot dS \quad (7-1)$$

Being φ the analysed fluid property. The first term corresponds with the magnitude its magnitude variation related with a fluid volume, closed system made always by the same particles. The second one is the same variation but in this case in

an opened fluid volume, that allow the mass transport through the limits. Finally, the third one is the convective flux of the variable that enters or exits the control volume.

7.1.1. Continuity equation

The continuity equation explains the mass conservation law, which establishes that in all systems the mass is not created nor destroyed, it's conserved. This property in a closed volume cannot change over time. Its expression is the following:

$$\frac{d}{dt} \int_{FV} \rho \cdot dV = \frac{d}{dt} \int_{CV} \rho \cdot dV + \oint_{CS} \rho \cdot (\vec{V} \cdot \vec{n}) \cdot dS = 0 \quad (7-2)$$

Being ρ the fluid density and V the volume of the studied region.

7.1.2. Momentum equation

In order to study this principle, it is necessary to analyse the second Newton Law:

$$\sum F = m \cdot \frac{dV}{dt} = \frac{d(m \cdot V)}{dt} \quad (7-3)$$

$$\text{momentum} = m \cdot V \quad (7-4)$$

If this expression is applied to the studied fluid volume:

$$\begin{aligned} \frac{d}{dt} \int_{CV} \rho \cdot \vec{v} \cdot dV + \frac{d}{dt} \int_{CS} \rho \cdot \vec{v} \cdot (\vec{v} \cdot \vec{n}) \cdot dS \\ = \int_{CS} \vec{\tau} \cdot \vec{n} \cdot dS + \int_{CV} \rho \cdot \vec{f}_m \cdot dV \end{aligned} \quad (7-5)$$

Where the third term refers to the superficial forces and the fourth one to the volumetric forces applied on the control volume.

This expression establish the second Newton law applied to fluids: The momentum variation of a fluid volume is equal to the sum of forces acting on it.

7.1.3. Energy equation

The first law of thermodynamics establishes that the total energy variation of a system (kinetic + intern) is equal to the work divided by the time (power) of the external forces, plus the received heat from the exterior.

$$\Delta E = \Delta Q + \Delta W \quad (7-6)$$

This expression applied to a fluid has the following form:

$$\begin{aligned} \frac{d}{dt} \int_{FV} \left(e + \frac{v^2}{2} \right) \cdot dV &= \int_{CS} \vec{v} \cdot (\vec{\tau} \cdot \vec{n}) \cdot dV \\ + \int_{CV} \vec{v} \cdot \rho \cdot \vec{f}_m \cdot dV &+ \int_{CV} (Q_r + Q_q) \cdot dV - \int_{CS} \vec{q} \cdot \vec{n} \cdot dS \end{aligned} \quad (7-7)$$

Being $(e + v^2/2)$ the total energy of the system, Q_r the received heat by radiation, Q_q the received heat by a chemical reaction and $q \cdot n$ the received heat in the system by thermal conduction.

7.2. Spatial discretization

In order to do the computations and simulate the fluid behaviour, the studied domain has to be spatially discretised. In this process the volume is divided in a finite number of regions, each of them has a point or node where all properties are assigned, like velocity, pressure, density or temperature.

There are principally three methods of discretization: finite differences, finite volumes and finite elements.

All methods, that need a previous creation of the geometry discretization or the so-called mesh, transform the initial differential system of equations in an algebraic problem, that will be solved by the used program.

The generated mesh in the case of this project was created with the software HyperMesh, that uses the finite element method. This procedure is known by its flexibility and it is accurate for complex geometries, like the one of this project.

After the creation of the discretised domain, it is compulsory to perform some checks in order to be sure our mesh satisfy the minimum requirements to be simulated. If the quality is not acceptable for the solver, the simulation cannot reach stability conditions and the time loss is then greater. Generally, the mesh checks focus on the element quality, for which exist some useful parameters as the 'skewness', 'warpage', 'aspect ratio' or the now explained 'jacobian'.

7.2.1. Jacobian parameter

The Jacobian ratio measures the deviation of a specific element with respect to an ideally shaped reference one. When this parameter is equal to 1, the element has a perfect shape. This value ranges from -1 to 1, the higher the distortion of the volume, the nearer it will be to 0. A Jacobian value of less than zero represents a concave element, which most solvers do not allow.

The ideal shape for the element depends on its type. The check process is performed mapping the ideal shape in parametric coordinates onto the current studied element in global coordinates. As an example, the parametric coordinates of an ideal quad element are (-1,-1), (1,-1), (1,1) and (-1,1).

The following figure 7.1, taken from the Altair student guide of element quality and checks, shows in a general form tria elements with different qualities. This type of element are the ones used in this project for the 2D mesh.

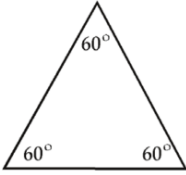
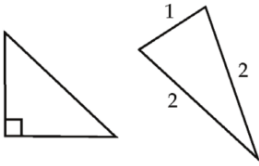
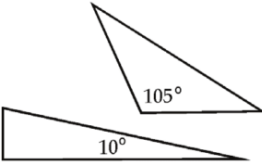
BEST	OK	VERY POOR
		

Figure 7.1 : Element quality examples [18]

7.3. Turbulent models

Previous equations allow us to study the fluxes in an easy way when they have laminar behaviour or zero viscosity. But when we try to simulate turbulent fluxes it is necessary to use models in order to solve the three-dimensional and chaotic movements that are characteristic of these fluxes.

The principal turbulent models can be seen in the figure 7.2, in this part of the document the turbulent model used in the project is explained with more detailed, the so-called *Spallart Allmaras*.

The DNS method (*Direct Numerical Simulation*) can be considered not as a model because with it all the Navier-Stokes equations of the fluid are solved. This method cannot be applied in many applications due to the high requirements of computer power and time.

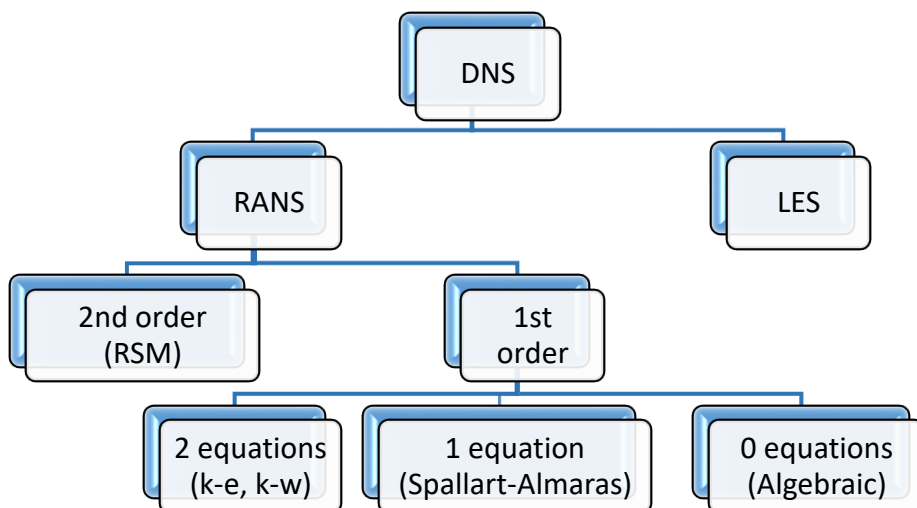


Figure 7.2 : Principal turbulent models scheme

On the other hand, LES method (*Large Eddy Simulation*) is a simpler alternative compared with the previous one where with a filtering method, big scale effects are solved while the little ones are approximated using models, to do this, different alternatives can be used.

RANS methods (*Reynolds Averaged Navier Stokes*) use the Reynolds average to divide the magnitude of a property in two values, the average and the variable. With this the Navier-Stokes equations change, and the system has an additional element, the turbulent viscosity. Depending on the strategy to model this element the different alternatives are obtained.

The most used hypothesis is *Boussinesq* (first order), based on the dimensional analysis with a lower computational cost than the other alternative, the RSM (*Reynolds Stress Model*). This model assumes the turbulence as isotropic and may not be accurate in some specific cases. The different models that use the *Boussinesq* hypothesis differ in the number of additional equations necessary to solve the system of equations.

One of the most used methods is the k-epsilon, solving two transport equations in order to compute the turbulent viscosity. This model is robust, cheap and with a good precision for a great variety of cases. Due to this, it is one of the most used methods, especially for external aerodynamics. One of its problems is that it is too diffusive, and it is not accurate enough in fluxes with low Reynolds number and with separation zones. Some modifications can solve this, the one called 'Realizable' improve the predictions of the standard model and the calculus when the flux is separated.

In the case of this project, the k-epsilon model was used in some simply and not detailed cases but for the definitive simulations, the chosen method is the *Spalart Allmaras*. On the next part, this decision will be explained, together with a general definition and characteristics of the model.

7.4. Spalart Allmaras turbulent model

Spalart Allmaras model was designed specifically for aerospace applications and it is gaining popularity as it shows good results in a great variety of situations. Its flexibility and robustness when the boundary layer is subjected to adverse pressure

gradients is desirable in the case of this project. It represents a good one equation turbulence model decision for aerodynamic flows. [19]

The model adds one transport equation to the original system in order to solve the viscosity-like variable ν , this is usually referred as the Spalart-Allmaras variable. The eddy viscosity term is computed in order to ignore the small-scale vortex (also eddies), just calculating the large-ones. The additional conservation equation contains convective and diffusive transport terms and expressions for the production and dissipation of the eddy viscosity variable.

$$\frac{\partial}{\partial t}(\rho\tilde{\nu}) + \frac{\partial}{\partial x_i}(\rho\tilde{\nu}u_i) = G_\nu + \frac{1}{\sigma_{\tilde{\nu}}}\left[\frac{\partial}{\partial x_i}\left\{(\mu + \rho\tilde{\nu})\frac{\partial\tilde{\nu}}{\partial x_i}\right\} + C_{b2}\rho\left(\frac{\partial\tilde{\nu}}{\partial x_i}\right)^2\right] - Y_\nu + S_{\tilde{\nu}}$$

Where G_ν is the turbulent viscosity production term and Y_ν the destruction term. This equation allows to determine $\tilde{\nu}$ for the computation of the turbulent viscosity μ_t , which is for interest for us, from:

$$\mu_t = \rho\tilde{\nu}f_{\nu1}$$

On the results part of this document, eddy viscosity contours are shown as it is a good indicator of the zones of the domain where the turbulence is dominant, something that obviously occurs on the rear part of the car and also on other recirculating zones.

III. NUMERICAL METHODOLOGY

This part of the document is dedicated to explaining what was the followed procedure in order to study the aerodynamic of the electric car, the details that were simulated and the used software.

To obtain the required results the steps were the following, as it is usual for this type of CFD studies:



After a first learning period, where the different used programs were tested with simple cases in order to be familiar with them, the first geometry of the electric car arrived.

The first simulations were simple, as the model was in the first design steps, and progressively the geometry was more and more complex until the definitive one, with the air ducts in the front part, the final wheels and other general details. With this geometry, the simulations were performed, at two different velocities as it is explained later, 160 and 270 km/h, and the obtained results were analysed.

After this, and in continuous communication with the client, some modifications have been made in order to improve the equilibrium of the car avoiding increasing the drag coefficient.

8. Geometry

The geometry of the car arrived directly from the client, that wanted an analysis of the external aerodynamics of its model. There were different phases because the received files were not complete from the beginning, but more and more detailed while the design of the car was being completed. The different received geometries can be resumed in the following points:

- First geometry of the external parts of the car – October first week
- A more detailed version in the door limits and lights – October third week
- Geometry of the air ducts, radiator and detailed wheels – November third week
- Little rear spoiler as a first modification – December second week

The figures 8.1, 8.2 and 8.3 show these different received geometries, that correspond with the base model of the car, the details added in order to arrive to the definitive case for the simulations and also the files corresponding with the different modification that were also simulated during the project, as the added rear spoiler.

The first of these images shows the standard received geometry. The wheels that we can see were removed and substituted by more detailed tires, to be nearer to real conditions. These new wheels can be seen on the figure 8.4, they are not the ones the final car has, as the definitive ones were not available during the simulation period.

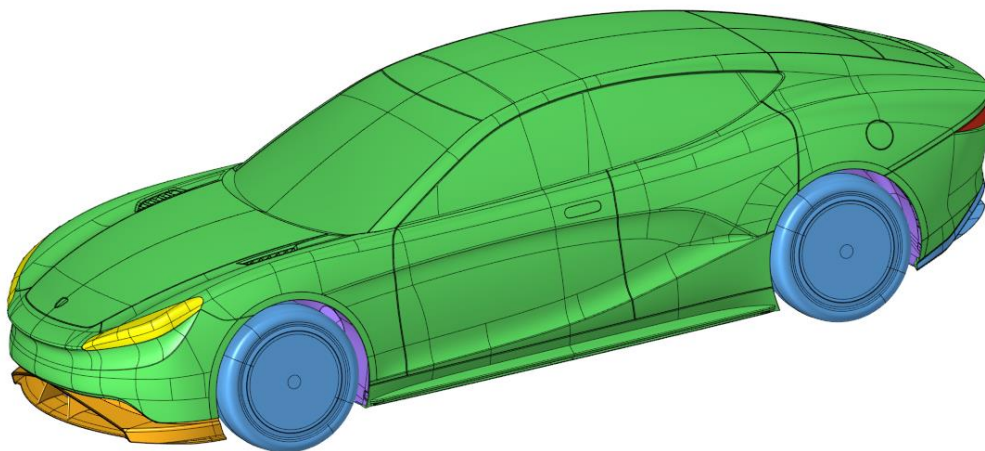


Figure 8.1 : General view of the received geometry

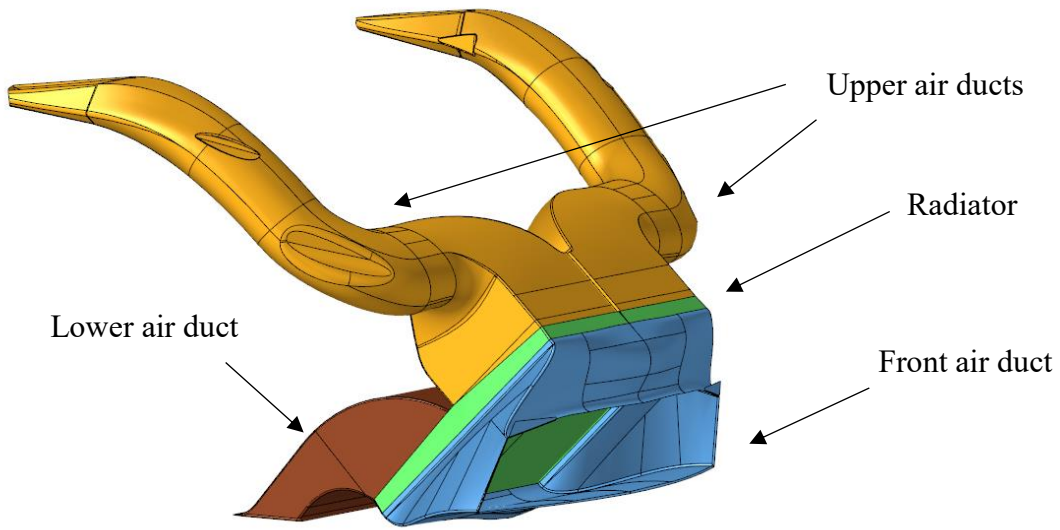


Figure 8.2 : Geometry of the interior ducts and heat exchanger

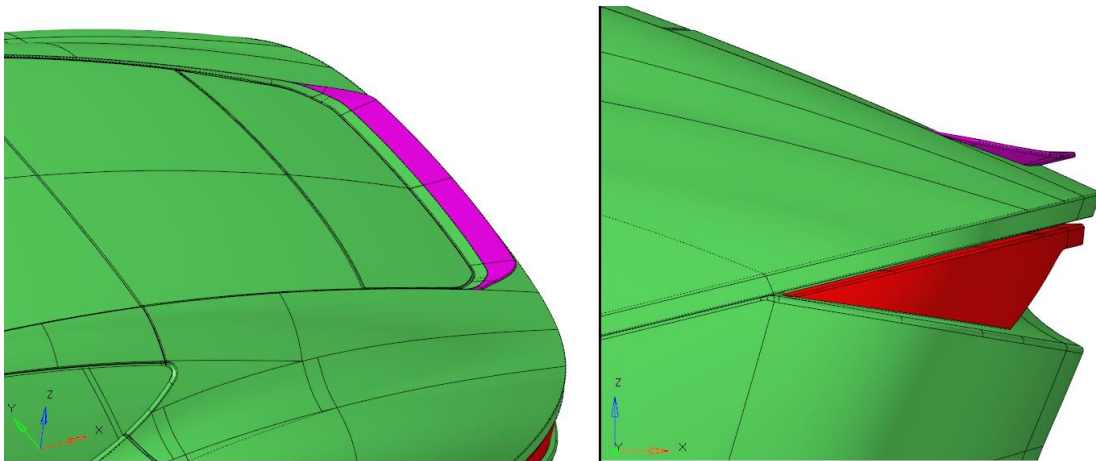


Figure 8.3 : Geometry of the added rear spoiler

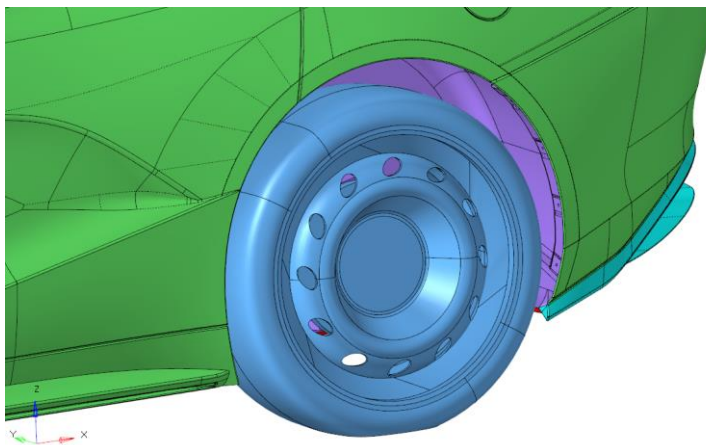


Figure 8.4 : Detail of the simulated wheels

The first simulations, with simpler shapes, were carried out in order to see what were the issues that could be found and to avoid future errors. After the arrival of the air ducts, radiator and final wheels the simulations were taken into consideration for the final results, due to the enough amount of details that made the geometry to be considered as definitive.

In all the received files, several steps were necessary in order to prepare the geometry to be simulated in a CFD environment. This procedure, as well as the spatial discretization of the domain, was performed in the software HyperMesh. The images below, shown in order to make clearer the followed process of cleaning the geometry, correspond to the base case of the car, with all the details and before the proposed modifications.

Basically, the necessary operations were to delete all the surfaces that were not part of the external skin of the car, made by the surfaces in direct contact with the air. Here we also consider the internal element as the air ducts and heat exchanger. After this important step, the surfaces that remained were joined, trying to conserve all the details that the real car have, like the joints of the doors and body of the car or all the little shapes of the bottom part of the model. During these operations it is important to think in advance and make the correct decision in order to have a good quality geometry for the mesh generation step. In order to show this geometry preparation, the figures 8.5, 8.6 and 8.7 are shown. In these images we can see the change on the air ducts and radiator geometries, but the process is equivalent on all the car's surfaces.

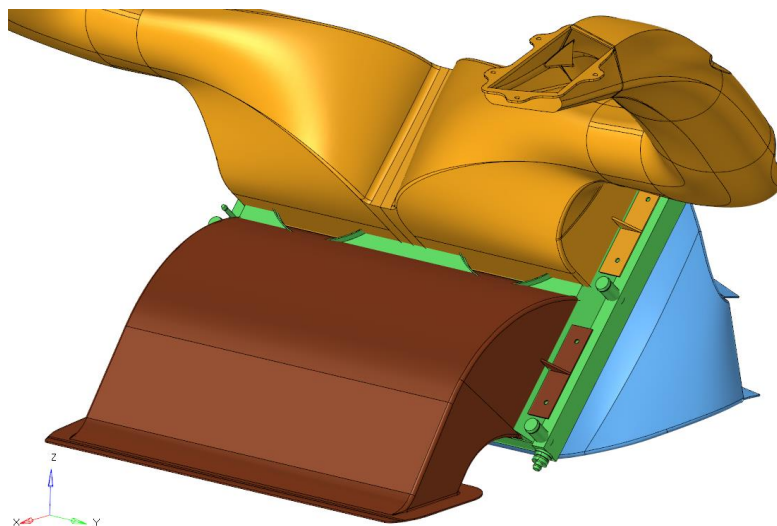


Figure 8.5 : Cleaning process, first step

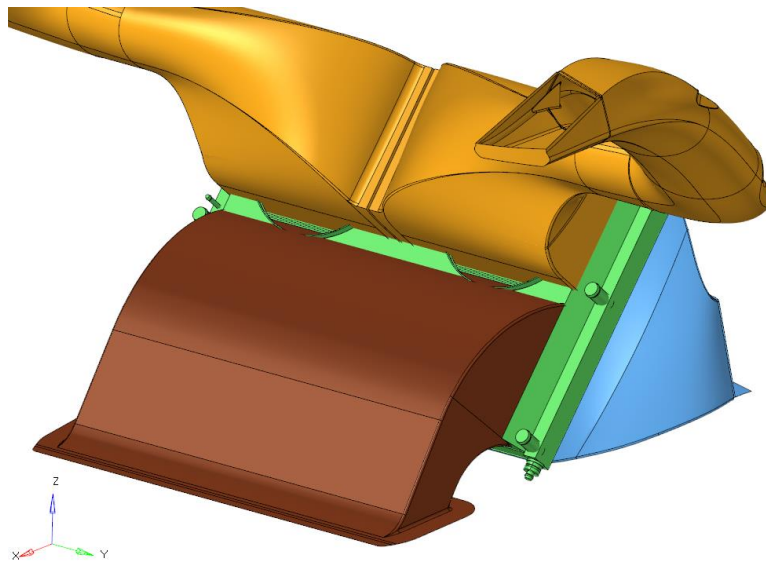


Figure 8.6 : Cleaning process, second step

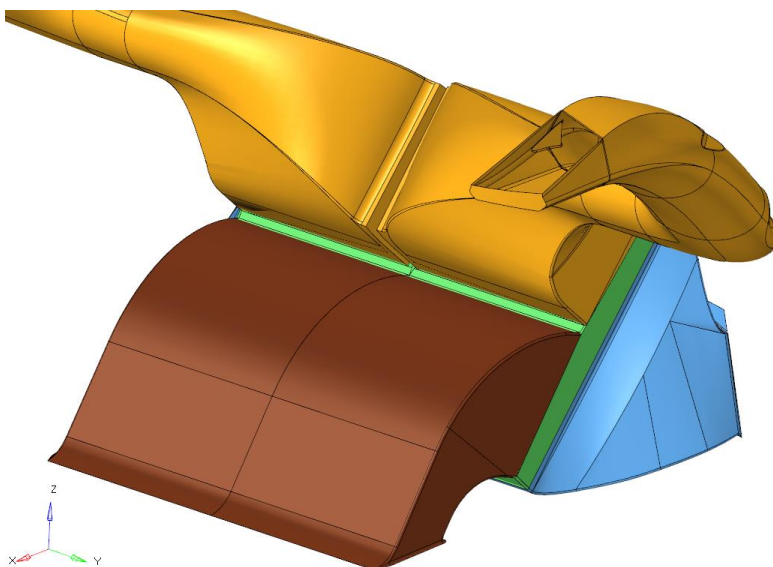


Figure 8.7 : Cleaning process, third step

Once the car was finished, the geometry of the wind tunnel, where the air is flowing during the simulation was created. An extract operation was later done in order to have an obstacle with the shape of the car in the wind tunnel, this is the general procedure that characterise this type of CFD simulations. As we can see in the figure 8.8, with the final geometry before the discretization, only one half of the domain is created, due to the symmetry we have in the case. The size of the domain where the air will be simulated is chosen considering the results that have to be

extracted from the simulation. Therefore, in the rear part of the vehicle the distance is greater, in order to be able to see the wake zone, very important in this type of studies. It is important also to have an offset in the front part, to be sure that the flow arrives without any perturbation to the car. The table 8.1 shows the measures of the domain, as a rule, it is recommended to have a distance equal to 1.5 car's length to the front and top parts and 3 times to the rear one.

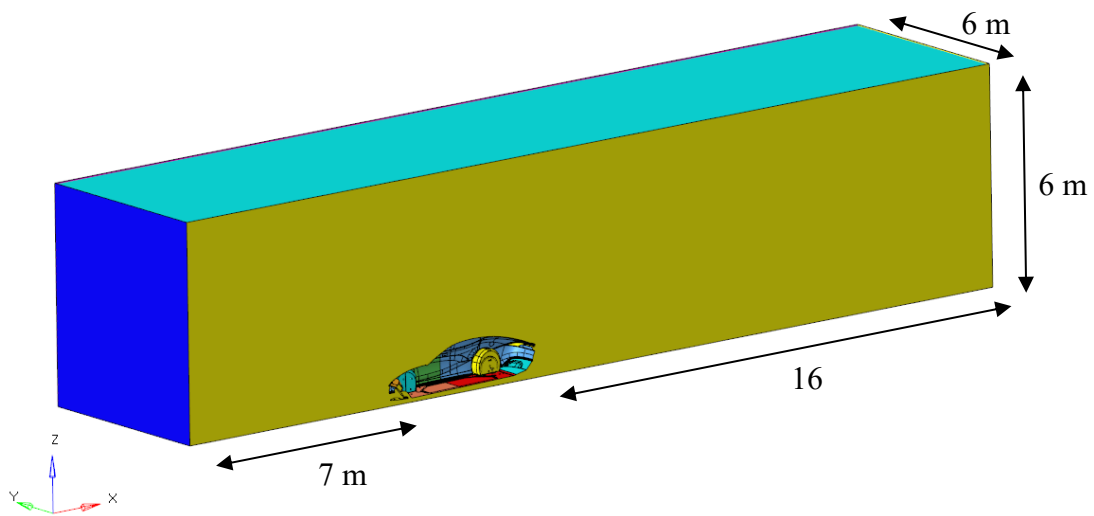


Figure 8.8 : General measures of the domain

Length	28 m
	7 m to front plane
	16 m to rear plane
Width	6 m
Height	6 m

Table 8.1 : Measures of the wind tunnel

All this process has the goal to obtain only the surfaces that are in direct contact with the air, the ones that are interesting for these type of simulations, including the wind tunnel. The geometry at this point correspond to a closed solid, in its interior is later created a three-dimensional mesh that will correspond to the studied fluid, in this case the air.

In the following table 8.2, the general measures of the studied model are shown. This data is important in order to create the air domain and also for the aerodynamic coefficient computation and the wheel's rotation velocity.

Length	5,11 m	Distance between wheels	3,04 m
Witdh	1,95 m		
Height	1,42 m	Geometry radius wheels	0,37 m
Frontal area	2,42 m ²		
Center of pressure coordinates		(1.464 , 0 , 0.084068)	

Table 8.2 : measures of the car model

The frontal area parameter, as it was explained, is a vital parameter that we need to be sure it is computed accurately. In the case of this project, the Virtual Wind Tunnel software of Altair has been used. This program has a tool that allow to get this value, the geometry has been imported from Hypermesh with this purpose. Virtual Wind Tunnel can be also used to perform the whole simulation, being a very user-friendly program. The truth is that AcuSolve, the chosen CFD solver, is more powerful and advisable generally.

The point used to divide the geometry of the car in order to obtain two halves is the centre of pressure. This allow to get the lift coefficient for the two divisions, useful to understand the balance of the car. The coordinates of this point were directly obtained from the client, constructor of the vehicle. We are only interested on the x-coordinate, as it is the one that serves to divide the car.

In order to compute the wheel's rotation velocity, parameter to introduce on the solver configuration, the distance from their centre to the ground is needed. This magnitude is not the geometry radius, as various factors affect this parameter.

On one hand, and depending on the velocity of the car, the wheels deform due to the weight of the vehicle. Therefore, the geometry radius must be decreased in order to represent real conditions, computing the so-called dynamic radius. Additionally, the tyres suffer a deformation due to the slip during their rotation. This slip has different direction in the traction and conducted shaft. As this is a 4x4 model, all wheels will have the same deformation. The reason behind this is that in real conditions the perfect rolling doesn't exist, and the tyres are additionally deformed. Taking all this into account, the following table 8.3 shows all the parameters needed to compute the real radius. The slip phenomenon is considered with an increase factor, different for each velocity, that is applied to the rotation velocity.

Velocity of the car (2 cases)	Geometry radius (Rgeom)	Dynamic radius (Rdyn)	Rotation velocity (v/Rdef)	Increase factor (slip)	Rotation velocity (ω -factor)
160 km/h	0.37 m	0.353 m	125.46 rad/s	1.05	132.04 rad/s
275 km/h	0.37 m	0.359 m	212.60 rad/s	1.08	229.61 rad/s

Table 8.3 : Computation of the rotation of the wheels

The values of the last column, that represent the real rotation of the wheels, have been introduced in the solver setup step.

9. Spatial discretization

As it was explained before in this document, a spatial discretization is needed in order to solve the flux and obtain the results. The domain occupied by the fluid is divided into a finite number of elements when the so-called mesh is created.

9.1. Bi-dimensional discretization

The first step, once the geometry is cleaned and closed, is to generate a bi-dimensional mesh in all surfaces. To do this the *surface deviation* tool of HyperMesh was used. This utility makes the elements finer in the parts where a curvature is found and represent a good general method to create the 2D mesh. During this step, different element sizes were chosen in order to refine the parts where the geometry had more details and the flux could have a more complex trajectory like the front spoiler, the air ducts or the wheels zones.

After this first creation, a re-mesh was performed to fix all the possible problem that are generated, like too deformed elements or superpositions and duplicates. The goal is to reach an acceptable quality of the mesh in all the surfaces, avoiding the problems at the moment of the 3D mesh generation. The bi-dimensional mesh was also created in the surfaces of the wind-tunnel, but this doesn't represent a problem as all surfaces are planes.

The figures 9.1 to 9.7 represent the two-dimensional mesh of the model, focusing on some details of the geometry of the car, once is finished.

The table 9.1 summarises the parameters introduced to generate the bi-dimensional discretization of the model. The ranges in the element sizes evidence the different measures used on the details of the car, as it can be also seen on the images.

Discretization method	Surface deviation
Minimum element size	3 mm
Maximum element size	5 – 50 mm
Growth rate	1.15

Table 9.1 : Parameters used for the 2D mesh

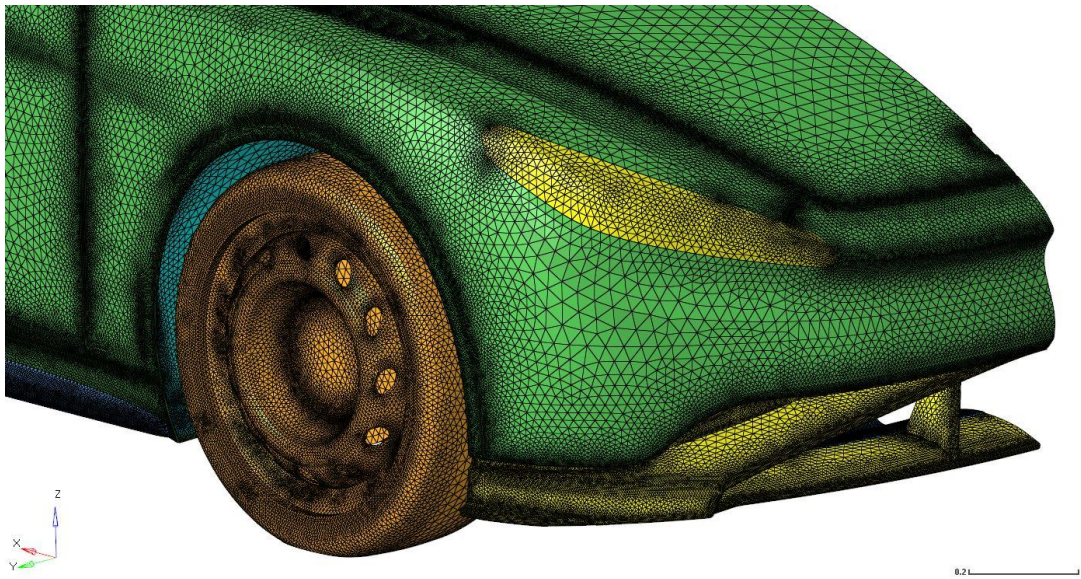


Figure 9.1 : Front view of the mesh

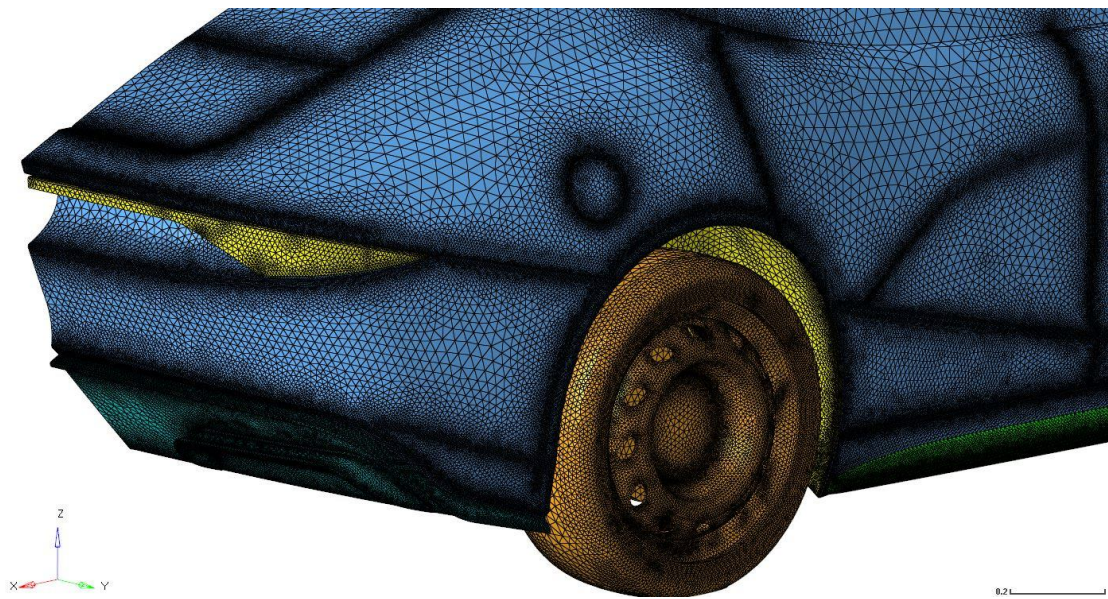


Figure 9.2 : Back view of the mesh

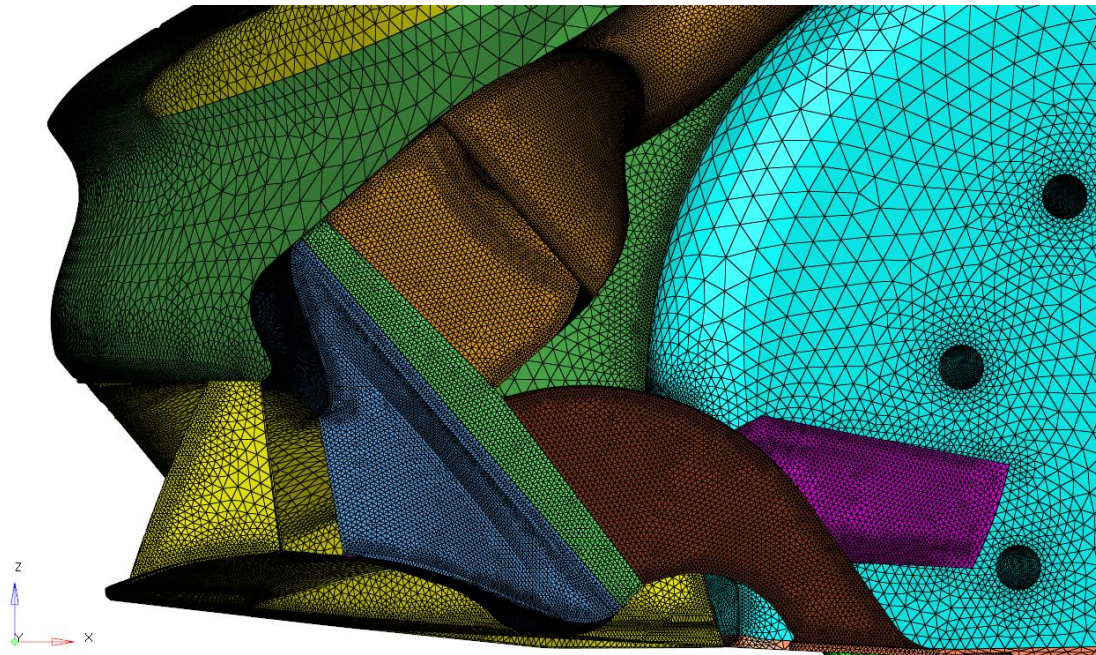


Figure 9.3 : Discretization of the interior ducts

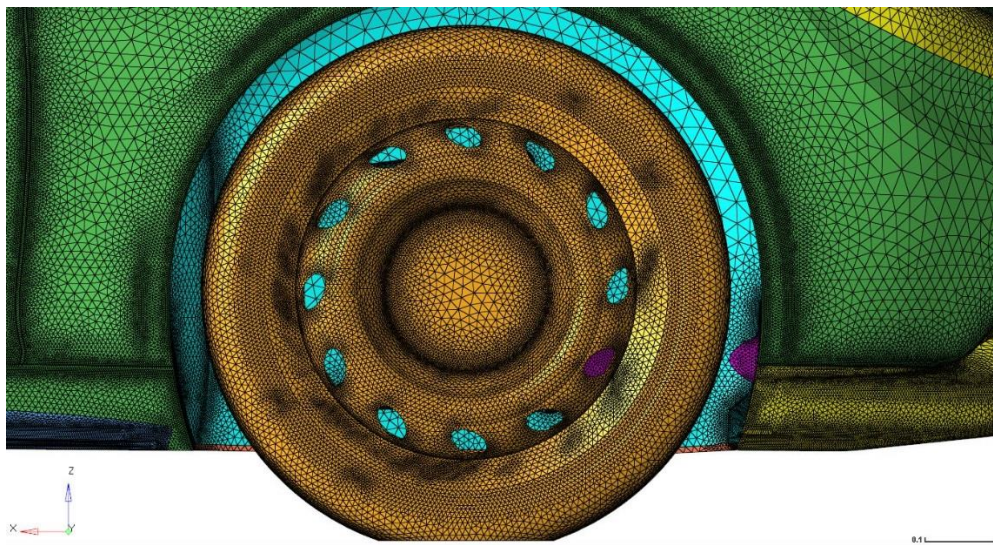


Figure 9.4 : Wheel view of the mesh

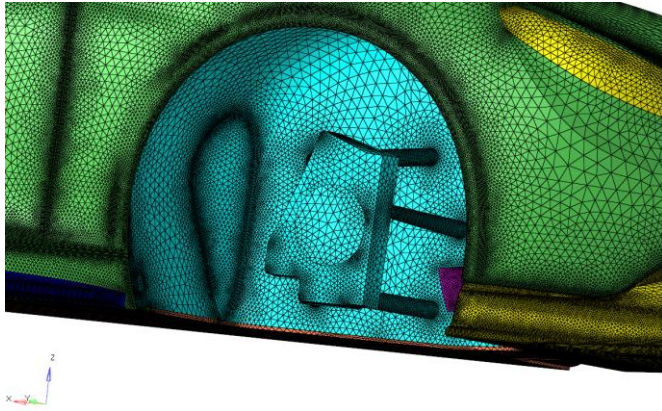


Figure 9.6 : Discretization of the suspension component

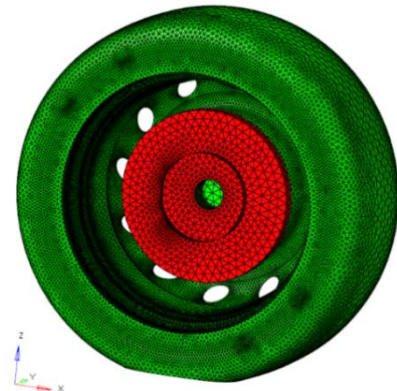


Figure 9.5 : Mesh of the wheel and brake disk

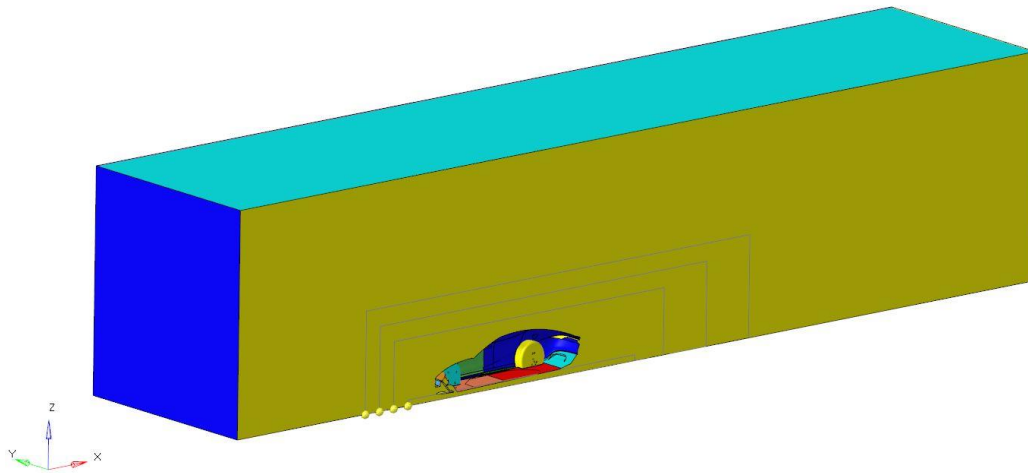


Figure 9.7 : General view of the mesh

9.2. Three-dimensional discretization

The next step is the generation of the three-dimensional mesh, that represent the volume where the air will be during the simulations. The previous superficial mesh will act as a base for the new one, that's why the previous step was so important.

To create the 3D mesh the *CFD tetramesh* function is used. Inside this panel, the boundary layer parameters are chosen, as well as the refinement boxes and maximum element size. Other options are also relevant, but these are the most important ones.

First, in the first configuration panel that can be seen in the figure 9.8, we choose the surfaces where we want to create the boundary layer, necessary to simulate in a

correct way the flux near the walls. In this case all the faces of the car and the ground near the model will have a BL. In the table 9.2 we can see the introduced parameters: First layer thickness of 0.05 mm, 3 layers with 1.2 of growth rate and 2 layers with 1.3. The decision to configure the BL like this was made after several tries until a good result was reached in all the details of the car. The computation of the first layer thickness is necessary to satisfy the y-plus requirement. The Smooth/truncate generation mode allows to truncate the last 2 layers when there's the possibility of a collision of the elements. The first 3 are fixed, to be secure of having this minimum boundary layer always.

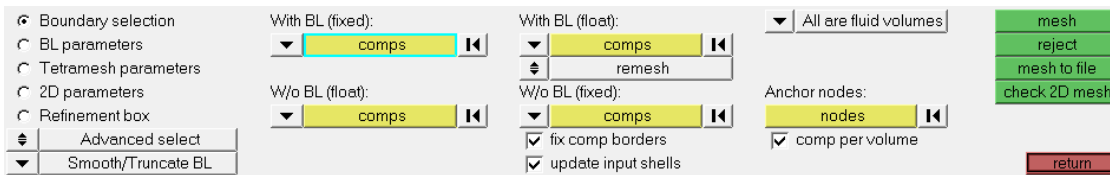


Figure 9.8 : Boundary selection panel

First group of layers (fixed)	3 layers	Second group of layers	2 layers
	0.5 mm first layer thickness		Growth rate of 1.3
	Growth rate of 1.2	Mode	Smooth/truncate BL

Table 9.2 : Boundary layer parameters

The computation of the first element height on the boundary layer was done with a tool of HyperMesh. It was necessary to introduce the studied fluid, in this case air, the freestream velocity and the required y+ parameter. The chosen thickness was the result given by the program, assuring a correct computation of the viscous effect on the fluid on the car's surfaces. The expression of the y+ parameter, together with its explanation can be found early on this document on the part 6.7.

Another important parameter is the maximum size of the three-dimensional elements. Like in the case of the boundary layer, after some tries 0.7 m was decided as the size of the biggest element in the domain. The process where we prove what is the optimal size of the elements of the mesh, not only the maximum one but also the elements of the details of the car, it's called mesh convergence, and it will be explained in the part IV of this document.

Finally, to finish the configuration of the 3D mesh and start its generation, it is necessary to define regions where the discretization will be refined, in order to simulate accurately the air flux near the car. The principal motivation behind the creation of this refinement boxes is to see the streamlines of the air in the rear part of the vehicle, where the wake zone is allocated. The figure 9.9 show the configuration panel where the maximum size and refinement boxes are introduced and in the figure 9.10 these boxes can be seen around the studied car.

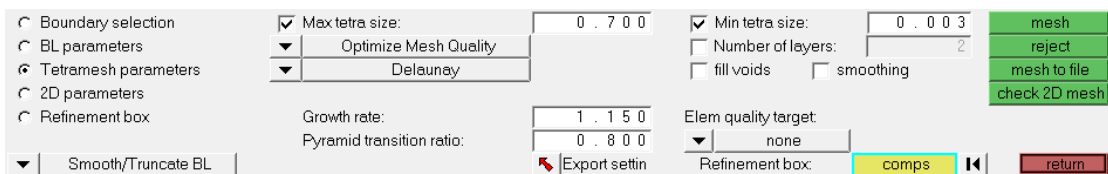


Figure 9.9 : Tetramesh parameters panel

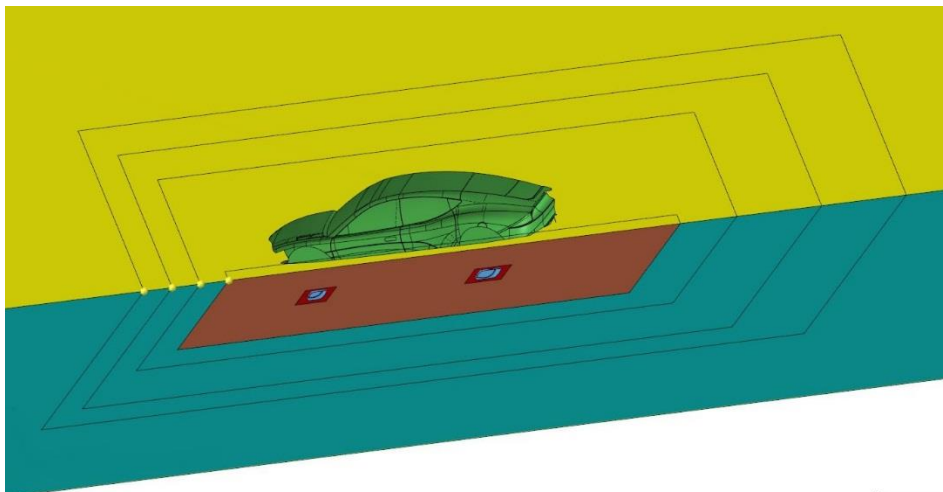


Figure 9.10 : Refinement boxes in the model

The refinement boxes generate smaller elements on the space near the car. On this kind of studies, a progressive growth of the elements is always wanted, to achieve convergence during the computation process. In the table 9.3, the maximum restricted size on each of these boxes is shown.

Refinement box 1 (ground)	40 mm
Refinement box 2	80 mm
Refinement box 3	150 mm
Refinement box 4	300 mm

Table 9.3 : Maximum element sizes in the refinement boxes

9.3. Discretization quality and component organization

After the configuration, the 3D mesh is generated, and the last step before the solver configuration is to check if the quality of all the element is satisfied, the boundary layer correctly generated in all the desired surfaces and the refinements applied in the configured volumes around the vehicle. This is done manually visualizing carefully the obtained result and also with the tool check elements, seeing parameters as the minimum Jacobian, that must be positive. The explanation of this important indication of the element quality is explained on the theory of this document, on the part 7.2.1.

During the geometry cleaning and the spatial discretization, the different parts of the car as well as the wind tunnel are separated in different components in the Hypermesh software. The reason behind this is the possibility to obtain the different results in a separated form after the simulation. With this strategy we can get the contribution to the drag coefficient of each part of the car, assign different boundary conditions to the different components or control precisely the visibility of the model during the post processing.

The geometry of the car was divided in two parts as we can see in the figure 9.11, with this configuration it is possible to get the value of the lift coefficient separately in

the front and rear part and obtain the balance of the model, important parameter specially at high speeds. To do this division the surfaces that were initially in the two halves were divided in two with the suffix 1, for the ones of the front part or 2, for the rear ones. The table 9.4 represent the names of all the components of the model used for the discretization and simulation process. In the figure 9.12 the different parts are identified in order to have a clearer view of the model.

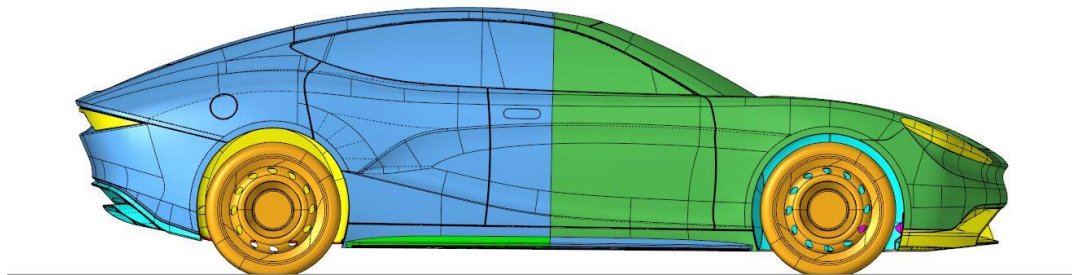


Figure 9.11 . Division of the surfaces in the model

inflow	symmetry	wall_1_Bottom	wall_1_SpoilerLateral
outflow	Ground	wall_2_Bottom	wall_2_SpoilerLateral
top	wall_1_Skin	wall_1_SpoilerFront	wall_1_LightFront
side	wall_2_Skin	wall_2_SpoilerRear	wall_2_LightRear
wall_1_AirDucts	wall_1_WheelhouseFront	wall_1_WheelFront	fluid_air
interfaces	wall_2_WheelhouseRear	wall_2_WheelRear	fluid_radiator

Table 9.4 : Components defined in HyperMesh

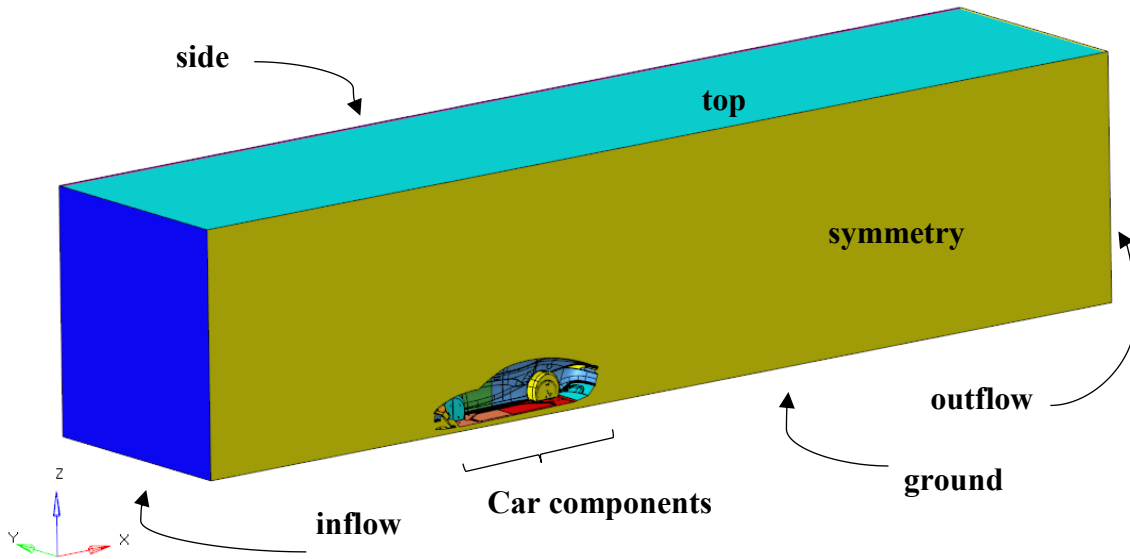


Figure 9.12 : Principal components of the model

During the generation of the 3D mesh, the volume of the fluid that corresponds to the heat exchanger is separated from the rest of the air in the domain. This is necessary because in the next step, the solver configuration, we need to configure a porosity property in this component, in order to simulate the effect that a real radiator generated in the fluid.

Also, in order to obtain the vertical force acting on the ground near the wheels, a division of this surface was made, that can be seen in the figure 9.13. In general, this is a common procedure in these types of simulations. The components are divided according with the required results after the computation.

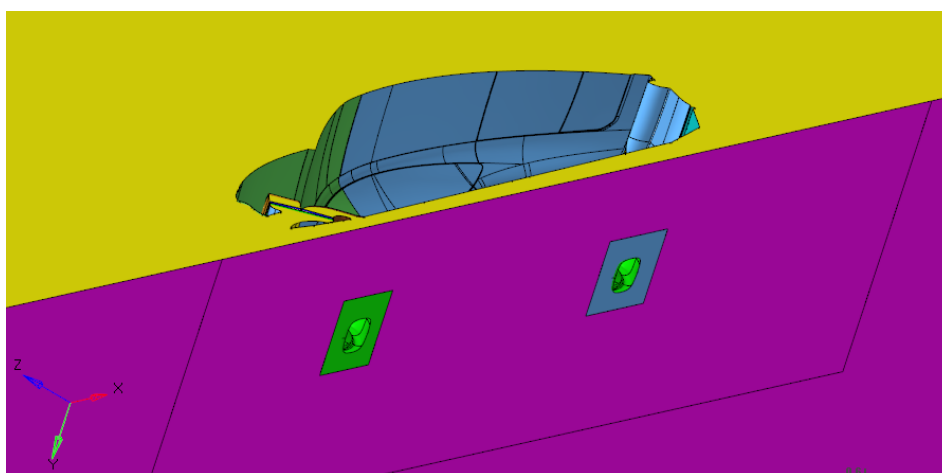


Figure 9.13 : Ground division in the wheels

10.Solver configuration

After the generation of the mesh, the next step is to configure the solver used to solve the equations and simulate the flux. At this point for this project two different software were chosen: AcuSolve and OpenFOAM.

AcuSolve is a program created by the company Altair, that are also the creators of the software used to generate the spatial discretization, Hypermesh. With this solver another program is necessary to configure all boundary conditions and the rest of parameter needed to start the simulation, AcuConsole.

On the other hand, OpenFOAM is a free software that are very flexible and can be used for a great number of different CFD simulations. The type of configuration is very different from a conventional way and it will be explained in this part of the document.

On both solvers, a critical point was the setup of the radiator component on the interior ducts of the car. This zone is modelled as a permeable fluid, that forces the air to flow on a specific direction and causes the pressure to drop, simulating the effect of the real heat exchanger.

Additionally, the configuration of the movement of the wheels and ground, and the definition of the boundary conditions and solution schemes will be discussed.

10.1. AcuSolve solver

The simulations performed with this solver were used to obtain the principal results of the project; as knowing the aerodynamic behaviour of the base model car, trying different modification to try to improve its efficiently and extract the final conclusions.

Almost all the configuration is performed in the AcuConsole software, and after that AcuSolve is started to compute and simulate the flux in the studied case.

After the mesh generation, explained in the last chapter, the file is exported to AcuConsole, using to this the direct tool presented in HyperMesh. After this step, and in the AcuConsole interface, different parameters related with the simulations and computation process are configured, shown in a compact form in the table 10.1.

Analysis type	Steady State
Flow equation	Navier Stokes
Turbulence equation	Spalart Allmaras
Max time steps	2000
Convergence tolerance	0.000001
Relaxation factor	0.5

Table 10.1 : General parameters of the simulation

The convergence tolerance is fixed with a very low value. The reason to this is having a simulation that is not going to stop, it will continue iterating until the maximum number of time steps. The strategy is to control manually the convergence with the residual ratio, and the evolution of parameters as the aerodynamic coefficients. When these values are constant, we know the simulation has arrived to stable conditions and can be stopped.

This visual control was performed with the AcuProbe program, which can be opened during the computation process. In the following figure 10.1, the evolution of the residuals is shown. As we can see, after xxx iterations the values are almost constant. The simulation was further computed until time step 500, to be on safe conditions. Drag and lift coefficients, together with other parameters were also controlled, to assure the solution was finally stable. This convergence control is also useful to avoid simulating a case for a long time that is not corrected configured, noticing the problem at the first steps of the computation. The visual control can be also performed with HyperView, watching the solution contours (velocity, pressure, eddy viscosity...).

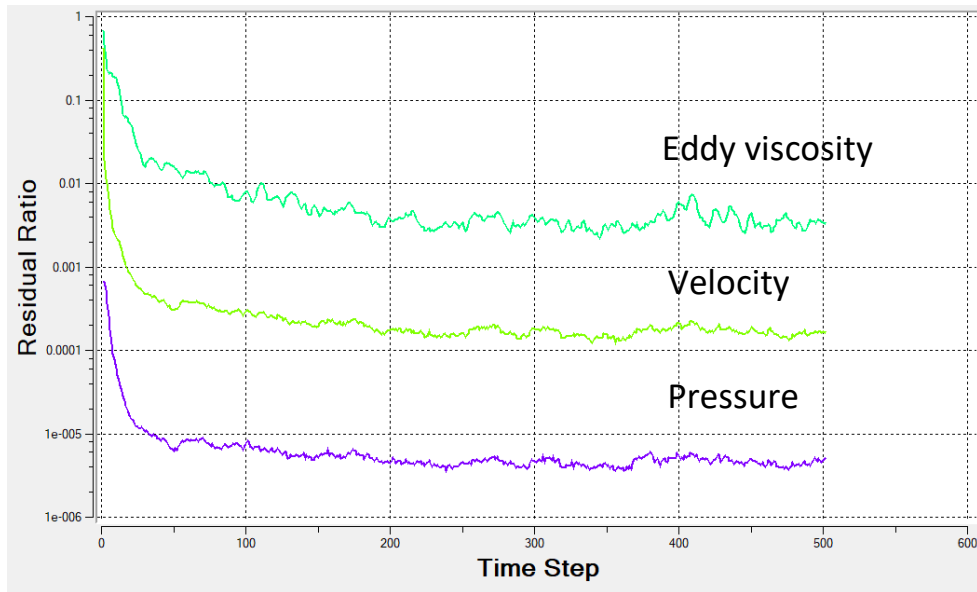


Figure 10.1 : Residual evolution during simulation

In this software the boundary conditions of each component, that were specifically separated in HyperMesh, are also configured. The table 10.2 summarises them.

ground	Type wall		X velocity
inflow	Type inflow	X velocity	Turb. Visc. Ratio = 3
outflow	Type outflow		Pressure 0
side	Type slip		
symmetry	Type symmetry		
top	Type slip		
air ducts	Type wall		Zero velocity
skin	Type wall		Zero velocity
spoilers	Type wall		Zero velocity
wheels	Type wall		Reference frame

Table 10.2 : Summary of the boundary conditions

Important parameters for the simulation are the rotation of the wheels, that are introduced with two reference frames and the velocity of the ground element. In the reality, the car moves at a certain speed and the ground and air have velocity zero. In CFD simulations the approach is the contrary, the surfaces of the car are stationary and the air and ground move at a constant speed.

The wheel's rotation velocity was calculated for each case using the process explained in the part 8 of this document. The values in rad/s were then introduced in the solver, together with the ground speed, which in this case is the same as the velocity of the car.

The tables 10.3 and 10.4 show the configuration of the wheels and ground for each case. The inflow surface was also configured with the air inlet speed, following tables summarise the introduced values.

160 km/h case				
ground	X velocity	44.44 m/s		
inflow	X velocity	44.44 m/s		
Front wheel	Rotation centre	-0.0601	0.9032	-0.0134
	Angular velocity	-132.04 rad/s		
Rear wheel	Rotation centre	2.98	0.9032	-0.0134
	Angular velocity	-132.04 rad/s		

Table 10.3 : Wheels and ground configuration in the 160 km/h case

275 km/h case				
ground	X velocity	76.4 m/s		
inflow	X velocity	76.4 m/s		
Front wheel	Rotation centre	-0.0601	0.9032	-0.0134
	Angular velocity	-229.64 rad/s		
Rear wheel	Rotation centre	2.98	0.9032	-0.0134
	Angular velocity	-229.64 rad/s		

Table 10.4 : Wheels and ground configuration in the 270 km/h case

10.2. Heat exchanger configuration

Finally, after the introduction of the heat exchanger component in the simulations, the porosity and direction properties are configured in the fluid that corresponds with the radiator. The table 10.5 summarises these parameters. The computations needed at this step are shown below, in order to obtain them, an experimental curve, in the figure 9.6, was used. The theory related to this process was explained in the part 10.2 of this document.

Density	1.225 kg/m ³
Permeability direction	45 degrees
Direction 1 permeability	1
Direction 2 permeability	0.001
Direction 3 permeability	0.001

Darcy coefficient	3320855.94
Forchheimer coefficient	21.78

Table 10.5 : Heat exchanger fluid configuration

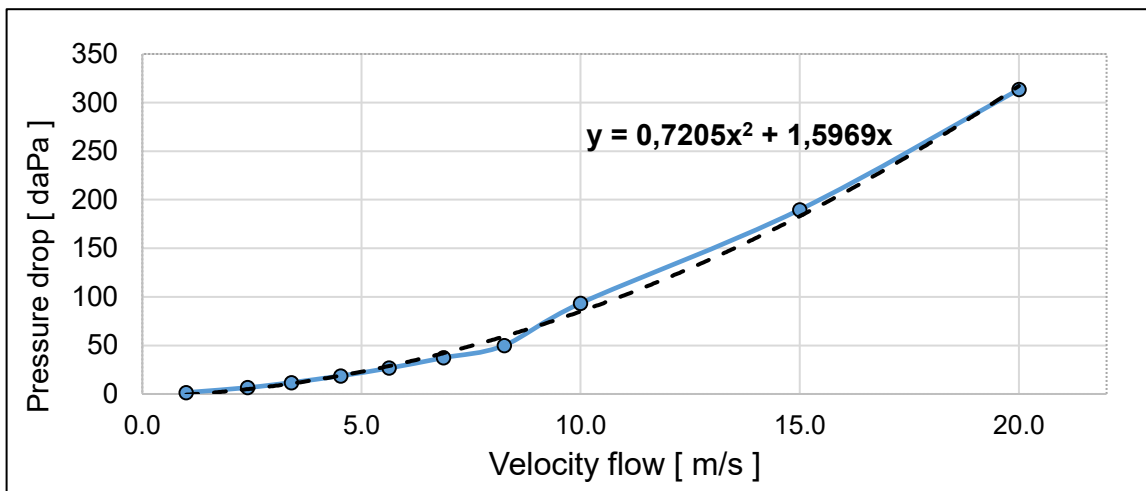


Figure 10.2 : Experimental curve of the heat exchanger

- Darcy and Forchheimer coefficients calculation:

From the experimental data, that can be seen on the previous figure, we get the A and B values, taking into account the general form of an exponential curve:

$$\nabla P = A u + B u^2$$

Now from the theory explained on the document, we know the expression of these two terms, that are related with the wanted coefficients:

$$A = \frac{C_{DARCY} \mu L}{k_x} \rightarrow C_{DARCY} = \frac{k_x A}{\mu L} = \frac{1 \cdot 1.5969}{0.0000178 \cdot 0.027} = 3320855.94$$

$$B = \frac{C_{FORCH} \rho L}{\sqrt{k_x}} \rightarrow C_{FORCH} = \frac{\sqrt{k_x} \cdot B}{\rho L} = \frac{1 \cdot 0.7295}{1.225 \cdot 0.027} = 21.78$$

These two values correspond with the principal direction of the heat exchanger. The other two, where the resistance to the air flow is very high, are calculated substituting the $k_x = 1$ by $k_x = 0.001$. This would simulate what happens on a real radiator, where

the air flux is oriented on a specific direction, in this case 45 degrees. The following figure 10.3 illustrates this phenomenon:

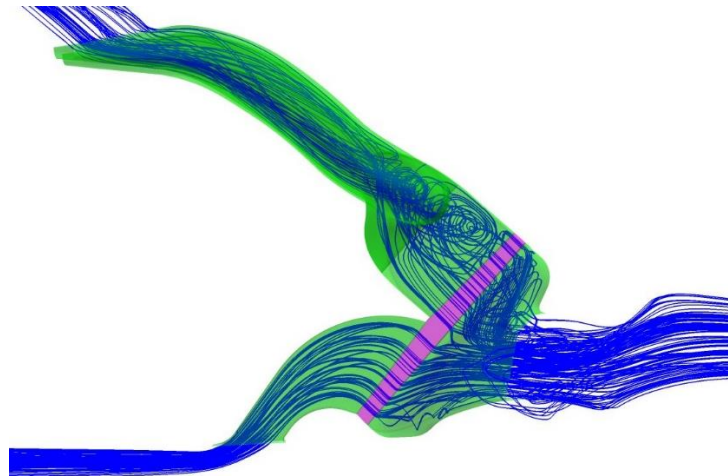


Figure 10.3 : Streamlines on the heat exchanger

The fluid decreases its pressure and is forced to flow at the 45-degree angle when passes through this element, something that occurs in the real case. On the other hand, the interfaces that were used to divide the fluid of the radiator and the fluid of the normal air are deactivated in AcuConsole, to allow the air to flow normally through the interior of the car.

10.3. Simulation launch

After all the configuration, the computation is started and AcuSolve launched. This is done directly from the AcuSolve interface. In order to use all the computer potential, a parallel simulation is performed, using all available processors. In the figure 10.4, the launch panel of AcuSolve is shown.

During the computation process, as it was explained before, the evaluation of the calculus can be performed, analysing the obtained residuals with AcuProbe, the visual contours with HyperView or directly with the text file generated by the solver, where the progress can be followed.

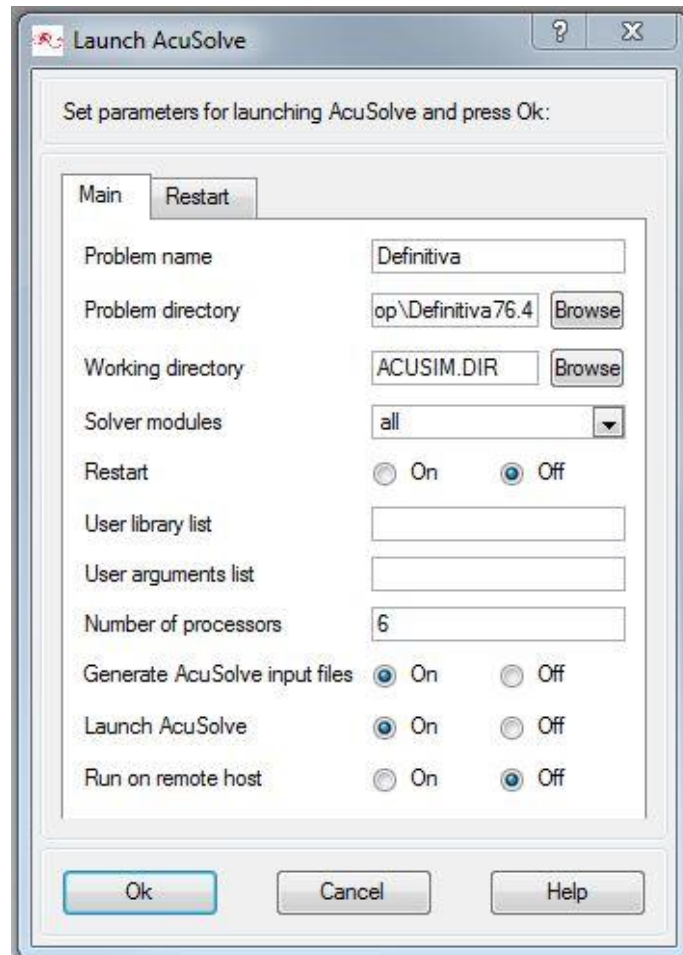


Figure 10.4 : Launch panel of AcuSolve

10.4. OpenFOAM solver

On the other hand, all the process starting from the discretised domain can be completed with OpenFOAM software. In this project this procedure was followed to validate the used method and to perform the so-called mesh convergence, both of them are explained in the following chapters of this document.

In order to configure correctly all the necessary parameters for the simulation, the OpenFOAM guide was used, together with several tries to reach an optimal simulation procedure.

The general structure of an OpenFOAM case, formed by three principal folders, can be seen in the figure 10.5.

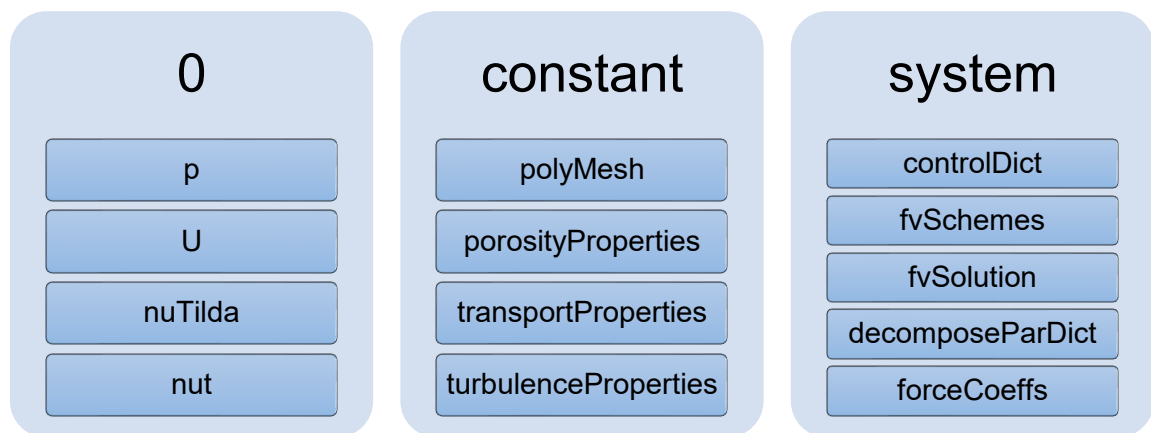


Figure 10.5 : General case structure of OpenFOAM

The zero folder corresponds to the boundary conditions. Inside it, for a Spallart Allmaras turbulent model, we can find files for the pressure, velocity, turbulent viscosity and `nuTilda`. Other type of models need other files, for example `k`, `epsilon` or `omega`. Each of these files are written in Linux code, and define the boundary conditions for the components defined in the HyperMesh software. As an example, in the figure 10.6 part of the velocity file is shown. The syntax is always the same for the rest of the cases. In the velocity file the boundary conditions of the rotation of the wheels and moving ground are introduced, in the same way were included in AcuSolve on the other strategy explained before.

```

boundaryField
{
  inflow
  {
    type          fixedValue;
    value         uniform (76.4 0 0);
  }
  outflow
  {
    type          inletOutlet;
    inletValue    uniform (0 0 0);
    value         uniform (76.4 0 0);
  }
  top
  {
    type          slip;
  }
  symmetry
  {
    type          symmetry;
  }
  ground
  {
    type          fixedValue;
    value         uniform (76.4 0 0);
  }
  wall_1_Skin
  {
    type          fixedValue;
    value         uniform (0 0 0);
  }
  wall_1_WheelFront
  {
    type          rotatingWallVelocity;
    origin        (-0.0601 0.9032 0.0134);
    axis          (0 1 0);
    omega         -229.6465;
  }
}
    
```

Figure 10.6 . Velocity file in OpenFOAM

Constant folder has additional parameters related with the turbulent model used, the properties of the fluid air and the porosity configuration of the heat exchanger. Table 10.6 summarises the information written in these three files. In the polyMesh folder all the information about the imported mesh from HyperMesh is located. Here are defined the components with the same names and the two fluid zones, the one that corresponds with the heat exchanger, where the porosity is defined, and the one of the open air.

As we see, the parameters used to define the porous zone that simulated the behaviour of the radiator are the same as the ones used on the AcuSolve case. This is because the definition method is the same so the values are exactly equal, with the same computation process, which can be seen on the previous part.

Transport model	Newtonian
nu of air	$1.45 \cdot 10^{-5} \text{ m}^2/\text{s}$
RAS model	Spalart Allmaras

Porosity configuration	Type		DarcyForchheimer	
	cellZone		Fluid_radiator	
	d	3320855	3320	3320
	f	21.78	0.022	0.022
	direction	0.707	0	0.707

Table 10.6 : General configuration of the constant folder in OpenFOAM

The system folder corresponds with all the configuration related with the way the simulation is launched and also some results are obtained during computation.

ControlDict, *fvSchemes* and *fvSolution* are the files that contain the parameters related to the computation of the fluid equations, the process of the simulation or the saved states during the process. In the table 10.7 the most important parameters are summarised.

Solver	porousSimpleFoam	
ddtSchemes	steadyState	
Relaxation Factors	p	0.3
	U	0.7
	nuTilda	0.7

Table 10.7 : General simulation parameters in OpenFOAM

The *decomposeParDict* file is used to configure the parallelization of the computation. As in the AcuSolve strategy, the maximum number of processors as possible were used in order to take advantage of all the computer power.

The introduced code in order to launch the simulation are shown below:

decomposePar.exe : To divide the domain and parallelise the computation

mpiexec -np 6 porousSimpleFoam -parallel > log : Launch the solver with parallelization

reconstructPar.exe : To join again the domain and be able to visualize the results

Finally, files as *forceCoeffs* and *forces* are configured to obtain some results as aerodynamic coefficients and forces in some specific components during the simulation. These two files were written in order to obtain the same results as in the AcuSolve solution, to have a good comparison and therefore validation of the method.

11. Post-Processing

After the simulation is completed, the results are analysed in different programs depending on the used solver. In the case of AcuSolve, there are several software each

of them specialised on a specific type of result, as it will be explained below. In the OpenFOAM case, the visualization software ParaView was used for the contour and flux results. On the other hand, numerical results were obtained directly from the generated text files during the simulation.

Both strategies give the same kind of results that allow to make a good comparison after the computations. This is useful to validate the used method, necessary to be sure about the extracted conclusions.

11.1. AcuSolve results

- **AcuProbe**: Software used to extract the numerical results during and after the simulation. The evolution of the residuals of the solution or the value of the aerodynamic coefficients and forces were obtained with this program.
- **Virtual Wind Tunnel**: Altair software specialised in CFD simulations. For this project this program was not used to mesh the studied model or perform the simulations, but it was useful due to its frontal area

computation tool. The discretised model was introduced in VWT just to compute this important parameter of the car.

- **AcuFieldView:** Another Altair solver specialised in the flow visualization. It can be used to obtain a great number of different results but in this project, it was useful to get animations and images of the streamlines of the air flux, both in the exterior and in the interior parts of the car.
- **HyperView:** Software used to obtain visual results as pressure or velocity contours. The possibility to see this results on specific components separately or in symmetry planes were useful to analyse better the behaviour of the studied case.
- **HyperGraph:** This program was used specifically to draw some graphical data as the profile of the pressure on the surfaces around the car.

11.2. OpenFOAM results

- **ParaView:** The visual results were obtained with ParaView, the natural postprocessing software of the OpenFOAM solver. Its great variety of tools allow to obtain almost the same kind of results as the programs mentioned in the AcuSolve strategy.
- **Text files:** Numerical results were obtained directly from the text files generated during the simulation. The configurations for the creation of this archives were written in the mentioned files *forceCoeffs* and *forces*.

IV. MESH CONVERGENCE

The mesh convergence is a very important process that have to be done to know what the optimal size of the elements of the mesh is in order to perform the simulations. After this procedure, that consist on several simulations with different mesh sizes, the adequate discretization is reached to simulate the definitive cases of the project.

If the size of the elements is too big, the complex geometry of some details of the car are not correctly taken by the mesh. This means that the results will not be the same as the one of the real car and therefore they are not satisfactory for the project. Besides, big elements near the car make the correct visualization of the streamlines very difficult because the complex turbulent flux cannot be simulated.

On the other hand, if the mesh is too refined, the time needed to perform the simulations is too long, and this makes impossible to perform all the computations due to the high computer requirements. The obtained results are correct, but too refined elements in the discretization make the simulations not efficient in time and power.

The mesh convergence was performed before the arrival of the final geometry of the car. Due to this, the simulations don't have the detailed wheels of the definitive model or the interior air ducts with the radiator. The used model, although is simpler than the definitive one, allow to make this convergence study because it has the same exterior shapes and general details. Later, when the definitive simulations were performed, the missing parts in this convergence study were tested with several meshing sizes to include them also efficiently discretised.

The different simulated cases differ in the minimum and maximum element size of the mesh and the refinement boxes defined near the model car. The next table 11.1 summarises the principal parameters and the number of elements of each case.

Case	Elements	Min. size	Refinement near the car
1	---	0.0005	0.06
2	20954349	0.001	0.07
3	13113511	0.002	0.08
4	9118645	0.003	0.1
5	6078717	0.004	0.12
6	4544891	0.005	0.14
7	3535086	0.006	0.16
8	2900589	0.007	0.18
9	2119688	0.008	0.19
10	2087147	0.009	0.2
11	---	0.01	0.3

Table 11.1 : Cases of the convergence process

The cases 1 and 11 were not simulated due to its too low or high number of elements. Case 1 was meshed with a very refined element size and due to this, the computation time was not acceptable as it was too high. On the other hand, case 11 had a too big element size and the convergence was not reached during the computation. As a result, the optimal element size of the mesh is located in the middle of these two limits. In order to find it, some results were evaluated, shown in the graphics below.

To clarify the differences in the discretization the figures 11.1 and 11.2 show two of the simulated cases, being respectively the mesh with 9 and 1 millimetres of minimum element size.

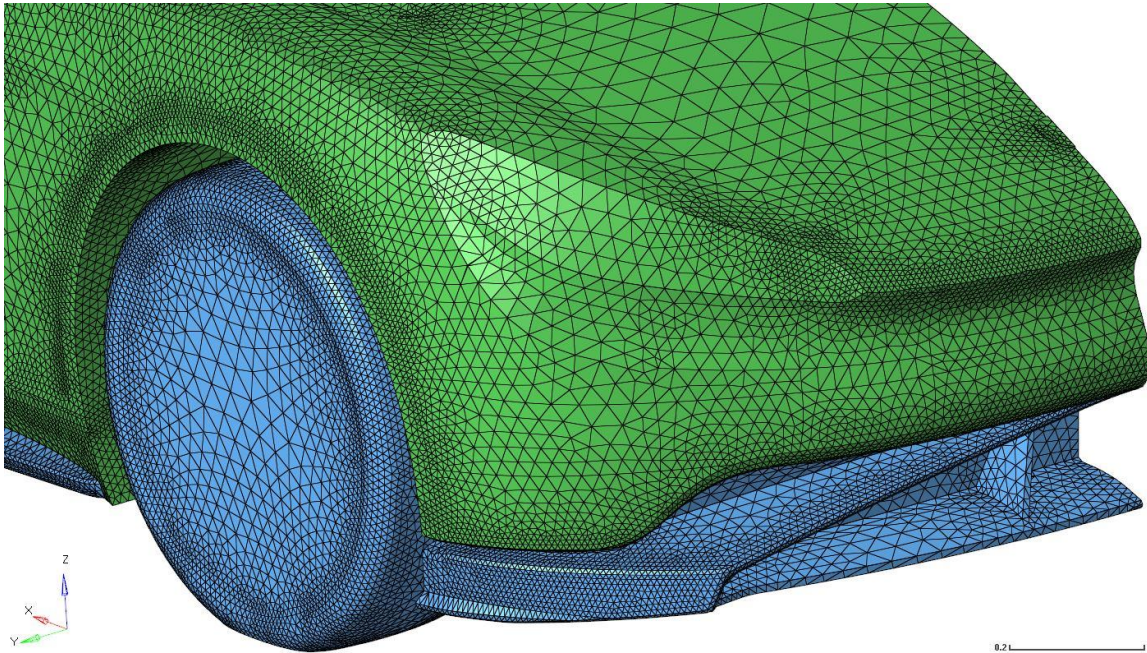


Figure 11.1 : Discretization with 9 mm of minimum element size

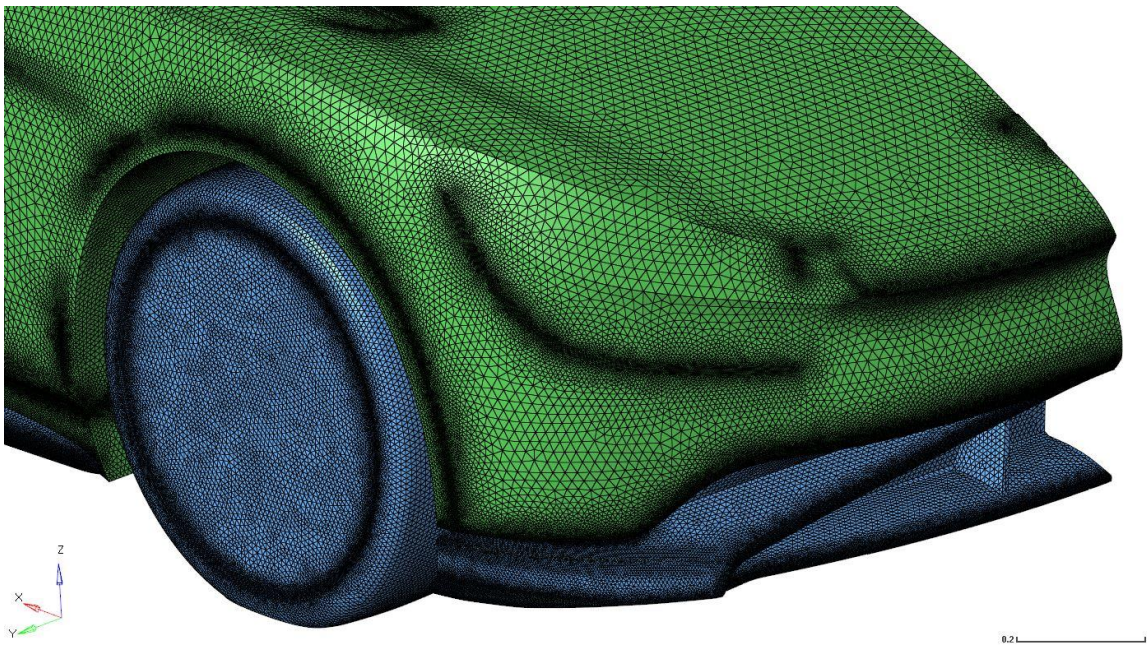


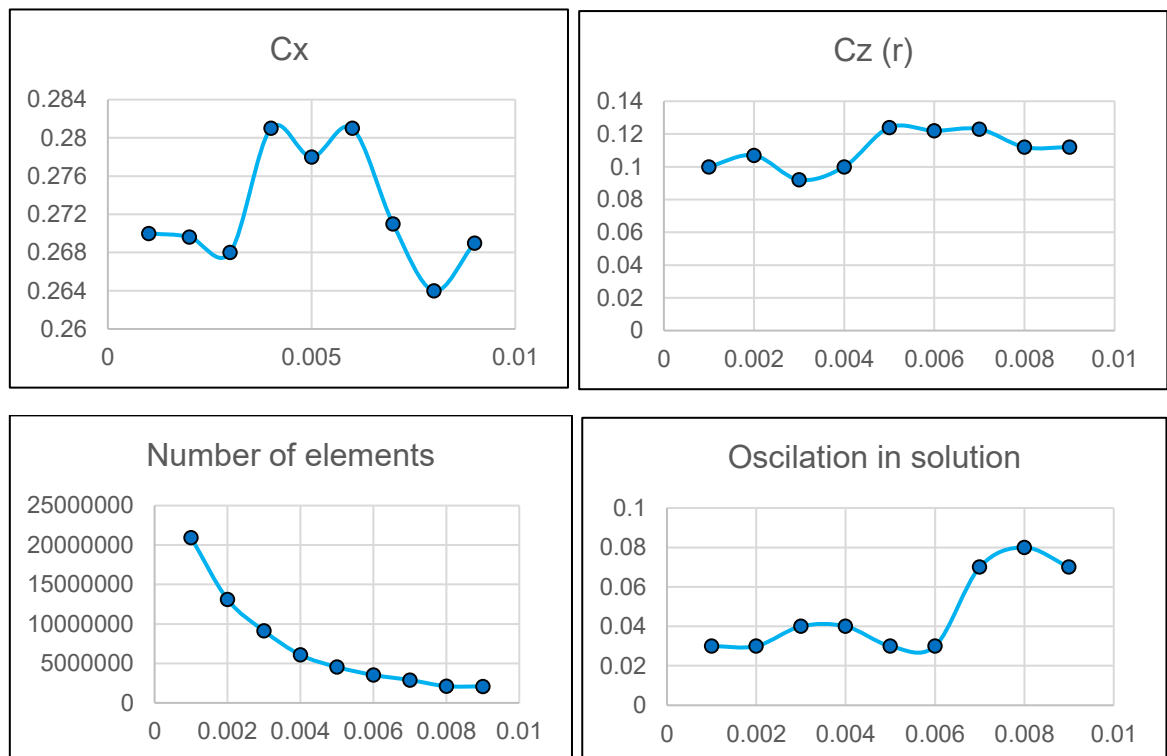
Figure 11.2 : Discretization with 1 mm of minimum element size

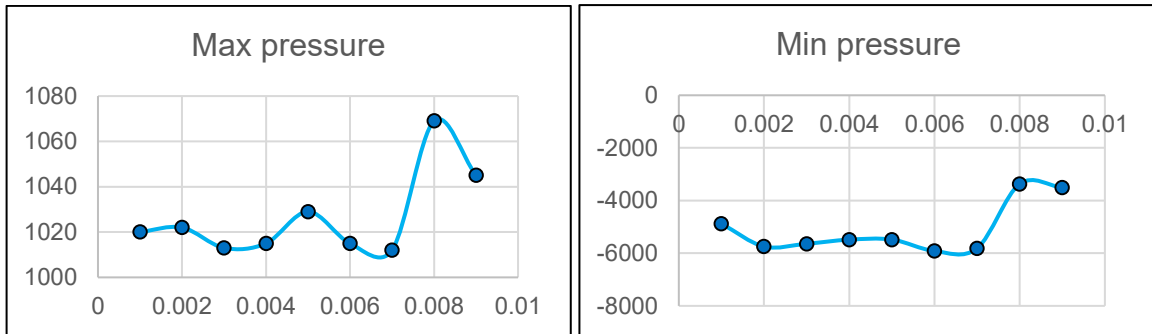
The set-up conditions of the computations are the same for all the cases, in order to have a good comparison and extract valid conclusion about the optimal mesh to

introduce in the definitive simulations. The boundary layer is also the same for all the cases, because as we saw it depends on the velocity, the reference length, the type of fluid and the wanted y^+ parameter. This configuration is similar to the one used for the definitive simulations, that was explained in the previous part of this document.

To make the comparison between the different cases, the drag and lift aerodynamic coefficients, as well as the maximum and minimum reached pressures were evaluated. The goal is to see the maximum element size that guarantees accurate results. When the computation is finished we do not obtain a stable number in the evaluated results, but we see an oscillation between a maximum and minimum values. The procedure is to extract the average to write down the final results. This is a normal procedure in this type of simulations but during this convergence study, it was clear that a big mesh lead to bigger oscillations in the obtained result. Therefore, this phenomenon was also taken into account for the conclusions.

To see clearly the result of the study, some graphics were created with the output data mentioned before. The next figures represent these graphics:





After the analysis of this data, from the minimum element size of 3 mm the drag coefficient maintains the same value. This mesh is also satisfactory for the lift coefficient and extreme values of the pressure, where the size could also be bigger. In the previous graphics, the red vertical line represents the chosen element size after the study.

In the definitive simulations, with all the details as the final wheels and air ducts, the minimum element size is lower due to the complex shapes of these components. Therefore, the final number of elements will be higher than the one seen in the previous graphics. This convergence study was useful to know what the optimal mesh for the general element of the studied geometry of the car is.

V. VALIDATION OF THE METHOD

The validation is a necessary procedure that allow us to know if the used method is correct in order to make the conclusions of the project. This process can be done simulating a case that was performed before in an experimental environment and comparing the results. In the case of this project the comparison is done with the two solvers mentioned above, studying the same case in both of them.

AcuSolve and OpenFOAM were the used solvers for this validation, following the procedure explained in previous chapters of this document and using the same set-up parameters to have a valid comparison.

The used geometry corresponds with the base case of this project, the electric car with all the final details and without any modification. The validation was performed after the convergence study and therefore the definitive geometry was already available to simulate these cases, including the interior air ducts with the radiator component.

The validation study was performed at 270 km/h (76.4 m/s), one of the studied cases in the definitive simulations. The results obtained with AcuSolve are the same we used for the final study of the car, as the base case without before the proposed modifications. On the other hand, the ones of OpenFOAM where obtained specifically for this validation.

To make the comparison of both solvers, the drag coefficient was chosen due to its importance in the design of the car, as it has direct influence in the consumption of the electric model. The table 11.1 shows this comparison with the relative error. As we see, the error is lower than 5%, so the used method can be considered valid.

76.4 m/s	OpenFOAM result	AcuSolve result	Relative error %
Drag coefficient (C_x)	0.288	0.28	2.63 %

Table 11.1 : Validation result

A comparison of the pressure and velocity contours has also been done, to be sure that in both solvers the air flux had the same behaviour and similar extreme values on the different components of the car. The figures 11.1 to 11.4 show these contours.

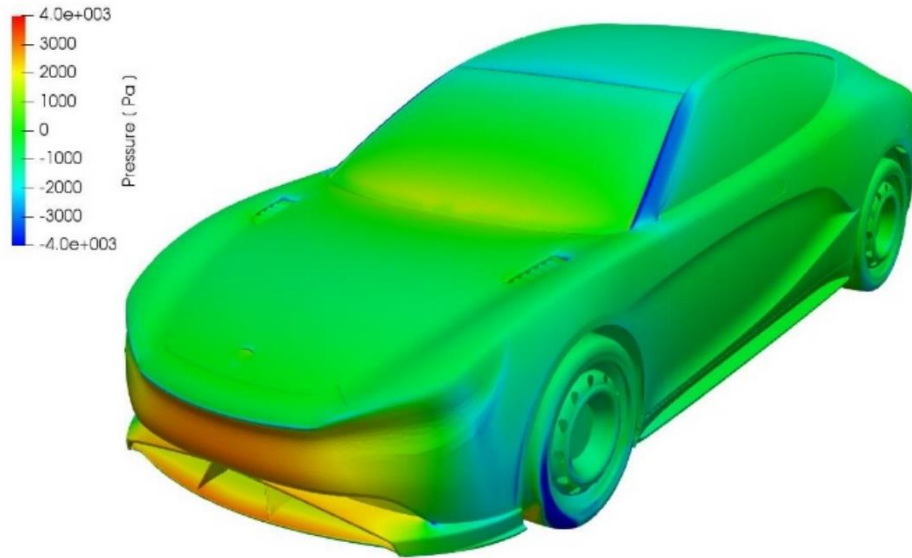


Figure 11.1 : Pressure contour in OpenFOAM

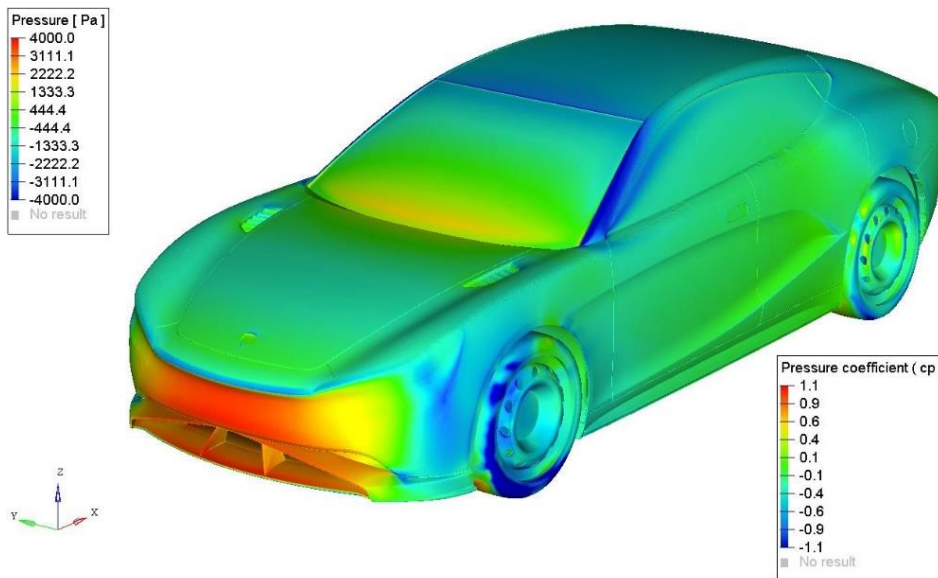


Figure 11.2 : Pressure contour in AcuSolve

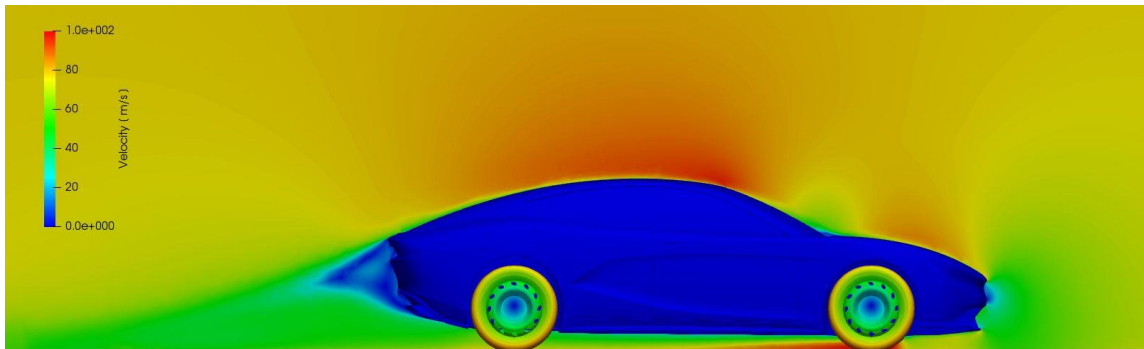


Figure 11.3 : Velocity contour in OpenFOAM

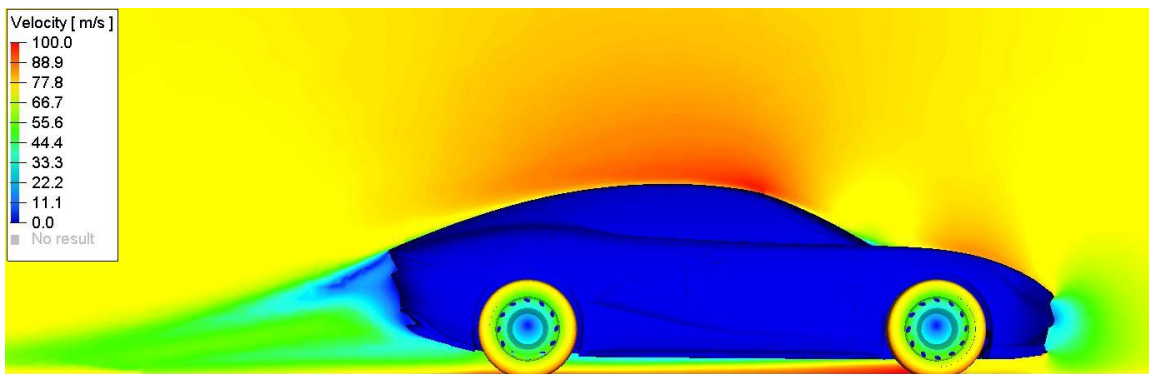


Figure 11.4 : Velocity contour in AcuSolve

After the validation study, the used method can be considered correct due to the similar results in both solvers. The definitive study and the proposed modifications can be then simulated with this procedure, in this case in the chosen solver AcuSolve.

VI. SIMULATED CASES

In this part of the document the different simulated cases of the project are explained. All these simulations were performed with the AcuSolve solver, following the process explained before in this document.

12. Base case

The simulations of the base case were performed with the final geometry arrived directly from the client. As it was explained before in the document, the geometry arrived in various steps, each time more and more detailed as the design process was advancing. The final geometry was considered when we had the detailed wheels and the interior duct for the air flux including the radiator component.

In the figure 12.1 we can see a general view of the model used in the simulations. After the study of this model, the problems that could be found on its aerodynamic behaviour were considered for the proposed modifications, with the goal of reaching an efficiency improvement.

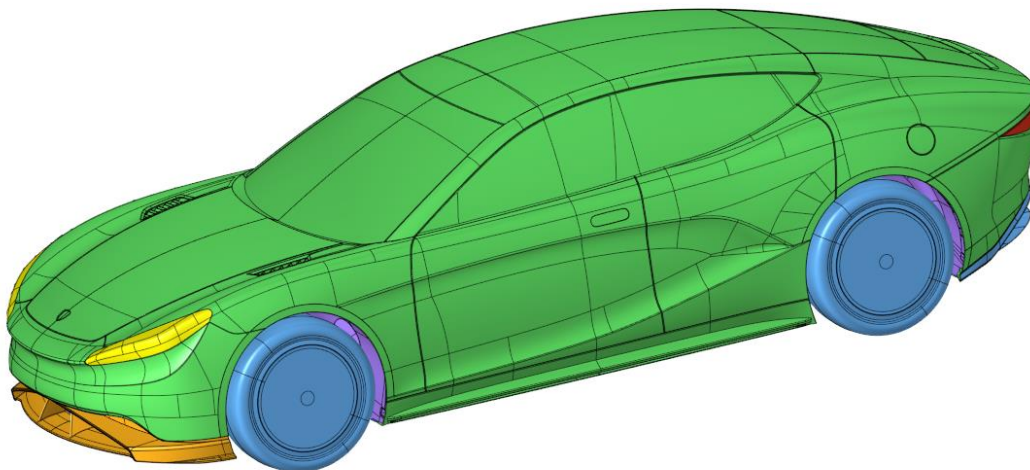


Figure 12.1 : Base geometry

The simulations of the base case were performed with the two mentioned velocities, 160 and 275 km/h. The solver configuration is the one explained before on this document, on the AcuSolve part.

For this standard case, many different results were obtained in order to find all the possible problems and to characterise completely the flux on this car model. This is the main part of the project, additionally, some modifications have been proposed, which are listed below.

13. Proposed modifications

The proposed modifications on the initial geometry are presented in this part, explaining the difference between the new and base case and also the expected behaviour after the change. The final results of the modifications, together with the base case, are shown in the next part of the document.

13.1. Added rear spoiler

After the simulation of the base case, a high up force in the rear part of the car was discovered and therefore some modifications in this part were proposed to try to lower this effect. The first one was to introduce a little rear spoiler, as we see in the figure 13.1, to create a high-pressure zone in its upper part and achieve the desired change.

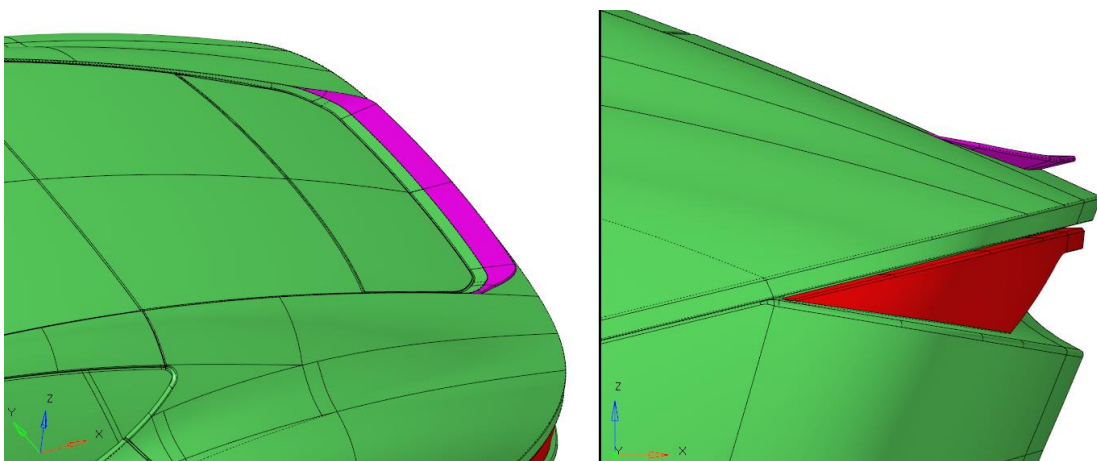


Figure 13.1 : Geometry of the added rear spoiler

The addition of this spoiler also increases the drag coefficient, which is not positive, so it is necessary to evaluate if this modification is generally positive for the car aerodynamic behaviour.

Together with the numerical values of drag and lift coefficients, in this simulated case the pressure and velocity contours were analysed, to understand in a better way the influence of the addition of this new component on the car. Besides, the streamlines of the air flux in the rear part were compared between this and the standard case.

13.2. Different car inclination

The way the air flows in the bottom part of the car is very important as it has a direct influence on the vertical aerodynamic force. In this case, the inclination of the vehicle was changed in order to see this effect.

The standard case has the model with a little inclination to the front, as the real model car is constructed. In the modified case this inclination is proposed to be eliminated, to analyse if this change has a big impact on the aerodynamic coefficients and subsequently on the behaviour of the car.

The figures 13.2 and 13.3 shows a comparison before and after this modification. Visually is difficult to notice the difference, as the angles have very low values. One part of the car that can be seen to differentiate them is the space between the tyre and the car on the rear wheels. The angle was changed rotating the surfaces of the car with respect to the front axis.

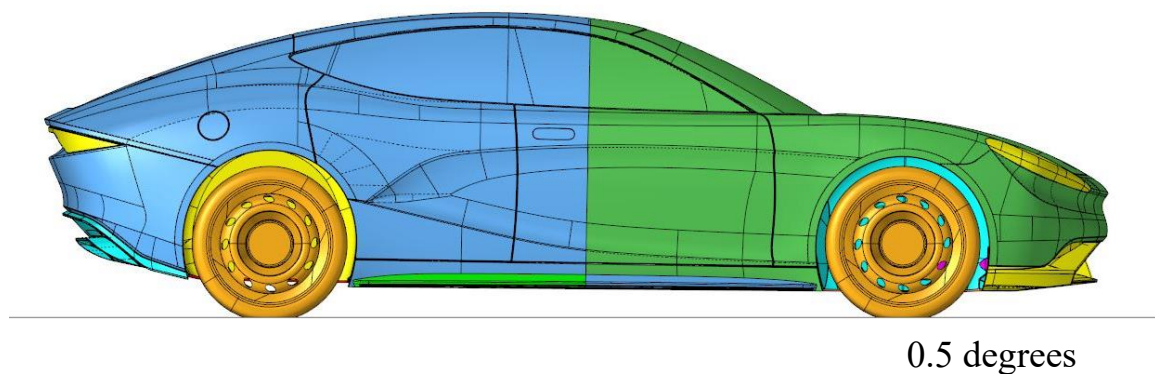


Figure 13.2 : Geometry before the inclination

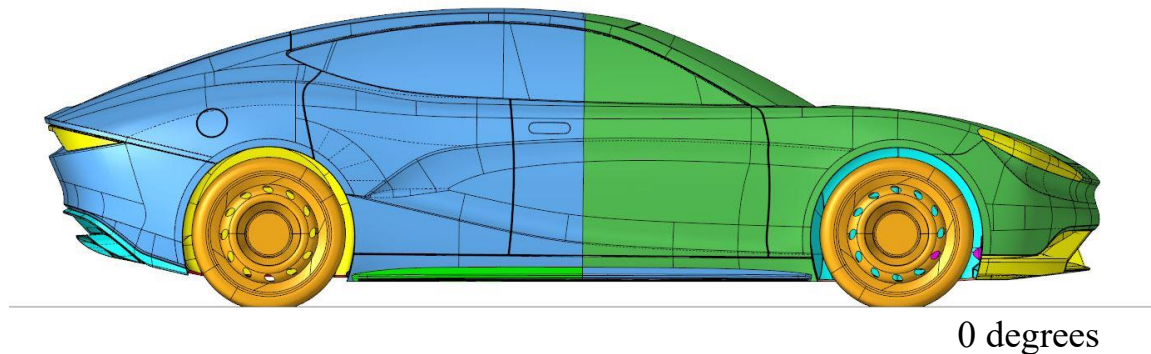


Figure 13.3 : Geometry after the inclination

The results taken after this new simulation were, together with the numerical ones, the pressure and the velocity contours, focusing on the node values of different points of the bottom gap with the road. The streamlines of the air flux were also analysed, to understand what is changing after the modification.

13.3. Optimized air ducts

From the animation results obtained with the standard geometry, the internal flux through the radiator of the car has been closely analysed. A negative phenomenon on the upper internal duct has been discovered, in form of a recirculation of the air flux. This may be caused by the low pressure that is generated on this zone, to try to solve it, or at least reduce it, a redesign has been applied to the components involved.

The proposed change is to reduce the area on the upper duct by a 20%, increasing the one on the lower duct. This change may increase the pressure and make the air flow easier. Additionally, the curvature near the radiator has been changed, to avoid the separation of the flux that was discovered. All the modifications to the original components were decided attending on the space limitations of the vehicle, to avoid collisions with other internal elements of that part of the car.

All these changes can be seen on the followings figure 13.4, 13.5 and 13.6 where a comparison between the old and the new design is shown.

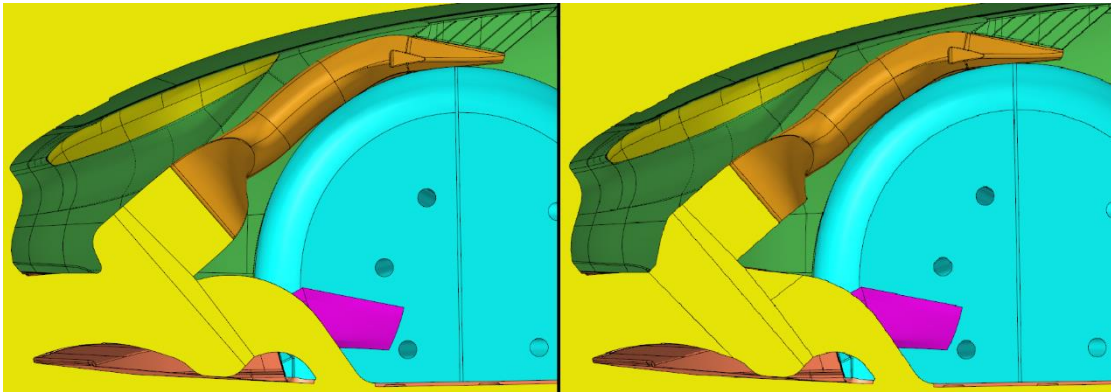


Figure 13.4 : Comparison of the interior redesign, symmetry plane

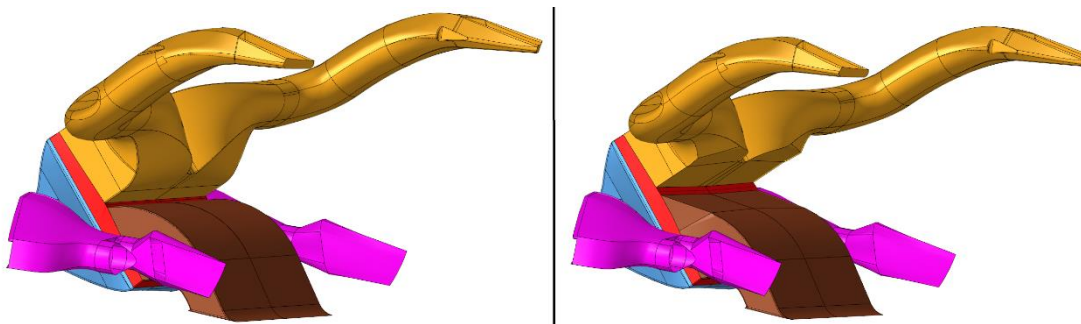


Figure 13.5 : Comparison of the interior redesign, interior ducts

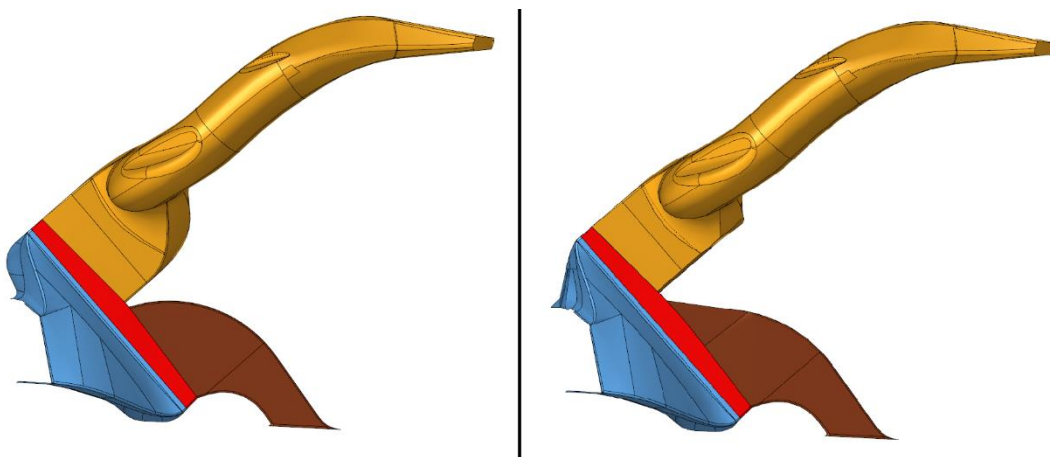


Figure 13.6 : Comparison of the interior redesign, lateral view

Alternative changes to the internal air ducts can be proposed. Due to the lack of time, in this project only this possibility was simulated but on the following part other possibilities are also discussed. This third modification was performed to show the change this redesign produces on the flux of the base case. Further tries can allow to reach the optimal internal flow through the internal ducts.

13.4. Other possible modifications

Analysing all the results of the standard case, further modification may have been added to the study, in order to complete the project and propose more improvements to the aerodynamics of the car. On the following part of the project, these possible modifications will be discussed, as the conclusions are extracted from the results. However, two of them are explained on this part, as they are especially useful to solve some problems of the flux and balance of the car.

- **Improved rear bottom spoiler**

To lower the up force in the rear part, a different design of the rear bottom spoiler of the car could be proposed. The goal is to accelerate the flux in that part of the model, to lower the pressure and generate a downforce, improving the balance of the car. The effect is similar to the one achieved with the added rear spoiler of the first modification, but in this case affecting on the bottom part of the car. The negative influence on the drag coefficient may be lower with this alternative.

- **Little rear spoiler**

Other types of rear spoilers can be tested in order to reach the optimal solution with this component. Different shapes, sizes and even positions of this flag on the car can be simulated to know what is the best one for the aerodynamic balance of the vehicle. The simulated case was performed with one possibility, but this may not be the most efficient.

- **Redesign on the interior ducts**

In addition to the modification proposed previously, that was simulated, different solutions can be performed to improve the flux through the interior duct of the vehicle. Some of these possibilities can be to deviate part of the flux that goes on the upper duct to the wheelhouse zone, or to increase the two exits through the hood. This can make the flow easier, reducing the recirculation presented on the standard case.

- **Redesign of the lateral part**

Near the front wheel, on the analysis of the lateral flux, a recirculation has been found. The redesign of the surfaces on this zone, like the addition of a little wing on the border of the wheelhouse can improve this behaviour.

VII. RESULTS

In this part of the document, all the obtained results are shown, with its analysis and extracted conclusions. The base case and the modifications were simulated with the same solver and configuration, in order to have a good comparison between them.

On each case, the type of results that are shown can be divided into three groups: The numerical output, directly taken from AcuProbe that allow us to assign a value to some important parameters, the visual contours, taken from HyperMesh and the streamline images, useful to understand the behaviour of the flux on the studied model.

14. Results of the base case

14.1. Numerical output

One of the most important parameters that we can extract from the simulations are the aerodynamic coefficients. They allow comparing different cars and conditions, as they are dimensionless quantities. On the following table, the drag and lift coefficients obtained with the standard geometry are shown. As they do not depend on the velocity, the values are the same for both 160 and 275 km/h simulated cases. The force values are obtained from the AcuProbe software, as it was explained before. For each surface, the force can be calculated, the program uses the pressure and the area of each face to compute it. As the car geometry was divided on two halves, we can get the force values of each one independently. The aerodynamic coefficient is directly obtained from their definition expression, showed on the theory part, using the velocity of each case and the frontal area calculated with Virtual Wind Tunnel.

Drag coefficient C_x	0,28
Lift coefficient C_z	0,32
Front lift coefficient $C_z (f)$	-0,014
Rear lift coefficient $C_z (r)$	0,344

Table 14.1 : Aerodynamic coefficient of the base case

The base value of the drag coefficient shows the good design of this car, as it is quite low compared with other cars of the same size. However, we must notice that this model was simulated without rear views and other details that are not included.

On the other hand, the lift coefficient values show the existence of an up force on the rear part of the car. This is a usual problem on long cars as the one that is being studied. This force may be a serious problem at high velocities, as the grip with the ground decreases, as well as the stability under critical manoeuvres.

It is important to analyse if the force values are acceptable, taking into account the maximum velocities or the car's weight, and propose some modification if it is necessary.

On the following table, the force values corresponded with the previous coefficients are presented. In this case we have to distinguish between the two simulated cases as the force depend on the velocity to the power of two.

160 km/h case		275 km/h case	
Downforce front part	-48 N	Downforce front part	-120 N
Upforce rear part	980 N	Upforce rear part	2980 N
Maximum pressure	1394 Pa	Maximum pressure	4632 Pa

Table 14.2: Numerical results of the base case

On both cases, the values of the force on the front part are very low, but in either case negatives so they don't represent any problem for the car's behaviour. On the contrary, the rear part of the vehicle suffers a high up force, that at the maximum speed of 275 km/h corresponds with 300 kg. The weight of this car is very high due to the battery component and its general size, but 300 kg may represent dangerous conditions at this limit speeds.

Because of this, some modifications are proposed to try to lower this effect and improve the aerodynamic efficiency. To know what the best change is we can do on the design, several results are analyse on the following pages.

Together with the force values, the maximum pressure on each case was also obtained. This maximum value, as we will see on the following part, are located on the front spoiler of the car, and are important to see if the component is prepared to these conditions.

During the configuration of the model, the different components of the car were divided in order to be able at this point to separate their contributions on the forces acting on the entire car. The following table represent this analysis, contributions of each part to the drag and lift coefficients are shown.

Aerodynamic contribution	Cx	%	Cz	%
SpoilerFront	0,017	6.07%	-0,015	-4,60%
Rear bottom spoiler	0,031	11,06%	-0,062	-19,02%
SpoilerLateral	0,0002	0,07%	-0,013	-3,99%
Wheels and wheelhouse	0,06	21,41%	-0,05	-15,34%
Air ducts and Radiator	0,04	14,28%	0,01	3,07%
Skin and lights	0,114	40,69%	1,056	323,93%
Bottom car	0,018	6,42%	-0,6	-184,05%
Total	0,2802	100%	0,326	100%

Table 14.3 : Aerodynamic contributions in the base case

Several conclusions can be extracted from this table. On both coefficient, the biggest contribution is found on the exterior skin of the car, as it represents the mayor part of the geometry. Focusing on the other components, the rotating wheels have a big negative impact on the drag, this is the reason some super sportive cars cover their tyres in order to decrease it. The rear spoiler also generates a good contribution to the drag, due to the wake turbulent zone that is formed on this region. If the goal was to reduce the air resistance, a focus on these components would be a good choice.

Concerning the lift coefficient, it is clear that the bottom of the vehicle has a big impact due to the ground effect. The acceleration of the flux on this part is positive to reach a depression in the gap between the car and the road, generating a downforce on the model. The rear spoiler also has a good contribution on this coefficient, as it is at the end of the bottom part. On the first proposed modification, a little rear spoiler is added to increase the pressure difference and lower the up force we found on this zone. The updated table, with the modified contributions after this change are shown on its part of the results.

The contribution of the interior ducts and radiator is important, especially on the drag coefficient due to the high pressures that are reached on the front part of the car. This is a normal effect; high pressures facilitate the air inflow on these components, which is necessary for the refrigeration of the engine and suspensions.

14.2. Contour results

The contour results are a good instrument to study what is happening on the model. The images show what the problematic zones are and allow understanding visually the effects that the air generates on the car.

The following figures are obtained from the 275 km/h simulated case. The colour distributions are the same for any velocity, but it is important to consider that the numerical values that are showed on the scales of the images correspond with the maximum speed, which represent the most unfavourable conditions.

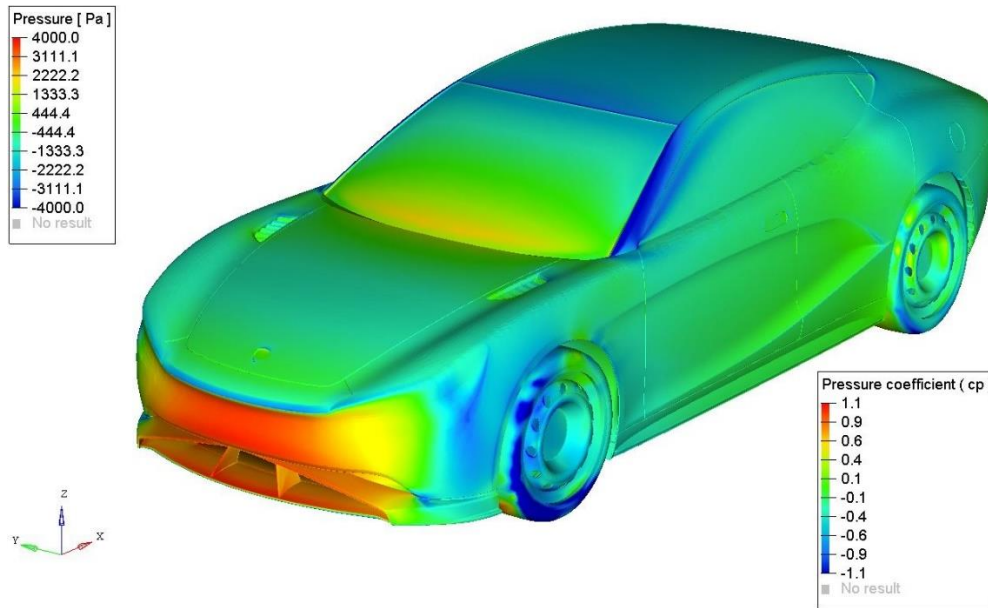


Figure 14.1 : Pressure contour

The pressure contour shown above is the typical it is found on a CFD analysis of a car. The maximum pressure value is found on the front spoiler, this is a good effect to facilitate the air inflow on the interior heat exchanger. On the other hand, the blue colour represent the parts with the lower value of the pressure. These zones are located on rounded shapes, as the tyres or the A pillar, because the flow accelerates generating a depression. The same contour is expressed with two different scales, as it is valid for both of them. On one hand we have the numerical values in Pascals, which would be different depending on the velocity. On the contrary, the pressure coefficient is a dimensionless value, explained on the theory part of this document, that will be the same on both cases. This last parameter is useful to make a comparison between different conditions and also car models.

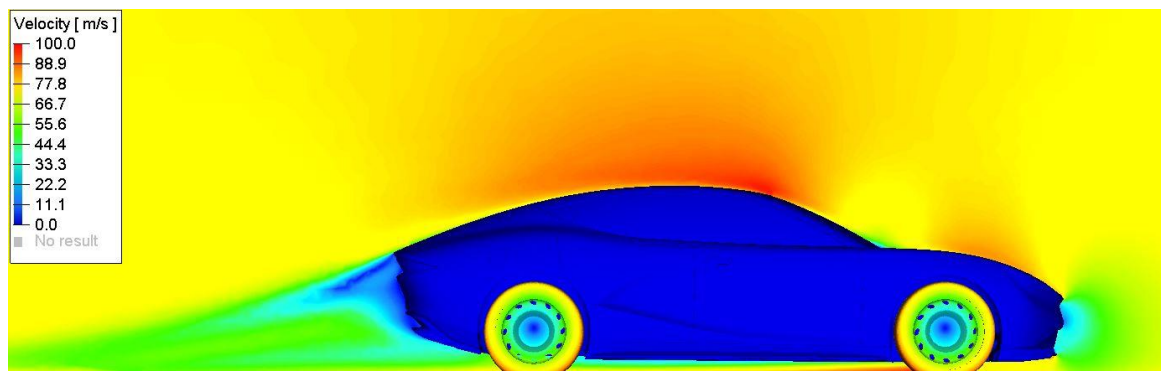


Figure 14.2 : Velocity contour

The velocity contour show the parts of the domain where the air flow decreases its speed, which may mean a separation from the surfaces of the car. Understand the point where this occurs is useful to know what the optimal position for the added rear spoiler is, that represent the first proposed modification. The wake zone on the downstream is easily seen on this contour, responsible of the mayor part of the drag force acting on the car. To see the effects the modifications have on this region is useful to see if the change is generating the effects we want to reach.

The acceleration of the air flux on the bottom part is also easily seen, but on the final part the air decelerated due to diffusor effect, this is one of the reasons of the high up force the model is suffering on its rear part.

Finally, we notice the rotation of the wheels with its centre in repose and the static rest of the car, as we have configured in AcuConsole.

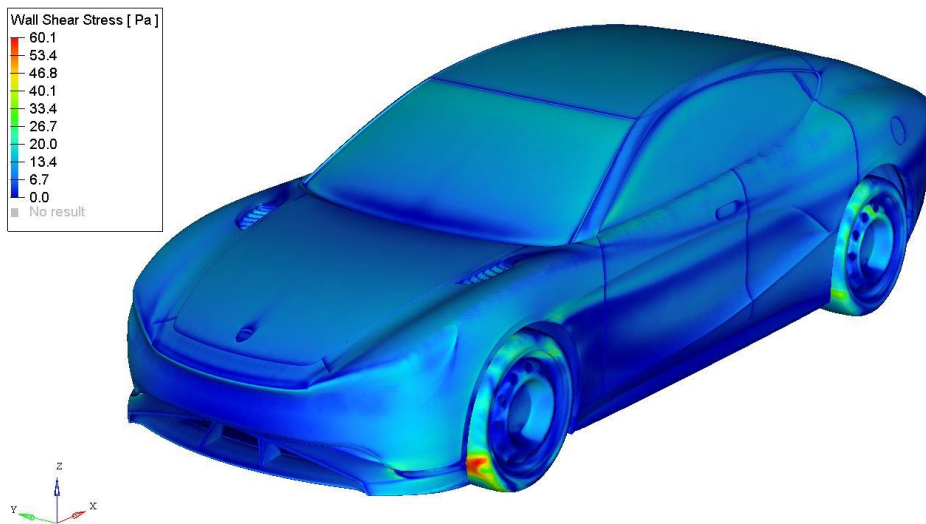


Figure 14.3 : Wall shear stress contour

The wall shear stress is a magnitude related with the tangential forces generated due to the friction between the fluid, in this case air, and the surfaces of the car. The value depends directly on the viscosity, therefore its effect on the behaviour of the car are not very important as air has very low viscosity. However, the contour shows the parts where the fluid has high speed, due to the curved surfaces the air encounters on its flow. These contours are then directly related with the pressure one, showed before.

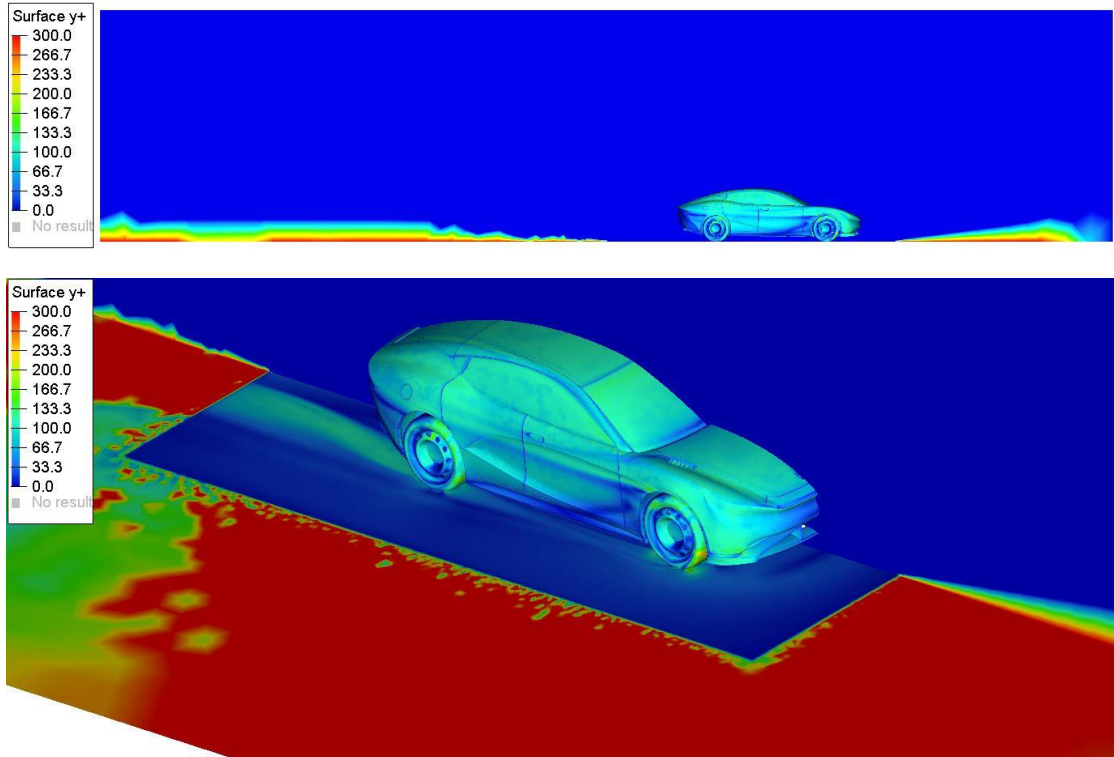


Figure 14.4 : Y-plus contours

The y-plus parameter should be lower than 300, and if possible lower than 100 in order to correctly take into account the viscous effects on the surfaces of the car. This is achieved, as we see on the above contours, thanks on the boundary layer created on all the vehicle's surfaces. The first element centroid distance to the wall is constraint to 0.5 mm and this assures a good y-plus parameter on the nearing of the car. From the contour, it is clear that the boundary layer was not created on all the domain ground, but only on the near zone of the model, to reduce the number of elements and computational time.

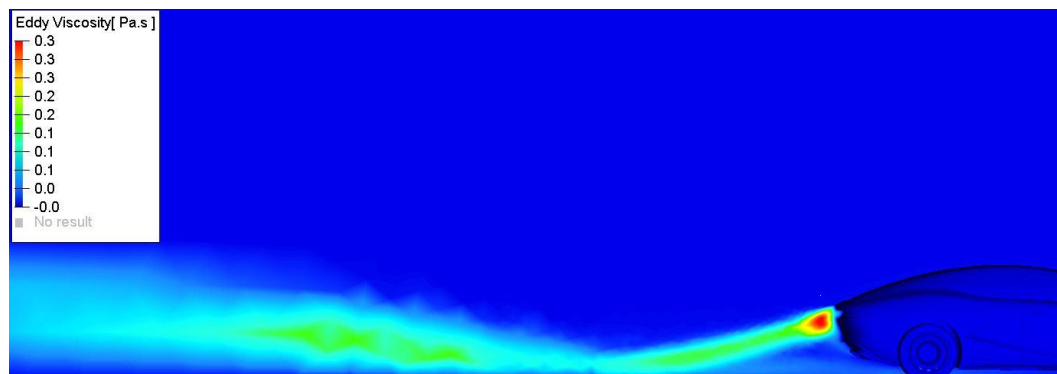


Figure 14.5 : Eddy viscosity contour

The eddy viscosity is a term added to the molecular viscosity in the momentum and energy equations to increase the stress values due to turbulent on the Spalart Almaras used model. This magnitude is useful to identify the parts where we have the highest turbulent effects. In this study, this corresponds mainly to the wake zone, on the downstream zone. After the addition of the little rear spoiler on the first modification, it is useful to compare the eddy viscosity contours, to see how the wake zone is increasing due to the new component.

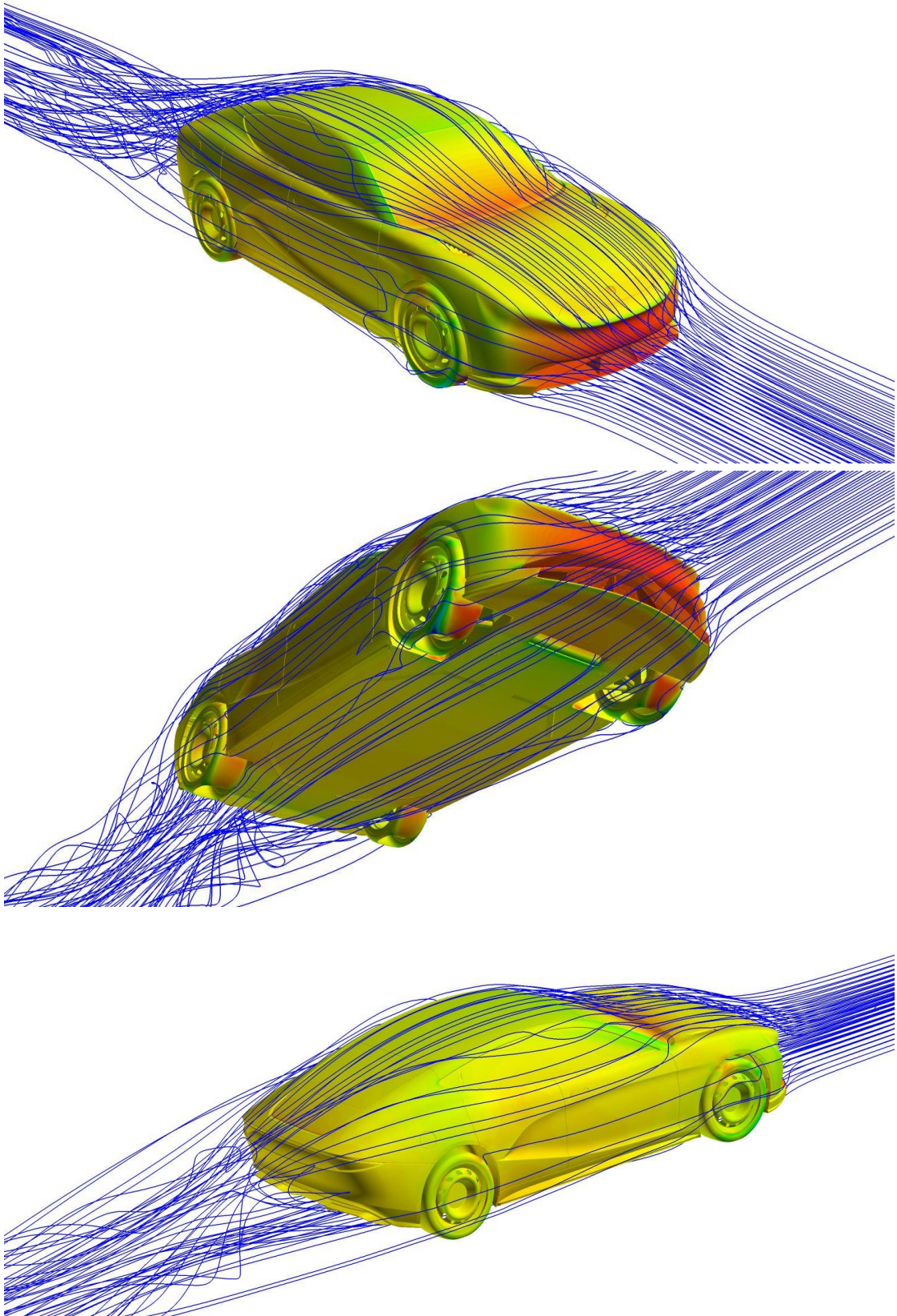
14.3. Streamlines of the air flux

The images and animations of the streamlines that can be extracted from the AcuFieldView software are very useful to understand how the air flux around the car on the simulated conditions is. On this part of the results chapter, we focus on the exterior general air flow and then on the interior parts of the vehicle, where the air enters and passes through the heat exchanger. This analysis allows to identify the problem due to possible flow separations or recirculation.

As in the contour figures of the previous part, the streamlines correspond with the 275 km/h simulated case, the most unfavourable one. However, the streamlines will look the same on either velocity.

It is important to notice that the flow showed on the program is generated introducing some points that are used as the origin of the streamline. Therefore, depending on the chosen points, the obtained image will be different. The results showed here were obtained after trying several origin options, to be sure of analysing completely the effects that take place.

On the first five figures, the external flux is represented. As we can see, the air follows the car shapes in a correct way. However, we notice a strange effect on the lateral side of the car, due to this, a more specific study has been done in order to understand what is happening. Besides, on the downstream zone, the flux recirculated and show a turbulent behaviour. These normal effects were already notice on the eddy viscosity and velocity contours, but at this point we see how is the real trajectory of the air particles.



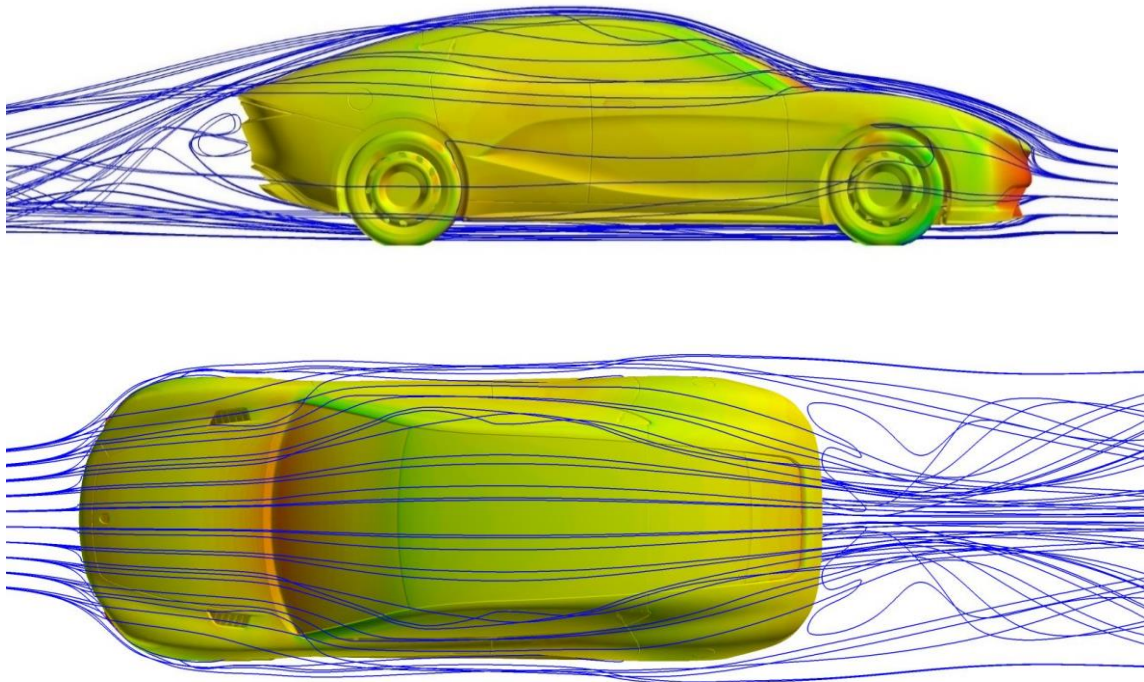


Figure 14.6 : Streamlines of the exterior air flux

The following three figures focus on the interior flux through the heat exchanger component. As we see, the flux enters on the front air ducts, passes through the radiator and then is divided into the upper and lower air ducts. The lower one seems to have a good behaviour, as no recirculation is taking place. However, on the upper duct, the flux experiments a low pressure and recirculates on a specific part. This decrease of pressure may be caused by the area increase after the heat exchanger. Two possible solutions are proposed in order to improve this behaviour. The first one, to decrease the area of the upper duct increasing the lower one, to make the flow easier on the upper half. The second one is to recirculate part of the flux on the upper duct to the wheelhouses, as it is a zone with a low pressure, making the exit of the air very easy. These modifications are explained on the conclusions of the document in more detail. These two possibilities were not simulated due to lack of time, but represent future work to be done after this project.

The flow on the brake ducts are not represented, to make the image clearer. On these zones the flux is generally acceptable, even though some recirculation take place, something that in many cases are not avoidable.

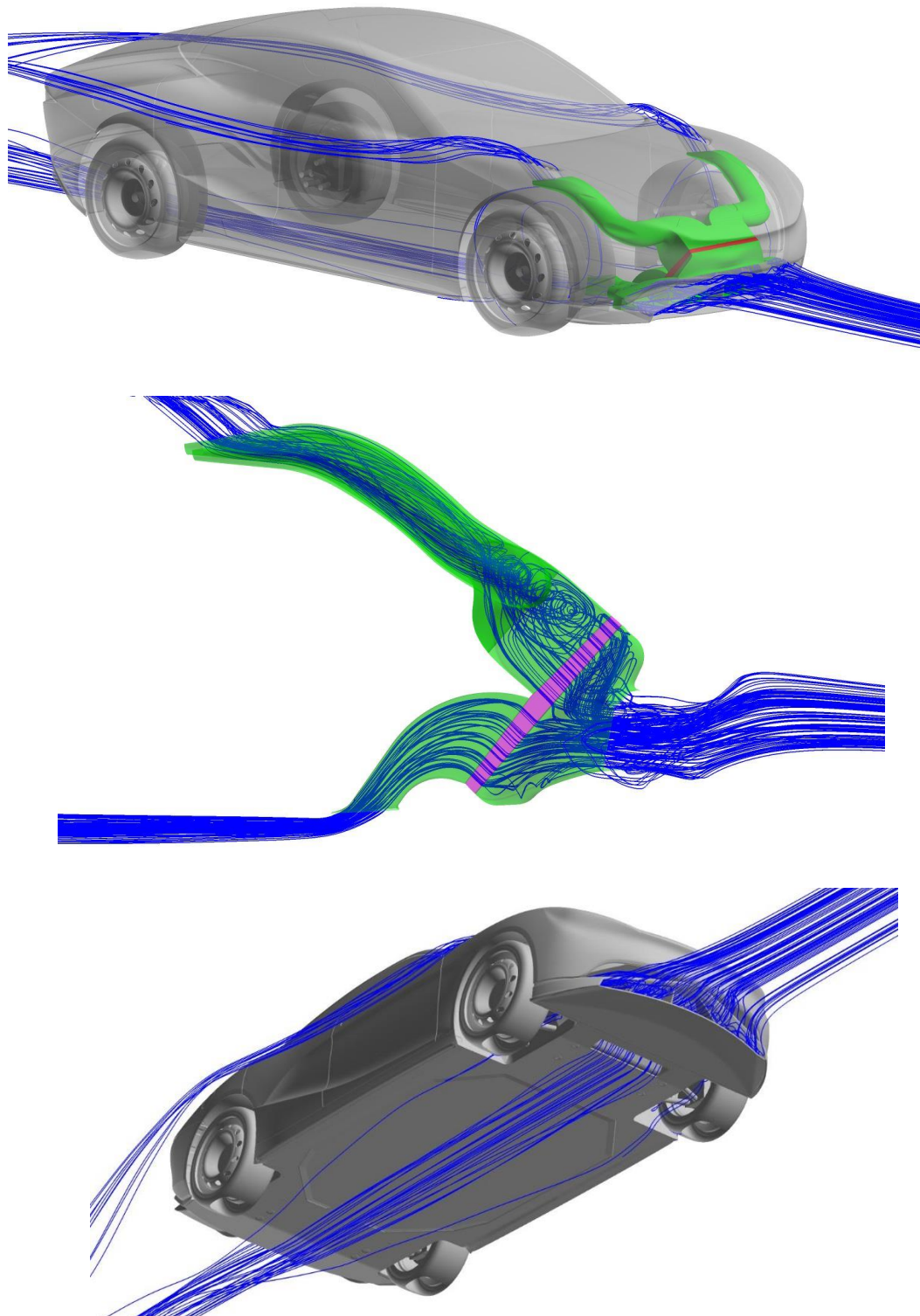


Figure 14.7 : Streamlines through the interior ducts of the car

14.4. Pressure profiles

Pressure profiles represent the trend of the pressure at some points of the car's surfaces. They are useful to identify the parts that may be causing a problem. In this case, the decision to show them is mainly related with the up force that we noticed on our numerical output on the rear half of the car. This negative result is caused by the low pressure that is found on the upper rear part. Seeing the curve, on its 'rear' segment, we appreciate a decrease on the pressure near the final part. The addition of an extra component as a little spoiler may improve the curve and the up force value that was found, decreasing it.

In the first modification part of the document, the pressure profiles before and after the addition of the rear spoiler are compared, to see how is the contribution of the new component.

Besides, on the ground surfaces, a deceleration of the air flux can be noticed, as the pressure increase progressively. This is mainly caused by the inclination of the vehicle. Also, the air that flows through the lower air duct, that could be seen before on the figure 13.7, can help to accelerate the lower flux and therefore improve the load balance of the car.

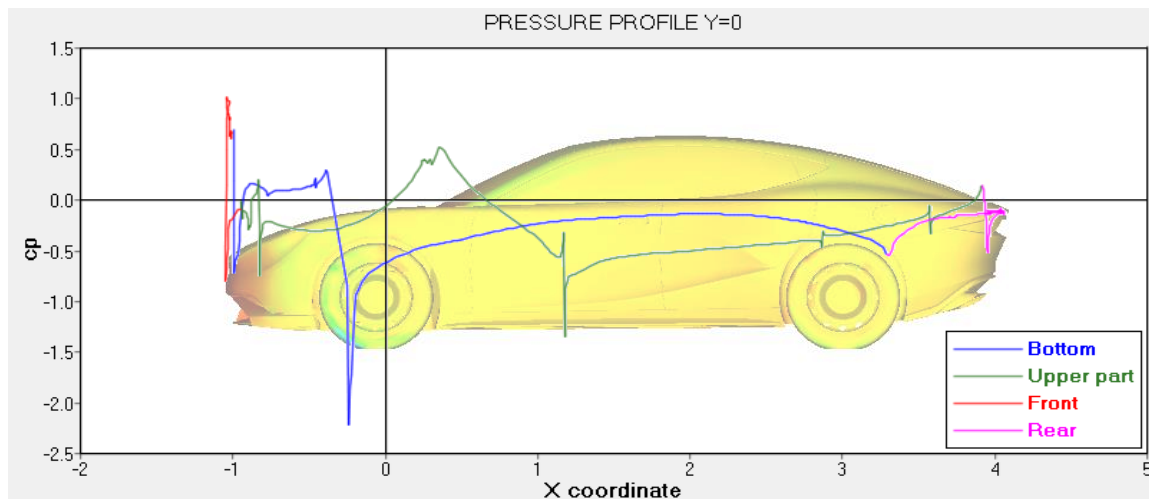


Figure 14.8 : Pressure profile of the standard geometry

Windows are an important component to take into account, especially at very high velocities where the effect that the pressure generates can be dangerous for the stability of the glass. For this reason, it is usual to see the trend of the pressure at some nodes situated at a certain distance with respect to the upper beam, In this case, one centimetre.

The most unfavourable point is located near the front limit of the window, where the pressure reaches the minimum value. These conditions are related with the maximum velocity of 275 km/h, and does not represent a dangerous result.

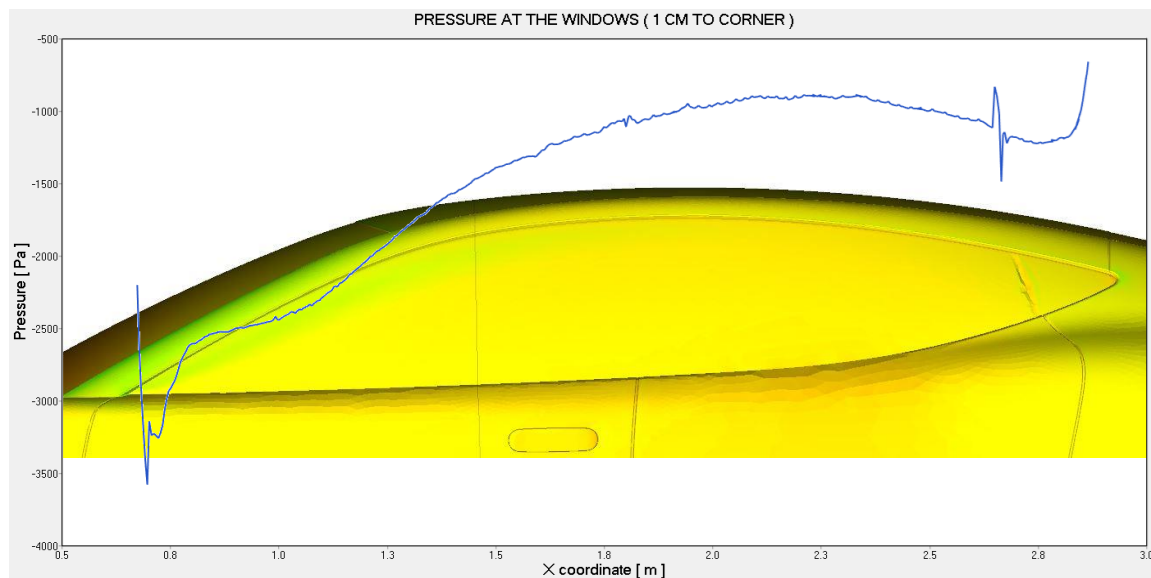


Figure 14.9 : Pressure value at 1 cm from the window corner

14.5. Study of the lateral flux

To analyse the lateral flux on the car, the following figures with pressure profiles and streamlines on this part were obtained. This study allows to know if there is some recirculation, especially on the upper wheel, and to propose some modification if it is necessary.

On the following figures, the pressure profiles on lateral points at four different heights were obtained. A low-pressure value could mean that the flux is recirculating

on that part. This can cause some problem that cannot be neglected, as the difficulty to refrigerate the suspensions and brakes or the generate noise.

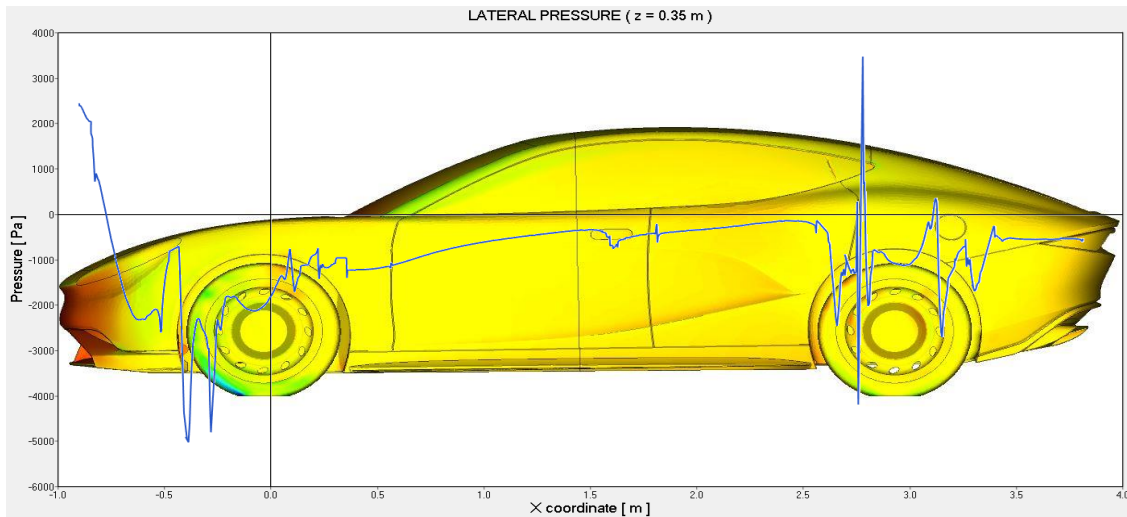


Figure 14.10 : Lateral pressure at z = 0.35 m

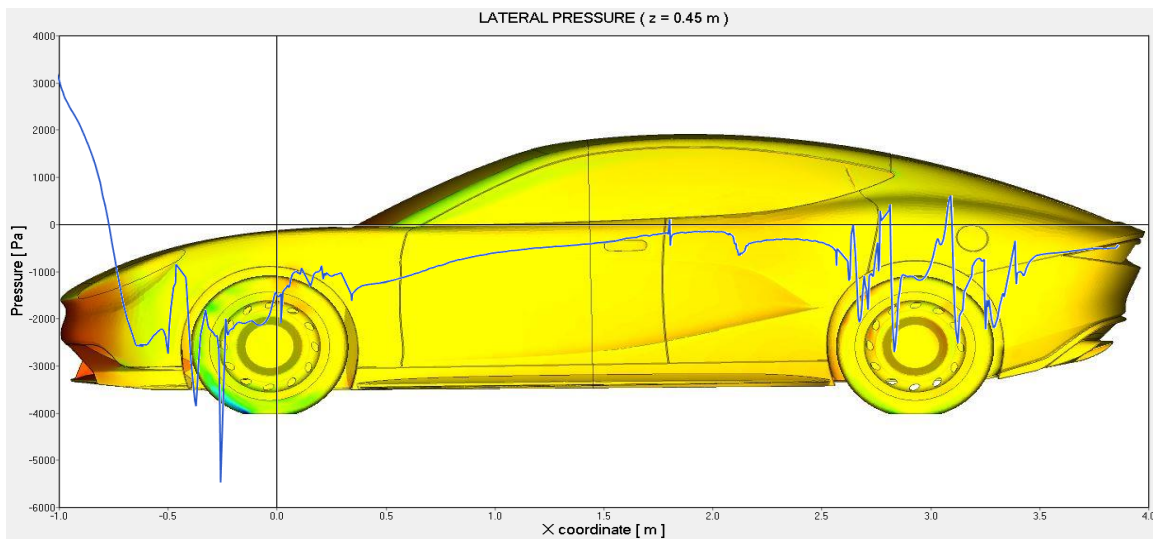


Figure 14.11 : Lateral pressure at z = 0.45 m

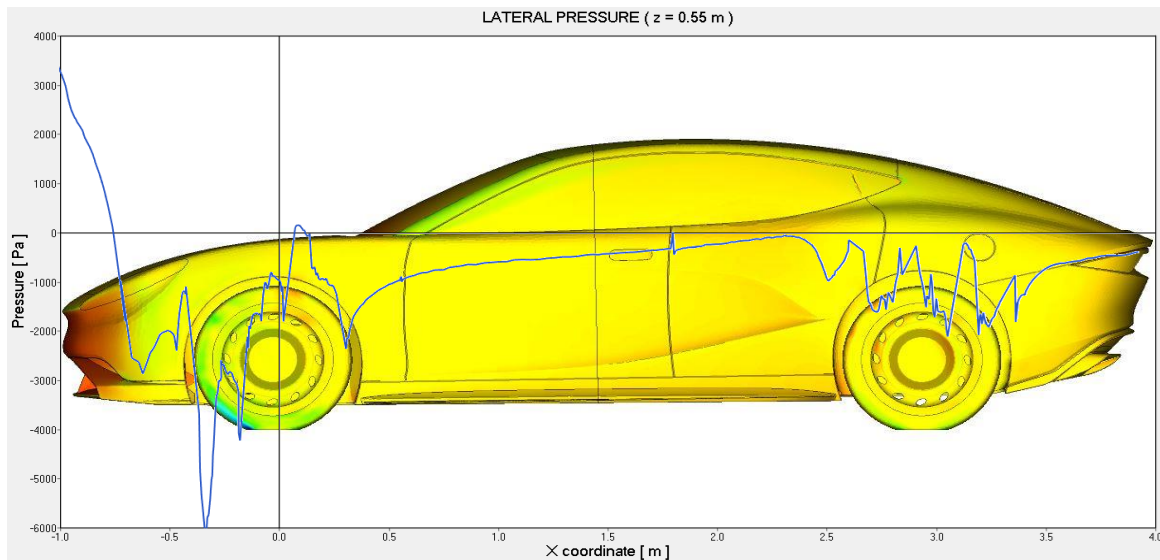


Figure 14.12 : Lateral pressure at z = 0.55 m

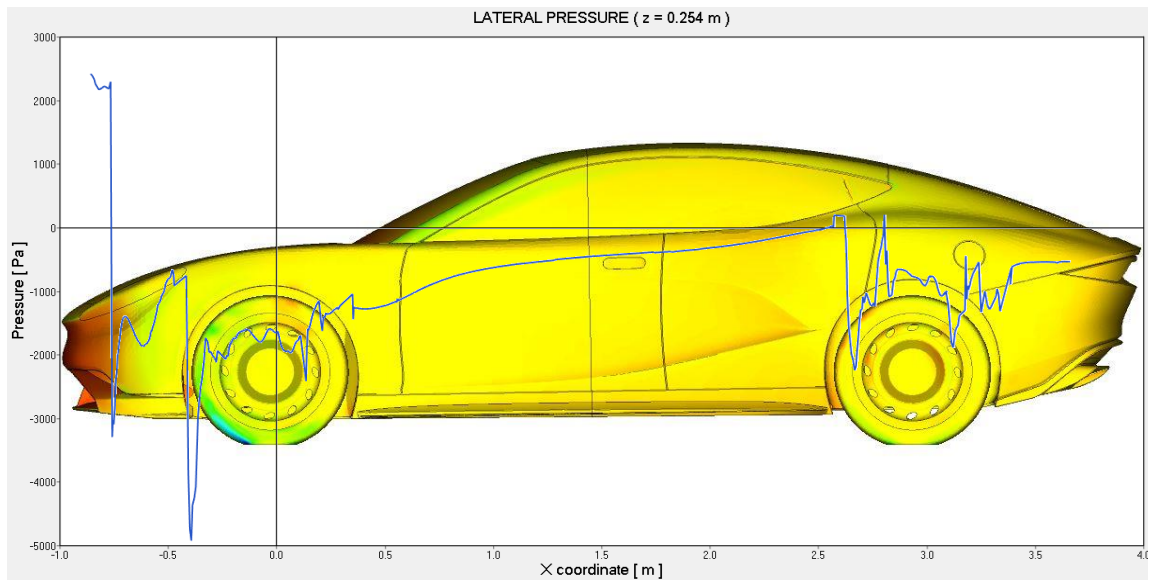


Figure 14.13 : Lateral pressure at z = 0.254 m

The streamlines images show this recirculating zone near the front axis of the car. A redesign of the lateral spoiler may help to solve at least partially this phenomenon. Besides, the figures show the trajectory of the flux that exit through the hood air outlets, which seems to be not problematic.

The streamlines showed here do not correspond with the total flux around the car, but just the portion that flown on the lateral sides of the vehicle.

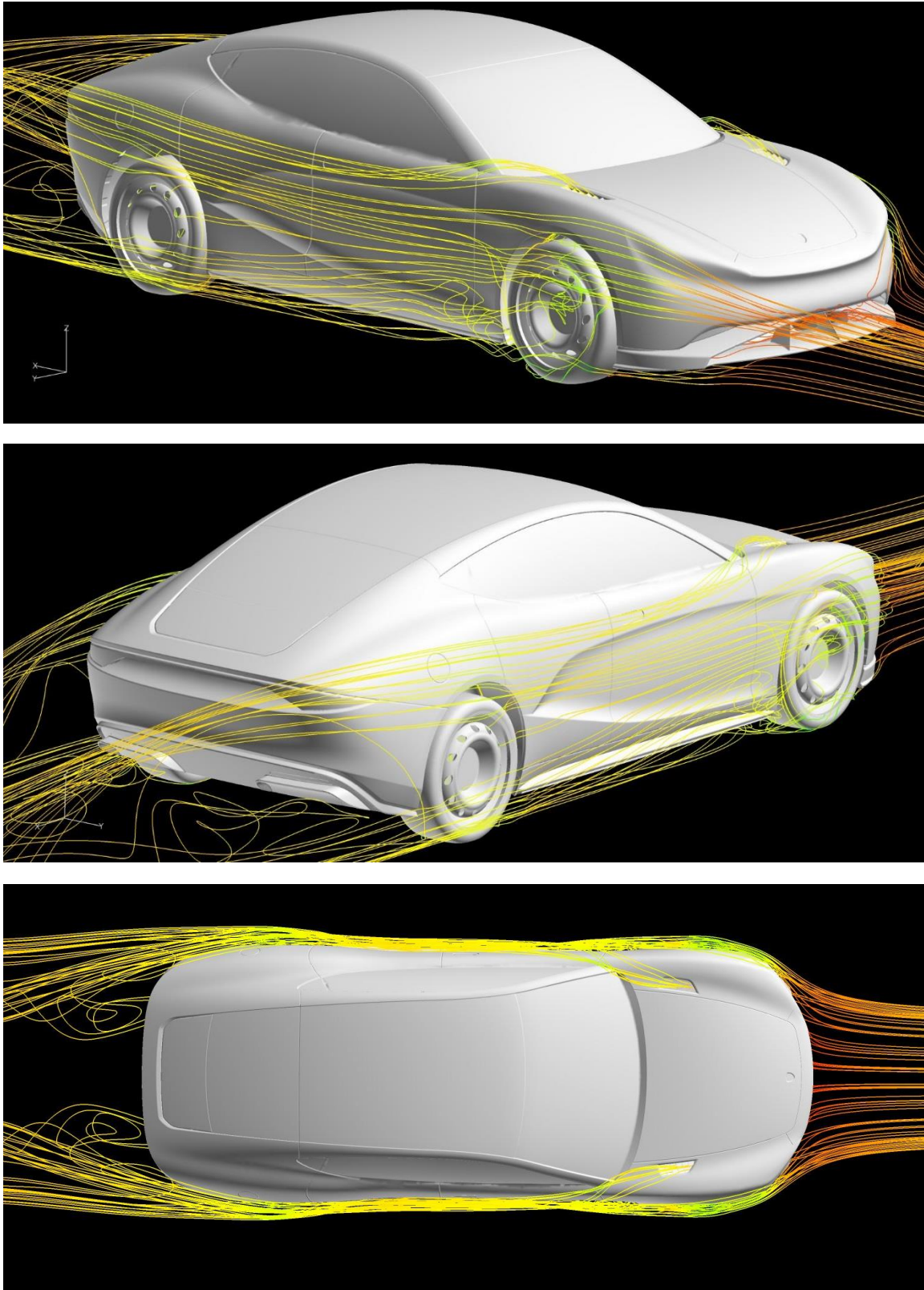


Figure 14.14 : Exterior streamlines of the lateral flux

15. Results of the proposed modifications

On this part of the results, the output taken from the two proposed modifications that have been simulated is shown. Other change possibilities, that were not simulated, are explained on the conclusions of the document.

On several points, the figures show a comparison of the new reached behaviour with respect to the standard case, which was widely discussed before.

15.1. Results with the added rear spoiler

The added rear spoiler is included in the model to try to decrease the high up force that acts on the rear part of the car. The high pressure that this element creates can help to achieve this purpose.

On the following table, the main numerical values extracted from the simulation are shown, compared with the same ones of the standard case to see the actual change.

76.4 m/s	Without rear spoiler	With rear spoiler
Drag coefficient C_x	0,28	0.305
Lift coefficient C_z	0,32	0.287
Front lift coefficient $C_z(f)$	-0,014	-0.02
Rear lift coefficient $C_z(r)$	0,344	0.307
Rear force $F_z(r)$ [N]	2980	2666

Table 15.1 : Numerical comparison with the added rear spoiler

As we see, the new lift coefficient has decrease thanks to the effect of the new spoiler. This change is mainly localized on the rear part, where the new component is situated; therefore, the up force has decreased from 2980 N to 2666 N, which

represents an improvement of the 10%. On the other hand, we also have a negative effect; the drag coefficient has increased, as expected, from 0.279 to 0.305.

If we take all into account, the addition of this spoiler may not be favourable as the decreasing on the rear up force was not notable enough. However, the modification achieved partially the desired goal, and further changes on this idea, as the place where the spoiler is located or its size and form, could mean a good improvement on the car's balance.

Other possibilities to reduce the rear up force may be more favourable, as the drag coefficient should, if possible, not be increased too much. These alternative modifications could be to redesign the bottom rear spoiler, which as a big impact on the lift coefficient, or the ground of the vehicle, part that does not have a big impact on the drag.

Aerodynamic contribution	C_x	%	C_z	%
SpoilerFront	0.015	4.91%	-0.02	-6.96%
Rear bottom spoiler	0.038	12.43%	-0.05	-17.40%
SpoilerLateral	0.0003	0.10%	-0.008	-2.78%
Wheels and wheelhouse	0.068	22.24%	-0.045	-15.66%
Air ducts and Radiator	0.04	13.08%	0.0094	3.27%
Skin and lights	0.125	40.88%	0.996	346.56%
Bottom car	0.0185	6.05%	-0.59	-205.29%
Rear added spoiler	0.001	0.33%	-0.005	-1.74%
Total	0.305	100.00%	0.287	100.00%

Table 15.2 : Aerodynamic contributions with the rear spoiler

As it was done for the standard case, the contributions of each component on the drag and lift coefficients is represented on the previous table. The new spoiler helps to decrease the up force located in the rear half of the vehicle, as it created a high-pressure region. From the values on the table, the contribution of the little added spoiler may seem very low, but this is because the high-pressure region affects not only the new component but also other surfaces on the car, as it will be seen in the following figures.

The rest of the values remain very similar compared to the base case. The increase of the drag coefficient can be located on the rear bottom spoiler and the rest of surfaces on that part, due to the increase of the wake zone generated by the new component.

On the following figure, the pressure contour focused on the location of the new spoiler are shown. The analysis of this contour is important in order to know which is the best position to locate the new element. Once this position was known, on the zone with the low pressure as we see on the image of the left, the simulation was performed, and the result was the expected. As it was explained before, it can be noticed that the region with the high pressure does not only affect the new spoiler, but also other surfaces near it.

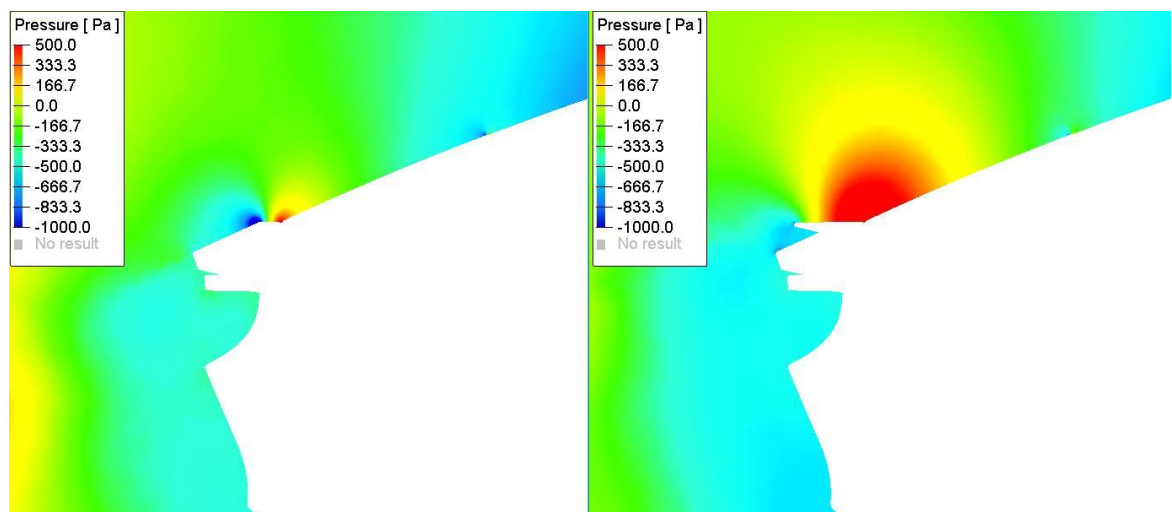


Figure 15.1 : Pressure comparison with the rear spoiler

The addition of the rear spoiler also causes a negative effect, the increase of the drag acting on the car. This is due to the new wake zone generated with the modified geometry. The region with low pressure increased in comparison with the standard simulation, and the forces acting on the car on the movement direction as well. The change on the downstream of the vehicle is clearly seen on the two following figures.

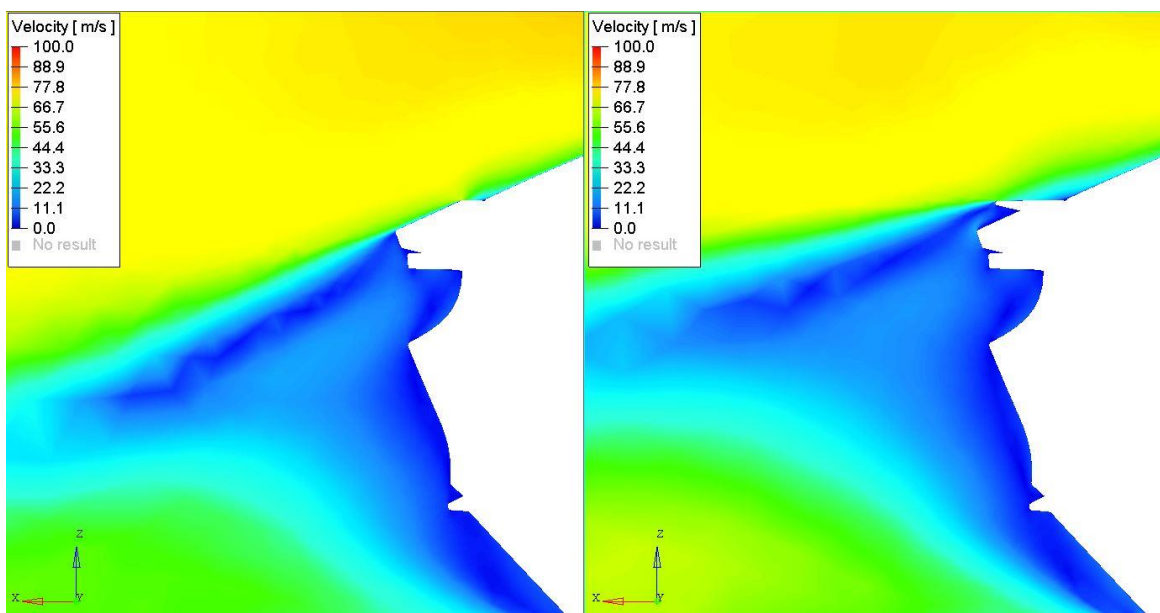


Figure 15.2 . Velocity comparison with the rear spoiler

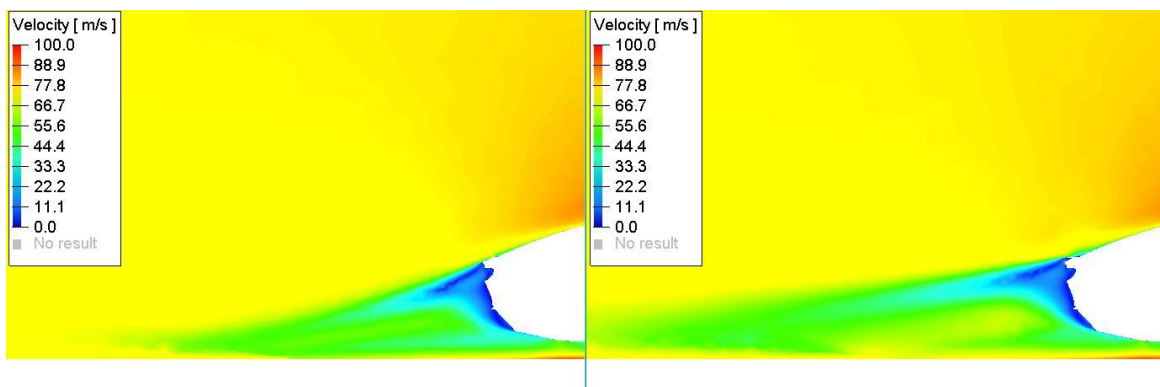


Figure 15.3 : Wake zone comparison with the rear spoiler

Pressure values on the top of the new spoiler have increased compared with the base case. The following figure illustrate this reality. As we see, the scale used on both images is the same, and the change can also be noticed visually.

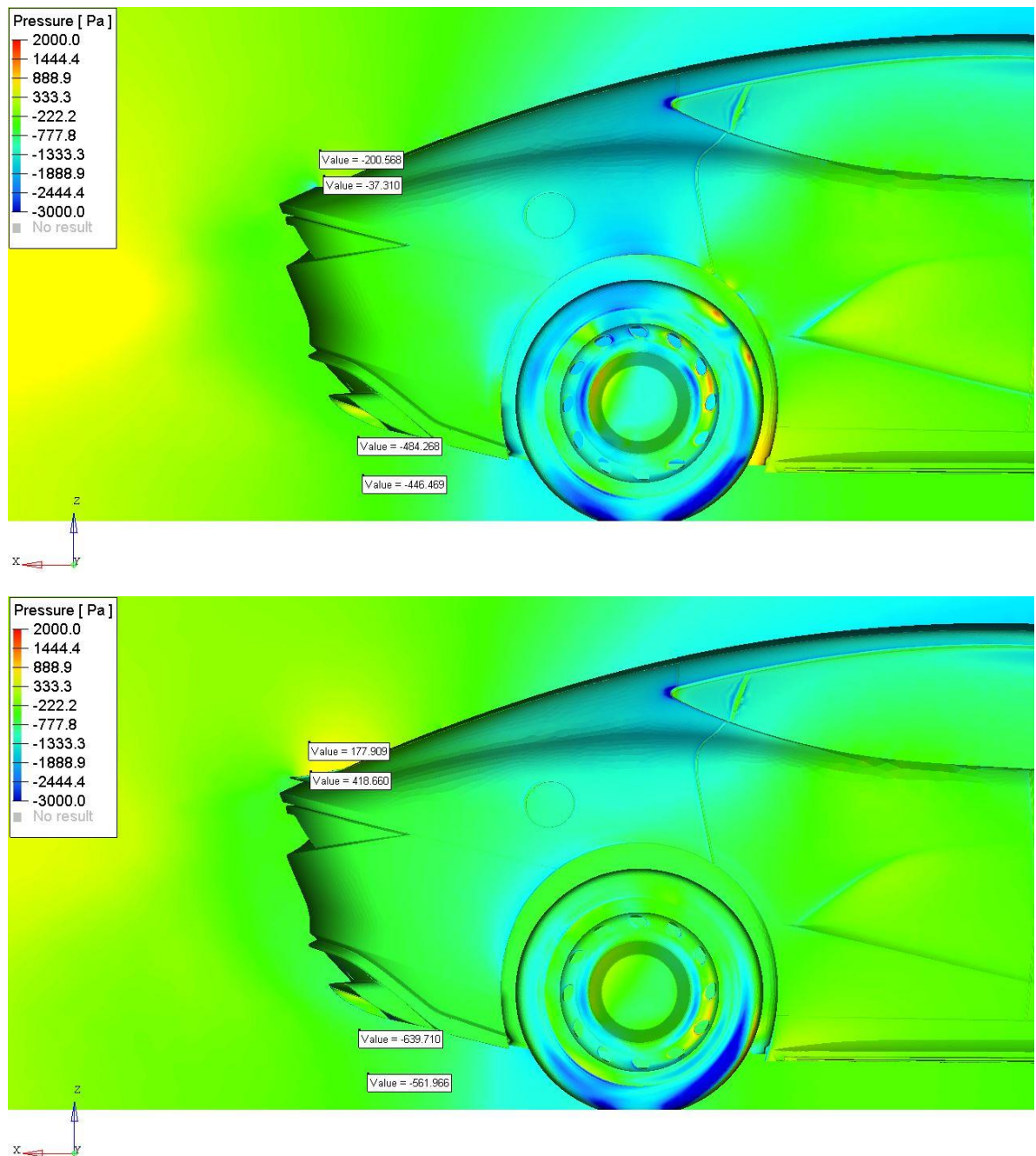


Figure 15.4 . Pressure values comparison

A pressure contour taken from an isometric view before and after the modification is shown on the next figure. We clearly see that on the new component a high pressure is acting on most of its surface. If this was not the case, the chosen position may not be the optimal one. Also, the shape or size of the spoiler can be discussed after the analysis of this type of contour results.

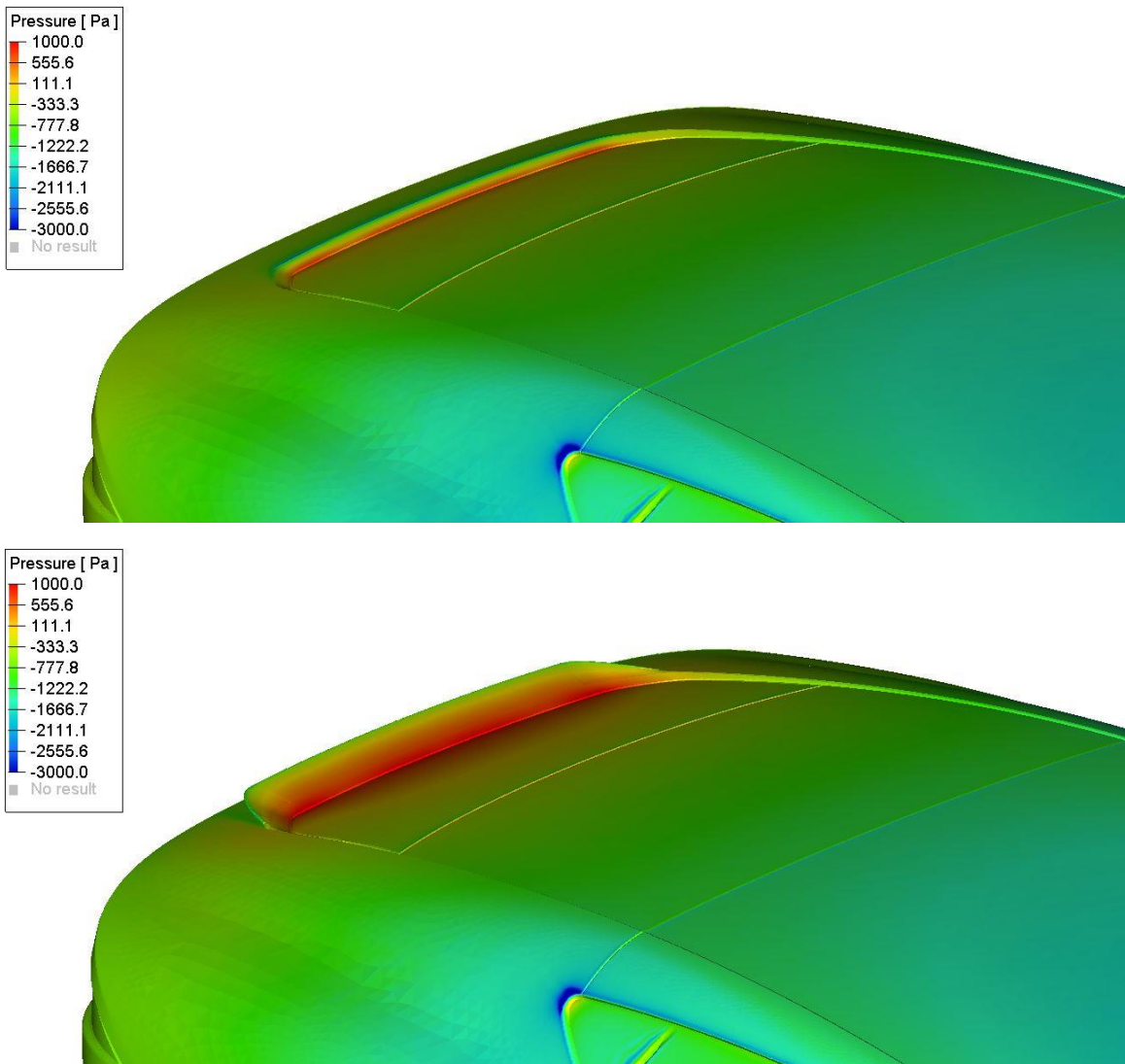


Figure 15.5 : Pressure contour comparison

As we saw in the standard simulation, the eddy viscosity is a useful parameter to notice what are the part with high turbulence behaviour. In this case it shows the drastic change after the modification.

This turbulence on the rear part influence highly on the drag force the car have to face to move within the air flow. Besides, noise can be generated and therefore the comfort and security of the passengers can also be negatively affected.

For this reason, the addition of the rear spoiler are a compromise between the reduction of the rear up force we obtain, and the drawbacks we encounter with its installation.

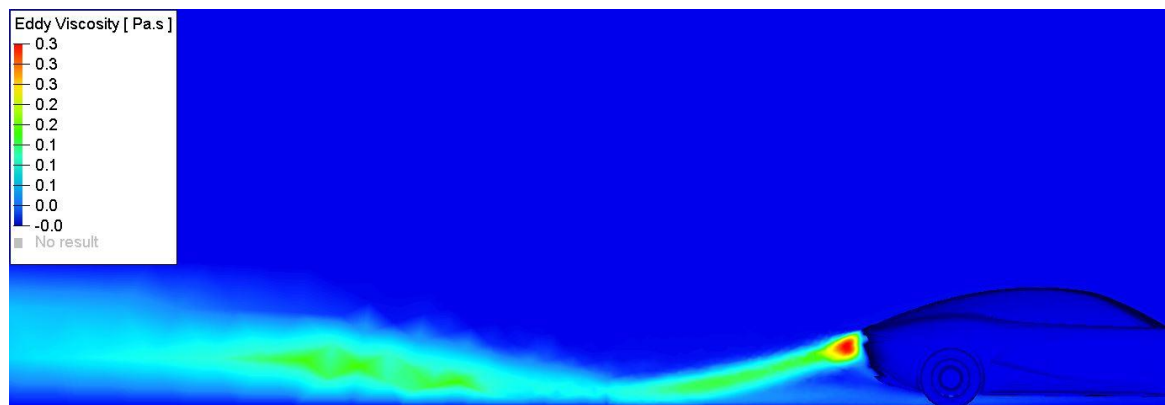


Figure 15.6 : Eddy viscosity contour without the rear spoiler

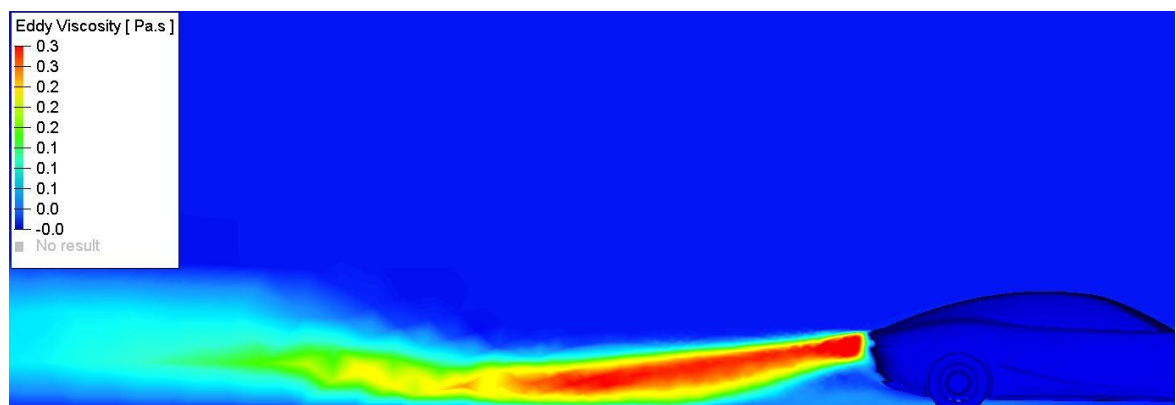


Figure 15.7 : Eddy viscosity contour with the rear spoiler

The following figure shows the streamlines of the upper flux of the car focused on the position of the spoiler. On the first one, the base case, a separation can be noticed before the end of the vehicle. The new component solved this, as we see the air flux adapts its trajectory.

This is the reason why after the installation of the new component the pressure on its rear part result to be higher in comparison with the base case.

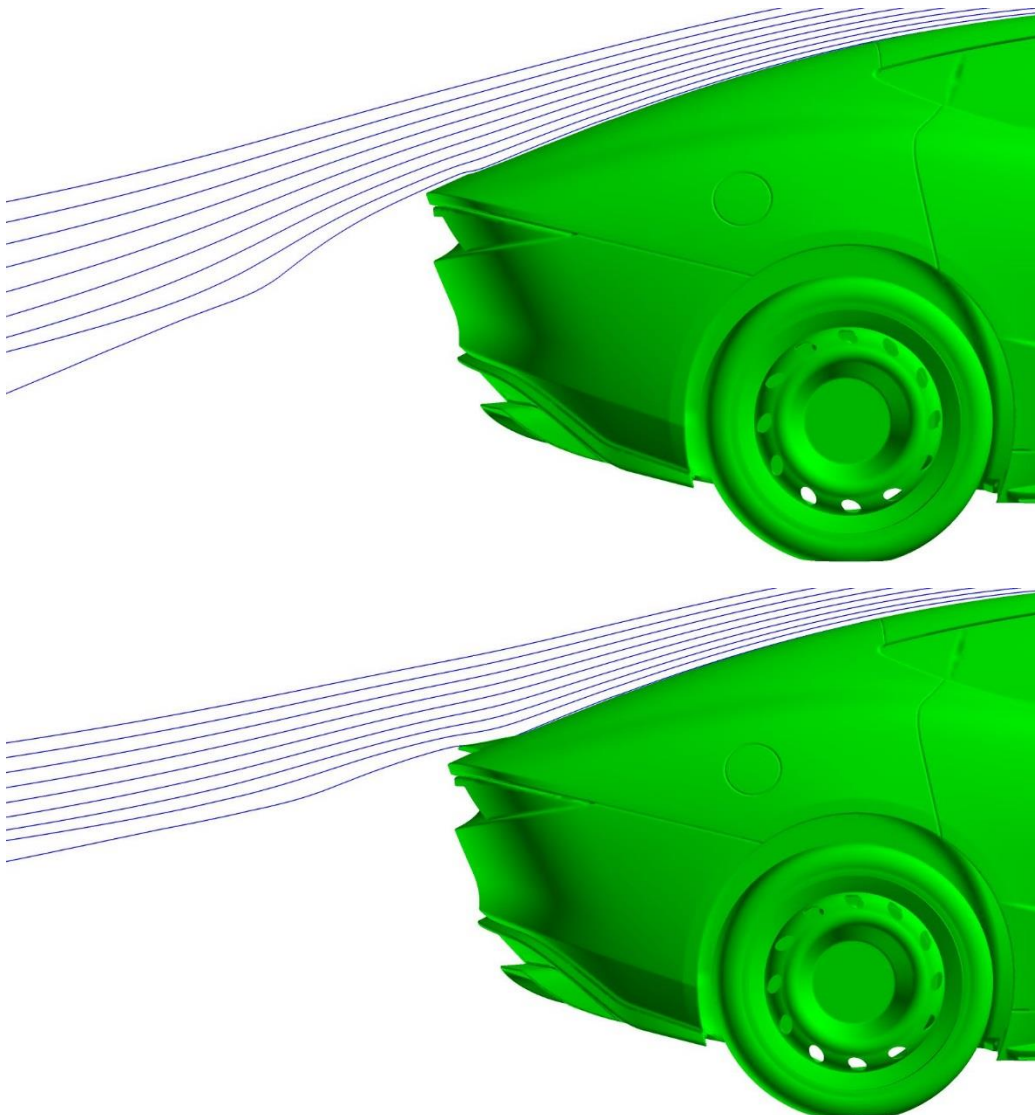


Figure 15.8 : Streamline comparison with the rear spoiler

Finally, the comparison between the two cases is also done with the pressure profile around the car on a middle cutting plane. The only part that changes, as expected, is the location of the new spoiler. The pressure, or in this case the dimensionless pressure coefficient, increase on this part, contributing to lower the existing up force presented on the standard geometry of the car.

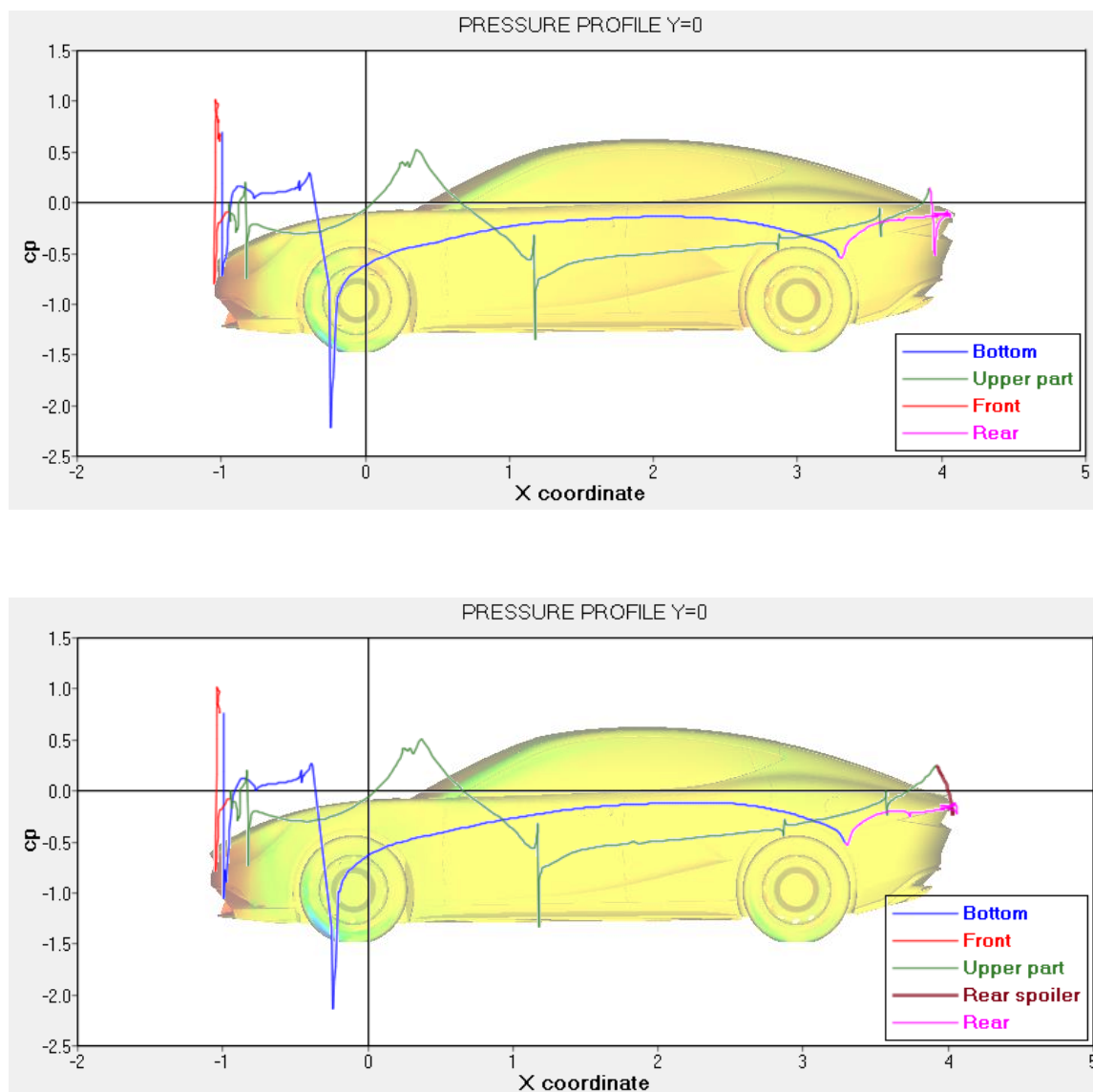


Figure 15.9 : Pressure profile comparison

15.2. Results with the different car inclination

The second modification consisted on a variation of the car inclination. The goal of this change is the achieve an acceleration of the lower flux in order to decrease the pressure on this gap and consequently increase the downforce.

The objective is to solve the high up force in the rear part, but this kind of modification affects all the vehicle, as we see on the following table.

76.4 m/s	Without inclination	With inclination
Drag coefficient C_x	0.28	0.307
Lift coefficient C_z	0.33	0.157
Front lift coefficient $C_z(f)$	-0.014	-0.126
Rear lift coefficient $C_z(r)$	0.344	0.283
Rear force $F_z(r)$ [N]	2980 N	2456 N

Figure 15.10 : Numerical results with the modified inclination

The lift coefficient values have decreased, both on front and rear parts, due to the acceleration of the flux on the bottom zone. On the other hand, the drag coefficient increases more or less the same quantity as with the added rear spoiler. Is impossible to improve everything, we have to 'pay' with something, but in general terms this modification gives better results compared with the previous one.

The up force acting on the rear half of the vehicle, which is the critical parameter, is decreased from 2980 N of the base case to 2456 N on this modification. This change represents an improvement of 17.6 %.

Aerodynamic contribution	Cx	%	Cz	%
SpoilerFront	0,017	5,55%	-0,022	-13,96%
Rear bottom spoiler	0,036	11,76%	-0,067	-42,51%
SpoilerLateral	0,00017	0,06%	-0,014	-8,88%
Wheels and wheelhouse	0,07	22,86%	-0,082	-52,03%
Air ducts and Radiator	0,041	13,39%	0,0096	6,09%
Skin and lights	0,127	41,48%	1,023	649,11%
Bottom car	0,015	4,90%	-0,69	-437,82%
Total	0,3062	100,00%	0,1576	100,00%

Table 15.3 : Aerodynamic contributions with the changed inclination

In this case the contributions of each component to the drag and lift coefficient changed generally compared with the standard geometry as the new modification affects to all the vehicle.

To fully understand what is changing with the new inclination, several contours have been extracted and compared with the equivalent one of the base simulation.

All surfaces of the bottom of the car are after the modification at the same height with respect to the road. This avoids the deceleration that took place before, as the frontal area that the air founded on its movement was increasing on its way to the end of the vehicle. This change on the velocity magnitude is shown of the following figure. It may be difficult to notice just visually because both contours are very similar. For this reason, the next two figures represent the same contour, focused on the rear part of the vehicle, with some values of the velocity magnitude plotted.

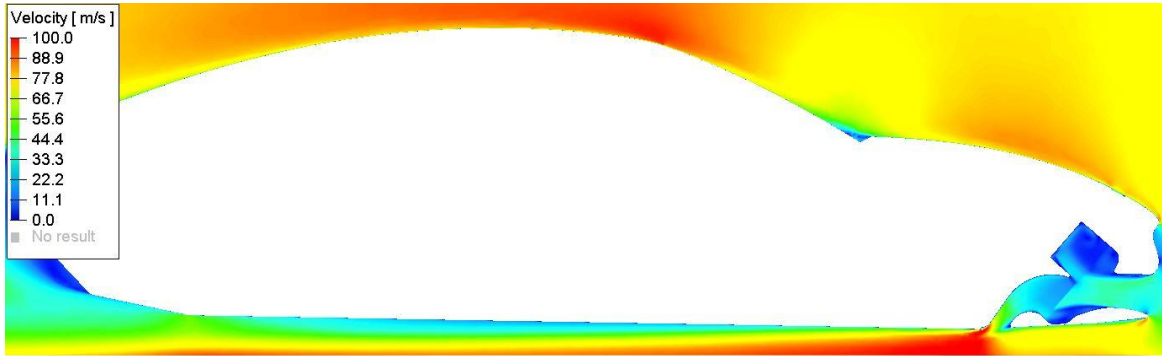


Figure 15.11 : Velocity contour in the base case

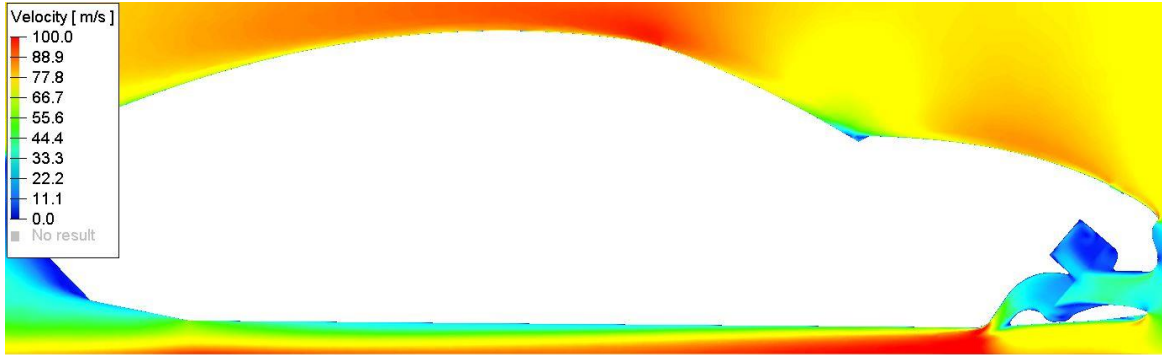


Figure 15.12 : Velocity contour after the inclination

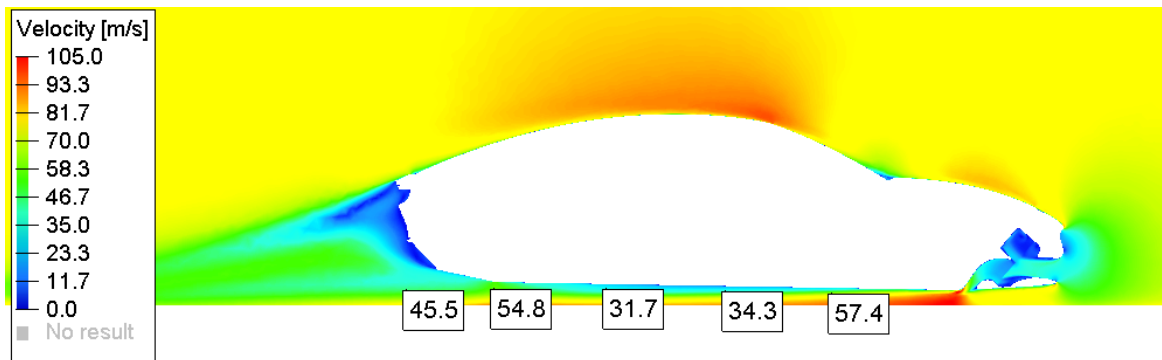


Figure 15.13 : Velocity values in the base case

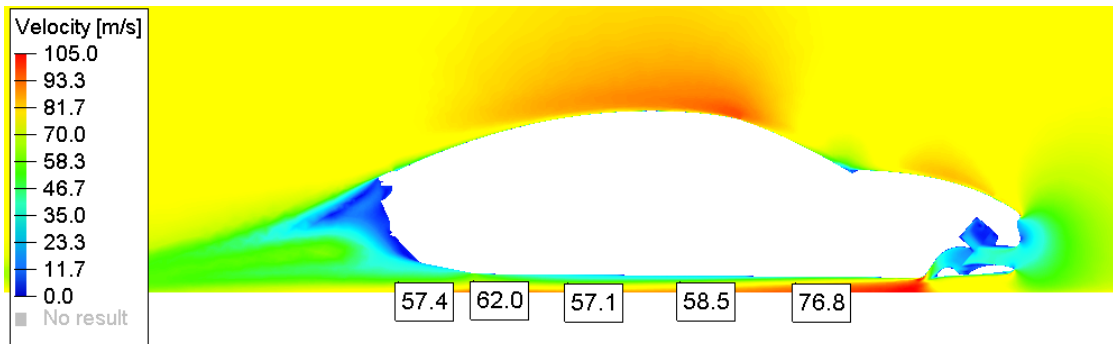


Figure 15.14 : Velocity values after the inclination

Several values can be showed to notice this effect. In this case, the same coordinated where used to report in an accurate form the increase of the flow velocity after the modification of the inclination of the vehicle.

Additionally, the pressure contours of this part of the vehicle are shown. As we see by the represented values, the pressure has clearly decreased, as expected, due to the higher velocity on the same zone.

This dependence between the velocity and the pressure was previously explained on the theory part of this document. Both magnitudes are strictly correlated and the effect on the velocity that was achieved with the new inclination also means a decrease on the pressure at the road-car gap.

A low pressure on this zone helps to amplify the so-called ground effect, which is responsible of most of the downforce the vehicle is able to generate.

As in the velocity case, some node values are shown to compare both cases. The scale on both figure was forced to be equal to make possible also a visual comparison.

Even of the difference is not as big as could be, we can conclude that the modification helped to achieved the desired effect, something that can be also proved from the numerical results previously shown.

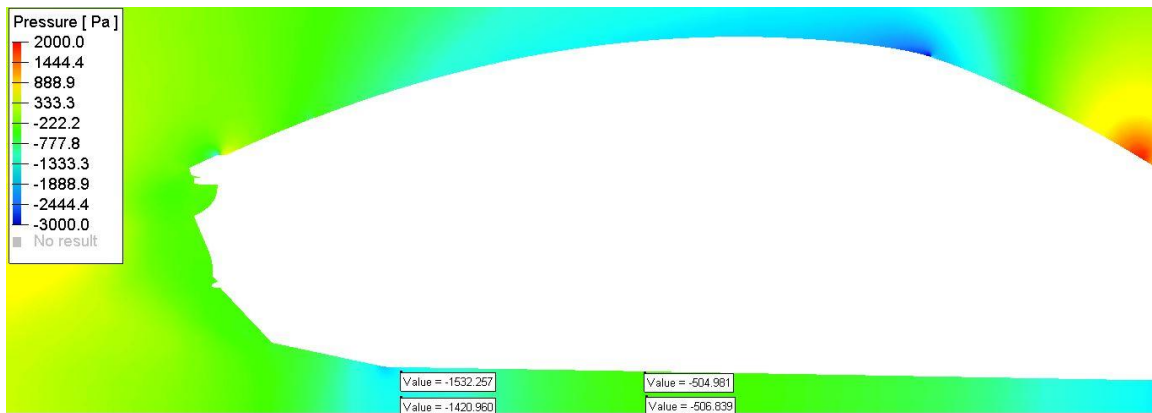


Figure 15.15 : Pressure values in the base case

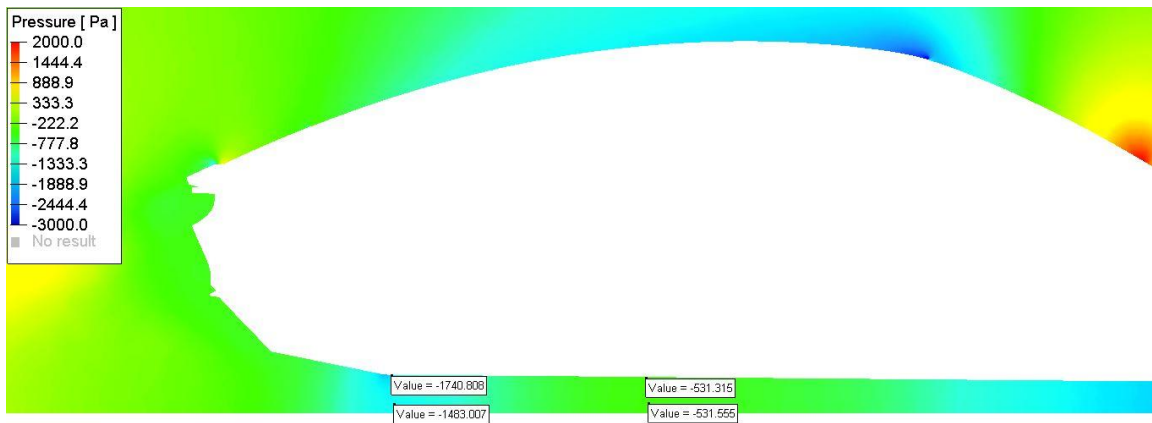


Figure 15.16 : Pressure values after the inclination

15.3. Results with optimized air ducts

The third modification consisted on the change of the internal air ducts of the car, trying to reduce the recirculation that was founded on the base case. The proposed solution was to reduce by a 20% the area on the upper duct, increasing the lower one. Additionally, the curvature of the duct on the radiator inlet was changed to reduce the separation that was founded, helping the fluid to follow the interior shapes. On the

‘simulation cases’ part of this document, a comparative image before and after the interior redesign can be seen.

To understand the change that these modifications generate on the flow, some results have been obtained and compared, as the pressure contours of the following images.

The values represented on the figures show up the increase of pressure on the upper ducts. The two plotted points were taken as a sample of what is happening on that part of the geometry. The magnitude of the change of pressure is not very big but it is enough to change the behaviour of the flow, as we it is shown below.

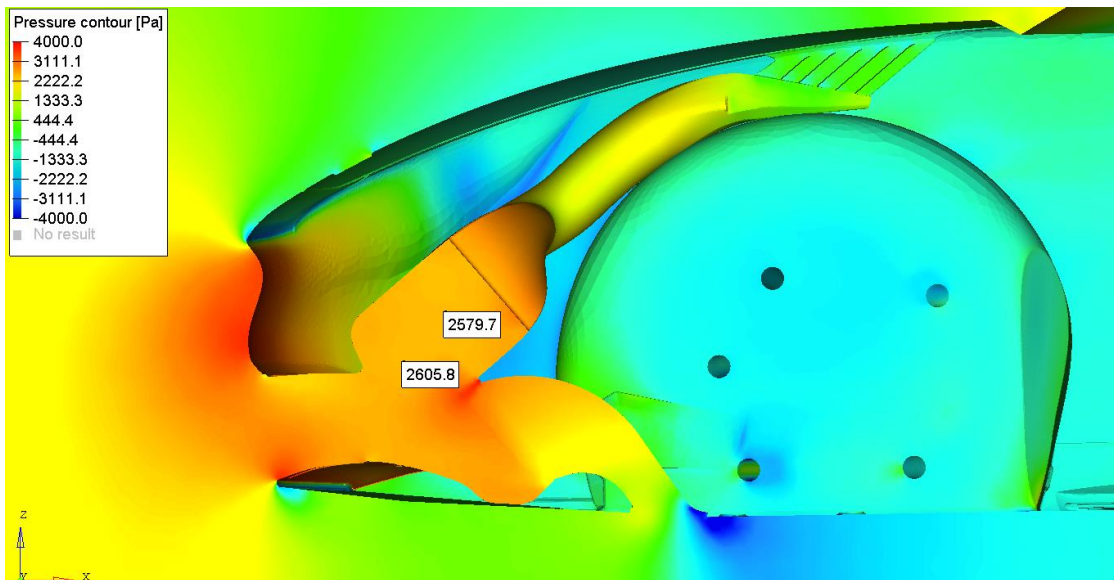


Figure 15.17 : Pressure at symmetry plane in standard air ducts

The two chosen nodes to show the pressure on the upper ducts are localised on two important points of the geometry; the entrance and exit of the heat exchanger. The higher these values are, the more efficient the flow will be due to the reduction of the turbulence. Although just two values are shown here, several points were controlled to know the effect the redesign had on the flux.

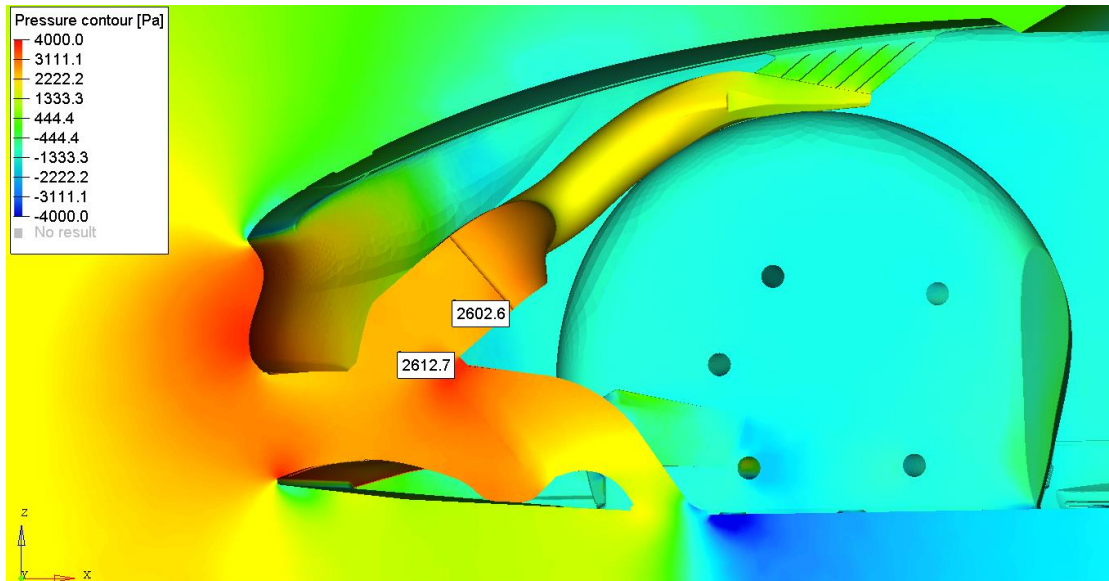


Figure 15.18 : Pressure at symmetry plane in modified air ducts

The pressure values can be also shown on the surfaces of the air ducts. To understand the change on the upper one, several points were evaluated before and after the proposed redesign. The conclusion is that the pressure is increased with the new geometry on all the upper trajectory of the interior flux, until the hood exits.

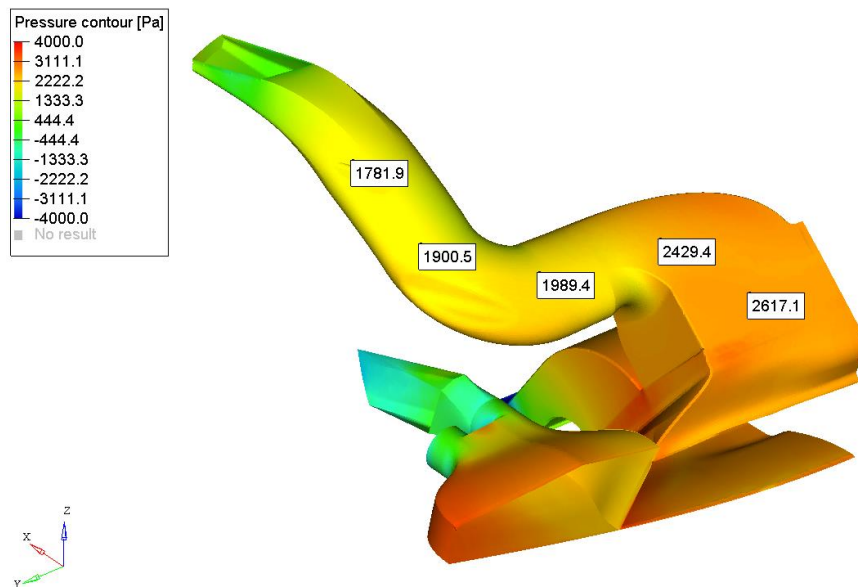


Figure 15.19 : Pressure at interior standard air ducts

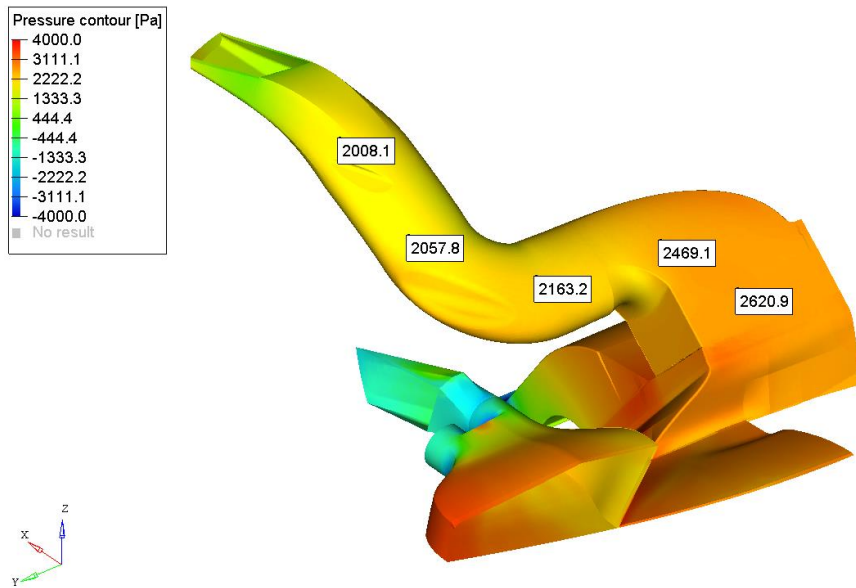


Figure 15.20 : Pressure at interior modified air ducts

As we see with the represented values, objective defined before the redesign has been achieved. The lower area the flow encounters make the pressure on the upper part higher in comparison with the standard case, where this area was a 20% bigger. The higher the pressure is on this zone, the easier the air will flow on the upper ducts, that was the goal of this change. Further tries can be performed to try to reach an optimal interior design, but the proposed change contributed positively on the desired goal.

The eddy viscosity parameter has already been analysed on the base case results before on this part of the document. In this case, this magnitude can be useful to determine of the turbulence on the interior flux has been reduced after the proposed modification. The following two figures show the eddy viscosity contour on a symmetry plane on the air ducts. As we clearly see, on the standard case a big turbulence zone was located on the start of the upper duct. This, in fact, was the reason to change the design of these components. After the change, the upper part present lees turbulence and the lower one has been sensibly increased, which does not represent a problem because on this last part the flow was satisfactory.

The turbulence on the interior of the airducts could mean a low efficient refrigeration process of the radiator, which can represent a very serious problem under certain conditions. Besides, noise can be also generated, affecting the passenger comfort.

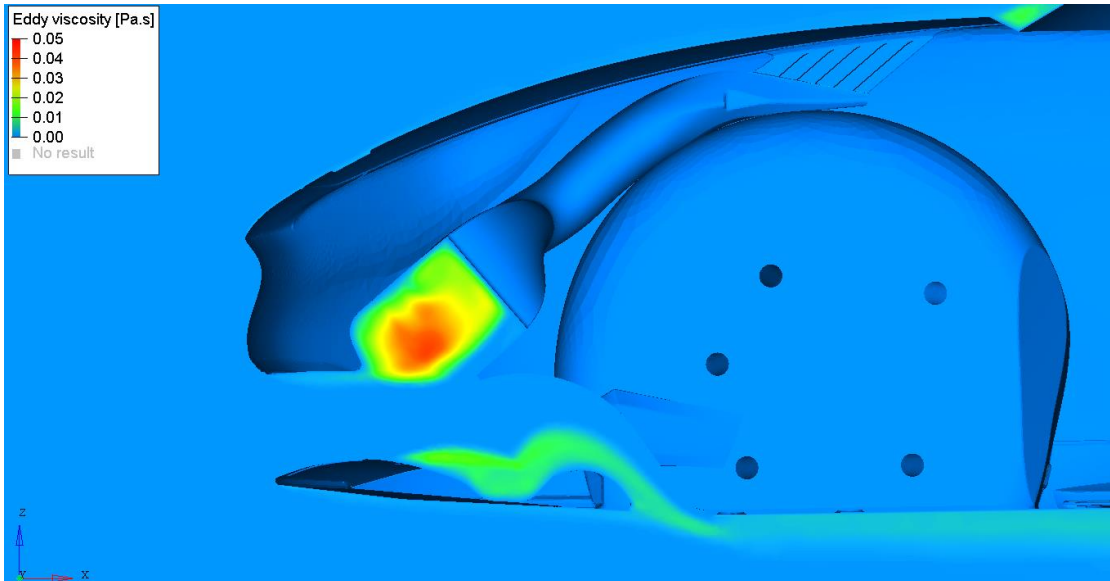


Figure 15.21 : Eddy viscosity contour at standard air ducts

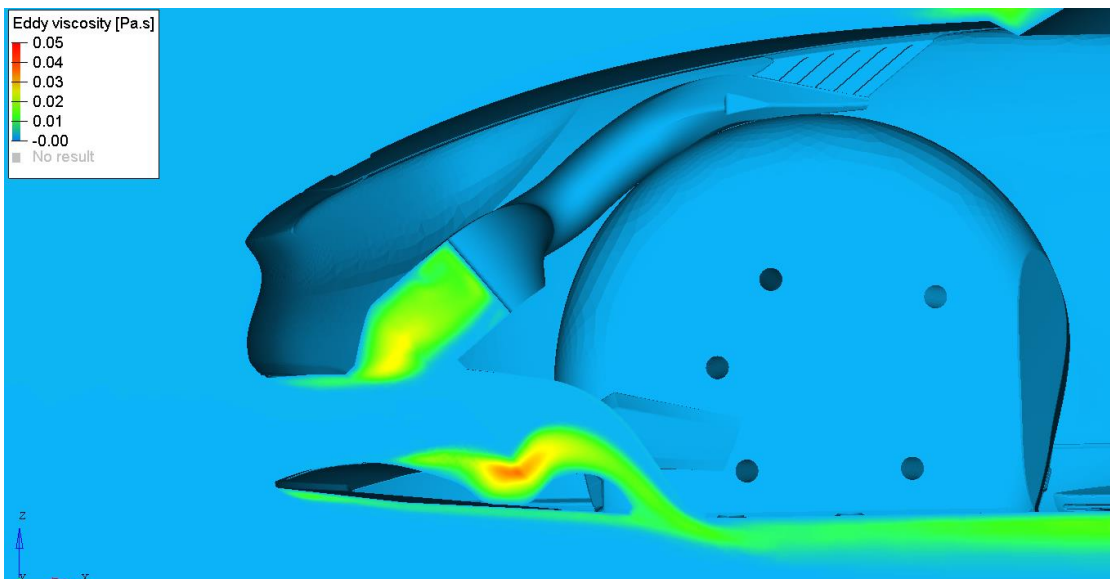


Figure 15.22 : Eddy viscosity contour at modified air ducts

Finally, the path the particles follow on the interior flux can be compared with the standard case and this can clarify if the initial founded recirculation has been reduced. The following two images show the streamlines generated on AcuFieldView, where several points can be selected as seed to the trajectories.

The observed results allow to conclude that, as we saw on the eddy viscosity contours, the turbulence on the upper duct has been sensibly reduced, and therefore the efficiency of the flow has been improved. Before arriving to the radiator component, the flow recirculates on both cases due to the low pressure generated on the curved zone. This effect, however, has been reduced due to the redesign of this particular curvature. The circular trajectory that can be seen on both cases is due to the curved shape of the upper duct, but the vortex presented on the standard case just after the heat exchanger has been successfully reduced.

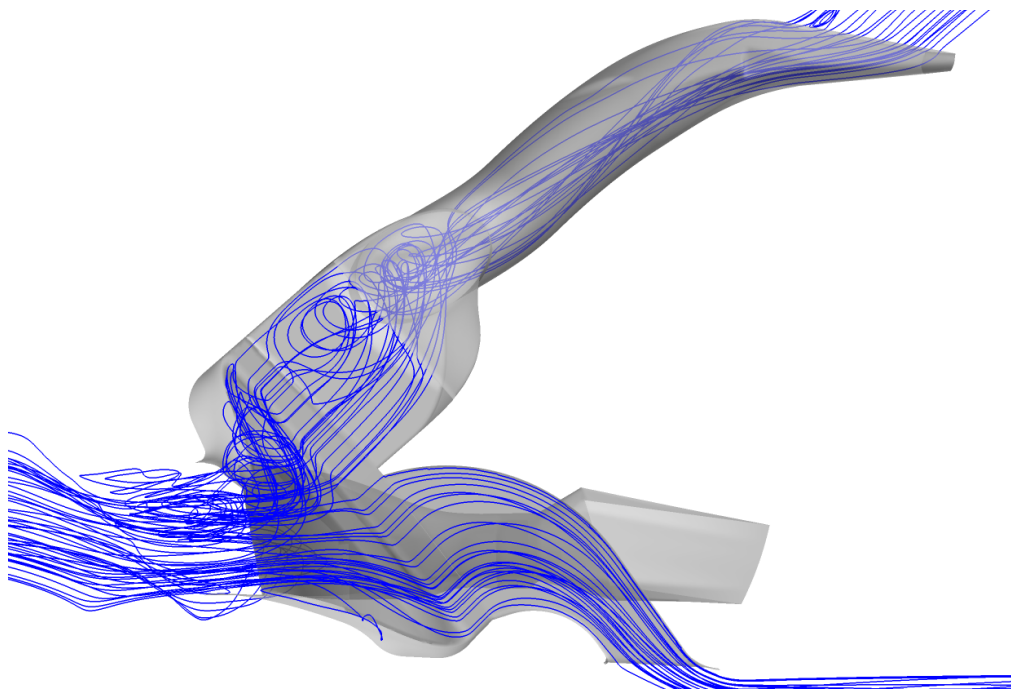


Figure 15.23 : Streamlines of interior flux in the standard case

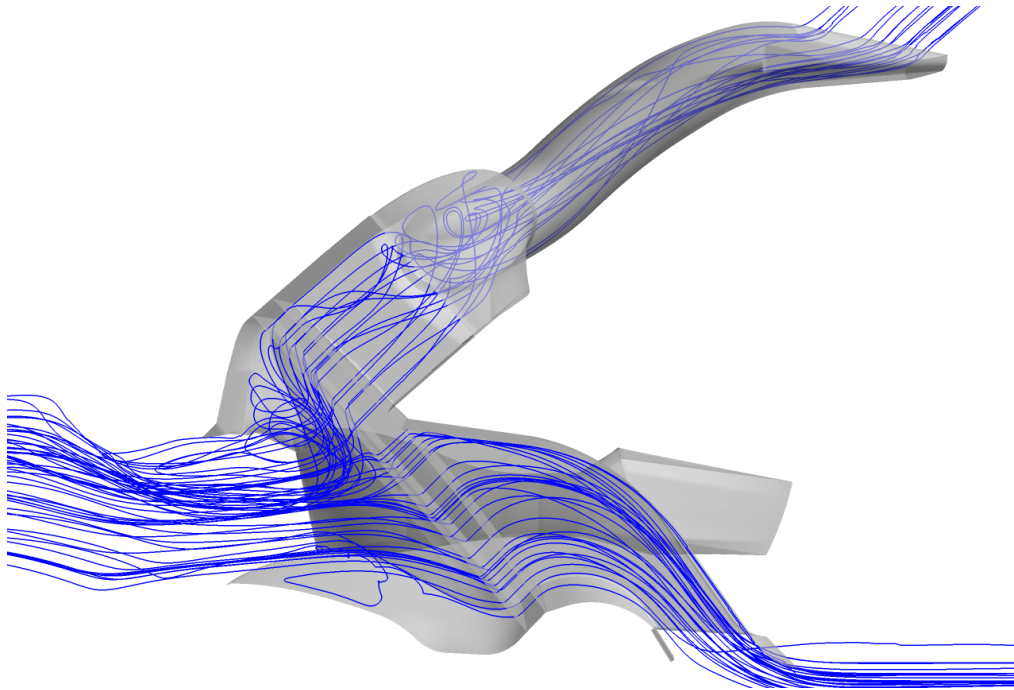


Figure 15.24 : Streamlines of interior flux in the modified case

After this comparison, the conclusion that could be extracted from the eddy viscosity contours can be confirmed; the recirculation founded on the initial case has been sensibly reduced, making the internal flow more efficient.

To obtain the previous streamlines, some points were chosen as seeds of the trajectories on AcuFieldView post-processing program. Some tries have been made in order to be sure of analysing the real behaviour of the flux on this zone of the geometry. As a prove to this, the following two figures show the streamlines obtained with different seed points. As we see, the conclusions that can be extracted are the same, and the general form of the result very similar.

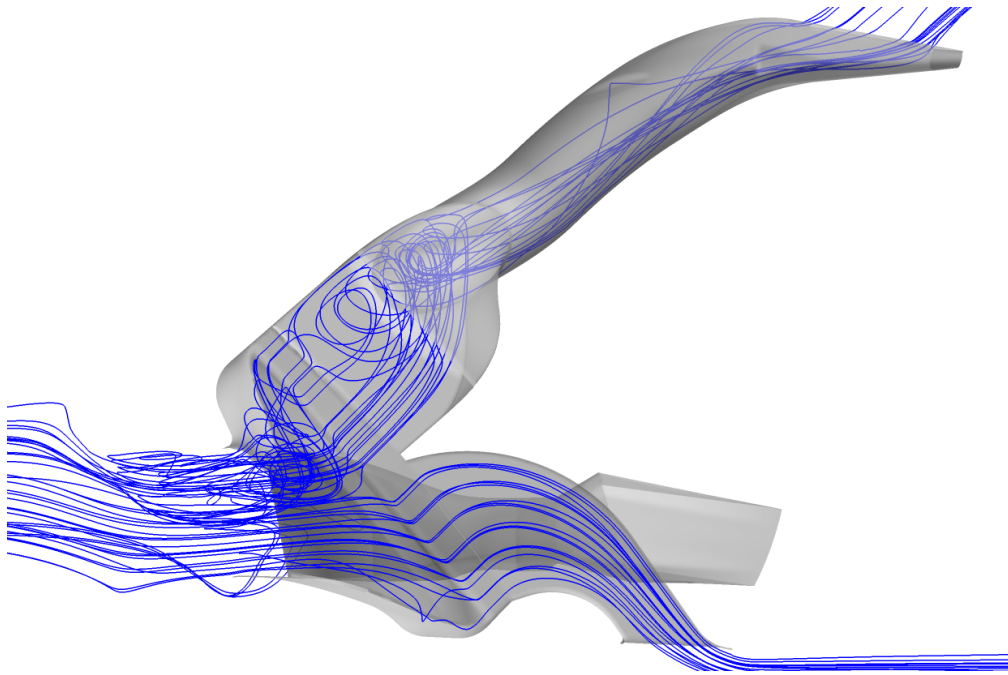


Figure 15.25 : Interior standard streamlines with a different seed

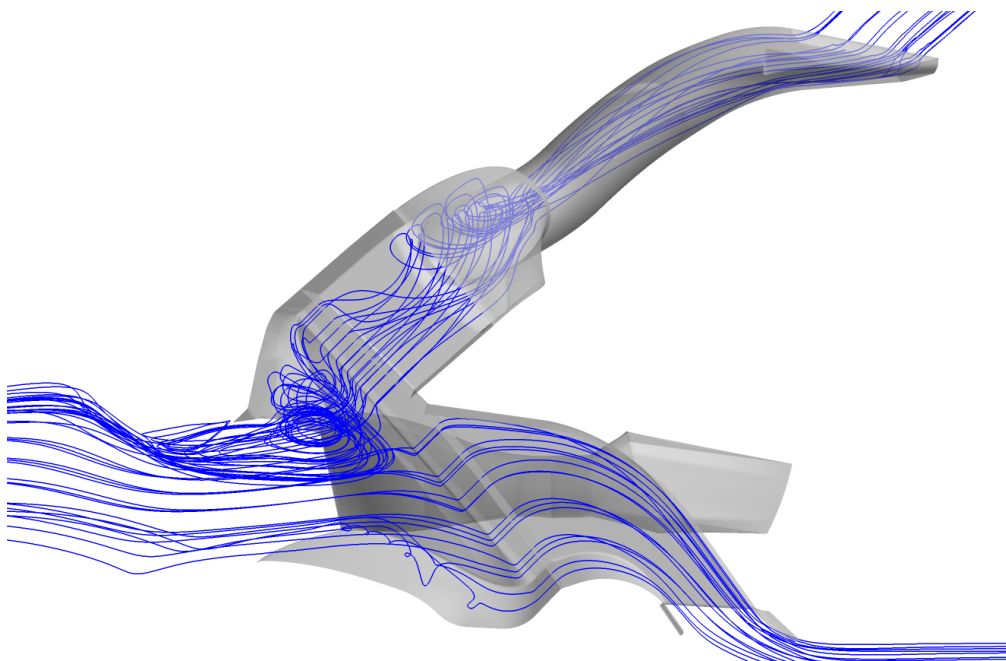


Figure 15.26 : Interior modified streamlines with a different seed

Even though a separation is still presented, the internal turbulence on the entrance of the upper duct has been reduced. The streamlines show an improvement of the flow, the air follows better the interior faces of the ducts and therefore can be considered more efficient. The proposed change is on the correct path and the refrigeration of the heat exchanger is then improved. As future work, additional tries can allow to find the optimal interior design.

With this the result's part of the document is concluded. All the obtained output, visual and numerical, have been shown together with the principal deductions that can be extracted from them. On the following part of the document, the conclusions of the project are listed, explaining the several performed simulations as a whole to make the process more understandable.

VIII. CONCLUSIONS

In this project a CFD study was performed on an electric supercar. The aerodynamic behaviour of this model was tested through different simulations in order to get the necessary results. The automotive electric industry is experimenting a great impulse over the last decades and a good knowledge on this field can help to be competitive on the market. Aerodynamic studies allow to find efficient designs that directly influence on consumption, security or comfort. On this part, the conclusions that could be extracted from the simulated cases are explained, together with the future work that are proposed in order to continue the work done on the project.

The geometries and configurations used for the simulations included many details of the real vehicle. The following list summarise the principal characteristics, that allow to think that the results represent correctly the real behaviour of the car.

- Together with the external aerodynamic analysis, the interior flux through the heat exchanger of the car was also simulated. The interior air ducts, with exits to the hood, the wheelhouses and to the road were modelled. The effect that the radiator has on the air flow was also considered with the addition of a permeable zone from experimental data, as it was explained. These details are not generally included on CFD analysis and add value to the project.
- The wheels of the car were modelled in great detail with the addition of the holes on the tyres. Besides, attached to them, the brake discs are included, being also rotating elements. Static with the rest of the car, the suspension bars join the wheels with the vehicle and affect how the air moves on that space. To conclude, these parts of the car are modelled with basic shapes but representing how the real components are.
- The simulation with the standard geometry has been analysed using several programs and types of results. Numerical output, visual contours and streamline animations helped to understand the behaviour of the flux and the possible improvements to be applied.

- The definitive simulations were performed with two different CFD solvers, OpenFOAM and AcuSolve Altair, that allowed to prove the correctness of the method. On both programs, the same configuration was done, adapted to each software.
- A validation process and a mesh convergence were included on the project. These are two important studies on projects that deal with FEM. The obtained results demonstrate that the used method is valid and the generated mesh optimal in terms of elements size for the computations.
- The study was performed in a company, a great opportunity to have the first contact with a professional environment. During all the procedure, there were a direct feedback with a client, constructor of the car. This allowed to have the necessary data to model accurately the vehicle and get good quality results.
- From the output taken on the base simulations several conclusions were extracted, which are explained below. To improve the aerodynamic efficiency, additional cases were carried out with modifications on the initial received geometry. The proposed changes try to eliminate recirculation of the flux and to reduce other negative effects founded on this supercar.

The base case was performed with the model directly received from the constructor of the supercar. After the cleaning of the geometry and discretization process, the case was simulated on the used CFD solvers. The principal conclusions that can be extracted from the results, that were shown on the previous part of the document, are the following:

- The external design of the supercar results efficient in terms of drag. The streamlines adapt to the shapes of the vehicle, that is designed to have a very low resistance with the air, to increase its autonomy. The obtained **drag coefficient is 0.279**, which is a very good value compared with other supercars of this size. It is important to notice that the geometry does not

represent exactly the geometry of the vehicle, therefore the final values of the aerodynamic coefficient must be obtained in experimental tests.

- The lift coefficient, which represent the vertical load acting on the car, result to be high on the rear half of the model. While on the front part, a downforce is obtained, on the rear shaft a vertical force upwards appears, proportional to the velocity squared. At high velocities, this force may be dangerous due to the losing of grip with the ground. The dimensionless **lift coefficient on the rear half is 0.344**, which at the maximum velocity of 275 km/h creates a vertical load of 2980 N. Although the high weight of this car does not make this result critical, some modifications to the original geometry have been proposed to reduce it.
- The **contribution to the drag force** of the rotating wheels and the lower rear part of the car are bigger in comparison with other components. While the tyres contribute with a 21%, the percentage of the rear spoiler is 11%, even though is a little part. In order to improve the drag coefficient, the design should be focused mainly on these components.
- The bottom part of the car, clearly creates a big **contribution to the lift force** with -0.6. Its percentage represent a 184% of the total lift coefficient and contribute positively with a ground force. The design of this part on sportive cars is essential to achieve the desired behaviour on road. The bottom rear spoiler also has a big impact, with 20% of contribution, being a component with high importance on both principal aerodynamic coefficients.
- The surfaces of the vehicle with the **highest pressure** are the ones on the front part, perpendicular to the movement. This is a usual result in this kind of cases and contributes to the easy inflow of the air to the interior ducts of the vehicle. This high pressure also generates a drag force on the vehicle due to the difference with the low pressure on the rear part. At the maximum velocity of 275 km/h, the peak value of the pressure is equal to 4 kPa.

- Downstream, a **turbulent wake** is generated due to the separation of the fluid. The minimization of this zone is important to reduce the drag force acting on the car. A separation of the flow is noticed on the upper part of the car, near the end. This is a normal effect due to the size of the vehicle, which length is 5 metres.
- The study of **the internal air flow** through the radiator component allow to notice a recirculation on the air ducts. While the flow to the lower and suspension ducts is satisfactory, the upper air duct, that finishes on the hood, present vortex near the heat exchanger. This is caused due to the decrease of pressure of this zone. Some modifications are proposed to solve it, as the recirculation of part of the fluid to the wheelhouse or the decrease of the area on the upper duct, to avoid this drop on the pressure.
- The air flow through the gap between the car and the road has a great influence on the grip of the vehicle, due to the so-called **ground effect**. The part of the internal air flow that exits through the lower duct, directed to the ground, contribute positively to this effect, due to the acceleration of the flow that it generates.
- The pressure acting at the **lateral windows**, taken at 1 cm from the upper end, is an important output to analyse to prove the integrity of these component at high velocities. At the most unfavourable simulated case, at 275 km/h, the lowest pressure is localised near the A-pillar of the car, and it is equal to -3.5 kPa. This value does not represent a dangerous result.
- The study of the **lateral flux** on the sides of the car showed up a recirculation near the front wheels. This is caused by the air exiting the wheelhouses, which present turbulence due to the rotation of the wheels and brakes, together with the presence of the suspensions. This phenomenon may cause not wanted noise and even an increase on the drag force, so a redesign of these part can be positive.

Additionally, to the base case, and from the conclusions of the obtained results, several modifications that can improve the aerodynamic behaviour of the car have

been proposed. Three of these changes have also been simulated, to see how the redesign affect the results.

- The first proposed modification is the addition of a **little spoiler** situated on the top rear part of the vehicle. This new component increases the pressure on its top and help to decrease the high lift force that was obtained on the rear half of the standard geometry. To know what was the best point to place it, pressure contours of the first simulations have been analysed. The obtained results show that this spoiler affect both drag and lift coefficients. While the lift is improved with a decrease on the rear part of the car, due to the new pressure difference, the drag is increased, which is not positive. The new lift coefficient decreased by a 10%, resulting on better behaviour of the car at high velocities, but the drag reached 0.305. After this simulation, it is necessary to evaluate if the change is generally positive or not, as the drag coefficient is a very important parameter that need to be maintained as low as possible.
- On the second simulated modification, a **different inclination** of the vehicle was tested. The purpose was to see its influence on the vertical force the car experiment on its rear part. The standard geometry has a 5 degree-inclination to the front and the modification was created with 0 degrees. The results show that after the change, the flux between the car and the road decelerate less and therefore the ground effect is improved. While the lift coefficient on the rear part improves a 17.6 %, the drag increase from 0.278 to 0.307. Again, as it happened with the added rear spoiler, it is necessary to evaluate if the modification is worth, from the aesthetic and engineering points of view.
- The third and final simulated modification consisted on a **redesign of the internal air ducts** of the vehicle. The proposed change was decreasing by a 20% the area on the upper duct, to increase the pressure and reduce the founded recirculation. An additional change on the inlet curvature of the ducts surfaces also helps the flux to follow better the interior faces of the

geometry. After the simulation the desired effect was reached, the pressure on the entrance of the upper duct was increase, allowing the air to flow easier on this component and exit through the hood. The comparative images and animations of the streamlines show an improvement of the flux, which is now more efficient as the turbulence founded on the standard case was sensibly reduced. Additional simulation tries can help to find the optimal solutions of the interior design of the ducts.

Due to lack of time, additional cases that could help to understand better the flux and to reach an optimal design were not simulated. From the results of the standard geometry, some conclusions were extracted, and simulations are proposed as possible future work.

- It was found that the rear bottom spoiler has a great impact both on the drag and lift coefficient. To test different designs on this component can be very interesting to try to reduce the high up-force of the rear part of the car affecting less the drag coefficient. In general, the change that can be tried should be pointed on reducing the pressure of the bottom rear part, accelerating the flux to improve the downforce on that zone of the vehicle.
- The little rear spoiler that was tested on the first simulated modification resulted to be not the most optimal solution due to its negative influence on the drag. Different wing designs and also trying different positions for their installation, may result on better results and can improve the aerodynamic efficiency and balance of the car.
- The recirculation founded on the air ducts must be eliminated if an efficient interior flux is wanted. In addition to the simulated redesign that was proposed and previously discussed, other change possibilities can be tested in order to try to reach an optimal solution. The deviation of part of the flux to the wheelhouses, where the pressure is low, or the area increase of the hood exits, can help the air to flow easier through the upper duct, improving the interior flux efficiency.

- Finally, the vortex on the lateral flux near the front wheels can create noises and unwanted forces on the car. A redesign of this part, including little wings on the border of the wheelhouses, can make the air to flow better on these zones.

All these simulations can be useful to complete the study that was performed here and to extract additional conclusions about the aerodynamic behaviour of this vehicle. The methodology and computation strategy used on this project can be used in the future to further analyse this and other model cars.

IX. BIBLIOGRAPHY

- [1]. Genta, Giancarlo and Genta, Alessandro. ***Road Vehicle Dynamics***. 2016, World Scientific Publishing Co. Pte. Ltd
- [2]. **NewWorldEncyclopedia**. Available:
<http://www.newworldencyclopedia.org/entry/Aerodynamics>.
- [3]. **LiveScience**. Available:
<https://www.livescience.com/47930-what-is-aerodynamics.html>.
- [4]. **Automoto** website. Available:
<https://www.automoto.it/news/alfa-romeo-g1-la-prima-del-biscione-all-asta.html>.
- [5]. **Alfa Romeo** website. Available:
https://www.alfaromeo.co.uk/promotions/Giulietta_Tecnica_Business_Contract_Hire.
- [6]. **Build your own race car**. Available:
<http://www.buildyourownracecar.com/race-car-aerodynamics-basics-and-design/>.
- [7]. **Lettera43** website. Available:
<http://www.lettera43.it/it/articoli/sport/2014/07/10/come-migliorare-aerodinamica-auto/189645/>.
- [8]. Katz, Joseph. ***Annual review of fluid mechanics***. 2006.
- [9]. W.Kieffer, S.Moujaes N.Armbya. ***CFD study of section characteristics of Formula Mazda race car wings***. 2006.
- [10]. Satyan Chandra. ***CFD Analysis of PACE Formula-1 Car***. 2011.
- [11]. Narayana, Mohd Aliff Bin Mohd Nor and Aswatha. ***CFD study for a rear spoiler for sedan car***.

- [12]. Sneh Hetawal. *Aerodynamic Study of Formula SAE Car*. 2014.
- [13]. S.M. Rakibul Hassan. *Numerical Study on Aerodynamic Drag Reduction of Racing Cars*. 2014.
- [14]. Mott, R. L. *Fluid Mechanics*. s.l. : Pearson Prentice Hall, 2006.
- [15]. **Ground effect on cars**. Available:
http://es.wikipedia.org/wiki/Efecto_suelo_en_coches.
- [16]. **Venturi effect**. Available:
<http://explicaciones-simples.com/2014/07/01/que-es-el-efecto-venturi/>.
- [17]. **OpenFOAM training**. Available:
<https://www.cfdsupport.com/OpenFOAM-Training-by-CFD-Support/node232.html>.
- [18]. Nitin S. Gokhale *Practical Finite Element Analysis*. 2008
- [19]. **Spallart Allmaras model**. Available:
https://www.cfd-online.com/Wiki/Spalart-Allmaras_model.
- [20]. **Altair Engineering**. Available: <http://www.altair.com>.
- [21]. **OpenFOAM user's guide**. Available:
<https://www.openfoam.com/documentation/index.php>.
- [22]. **OpenFOAM, tips and tricks**. Available:
<http://www.wolfdynamics.com/wiki/Oftipsandtricks.pdf>.
- [23]. **CFD support**. Available: <https://www.cfdsupport.com/index.html>.
- [24]. **CFD online**. Available: <https://www.cfd-online.com/>.
- [25]. Anderson Jr., John. *Fundamentals of aerodynamics*. 2005.
- [26]. Lorenzo, Oscar. *Estudio CFD de los efectos aerodinámicos del cruce de trenes de alta velocidad*. 2015.